PROGRESS REPORT
Covering Period from 15 March 1965
to 15 September 1965

RADIATION DAMAGE TO SEMICONDUCTORS BY HIGH-ENERGY ELECTRON AND PROTON RADIATION

John C. Corelli

Sponsored by the National Aeronautics and Space Administration

under Grant NsG-290

Department of Nuclear Engineering and Science
Rensselaer Polytechnic Institute
Troy, New York

Table of Content

I. Introduction and Summary

The results presented in this report were obtained during the six month period 15 March 1965 to 15 September 1965. The following personnel were actively engaged in the research program:

Faculty

Dr. John C. Corelli (Half time)

Adjunct Professor James W. Corbett*

Adjunct Professor George D. Watkins* (Left September 1, 1965)

Graduate Students

Mr. Li-Jen Cheng

Mr. John E. Fischer (AEC Fellow)

Mr. Arne Kalma (NASA Trainee as of September 1, 1965)

Mr. Orrin H. Merrill (Left September 1, 1965)

Mr. William Bohlke (Started September 10, 1965)

Undergraduate Participants and Thesis Students (Physics Department)

Mr. Martin Gaerttner (Left September 1, 1965)

Mr. Martin Weinhous

Research Technician

Mr. James W. Westhead

A brief summary of each phase of the research progress is given below.

1. Infrared spectroscopy using polarized light and stress alignment experiments on defects induced in silicon by $\approx$45 Mev

*Served as part time consultants, lecturers, etc., and are full time scientists at the General Electric Research and Development Center, Schenectady, New York.

electrons have shown that the 1.8 micron absorption band is due to the divacancy defect first studied by Dr. G. D. Watkins and Dr. J. W. Corbett. A substantial body of evidence from annealing of the dichroic ratio and symmetry studies leads to the identification of the 1.8 micron band with the divacancy (in one of its three charge states). From the annealing experiments we conclude that the kinetics are first order with an activation energy for defect migration of $\approx$1.2 ev.

2. The study of radiation-induced oxygen-defect complexes in oxygen-doped germanium has been extended by performing a cold temperature irradiation ($\approx 125^{o}K$) with $\approx$48 Mev electrons and examining the defects using infrared spectroscopy. In addition to yielding a simpler defect absorption band pattern (when compared to $300^{o}K$ irradiation of the same material) sufficient evidence is given that leads to the conclusion that a defect band at 618 cm^{-1} may be the germanium A-center, i.e., a simple complex consisting of a substitutional oxygen coupled to a single vacancy similar to the analagous radiation-induced defect found in silicon (Si-A center). Results of the annealing experiments run on this sample from $125^{o}K$ up to $370^{o}K$ are presented.

3. The study of lifetime and trapping in 6 - 50 Mev electron-irradiated germanium has been extended to include measurements of carrier concentration and conductivity on bridge-type samples cut from the same ingot as the parallelopiped lifetime samples. The irradiations are made at $85^{o}K$ (49 Mev electrons) and detailed annealing experiments are run on the electrical property sample and the lifetime sample (irradiated simultaneously) from $\approx 90^{o}K$ up to $\sim 550^{o}K$ to $600^{o}K$. The experiments thus far have been run on

indium - arsenic - and antimony-doped germanium. The following conclusions have been reached - 1) there is a close correspondence between trapping levels (lifetime $\gtrsim 10^{-3}$ sec) and defect acceptors (carrier removers) and the dominant trap level lies 0.16 eV above the valence band, 2) the energy dependence of trap introduction for both As- and Sb-doped germanium is roughly the same as we have observed in the energy dependence of carrier removal, 3) the dopant (in this case arsenic or antimony) has no significant effect on the introduction of long lived traps, 4) heat treatment to $\approx 550^{\circ}$K (15 minute isochronals) is sufficient to restore in the samples, the pre-irradiation lifetime, carrier concentration and conductivity. No long-lived trapping occurs in p-type germanium.

4. Electrical properties (temperature dependence of carrier concentration and conductivity) of $\approx$50 Mev electron-irradiated germanium were studied on samples irradiated at 325°K and at 82°K. In the 82°K irradiation 1Ω-cm n-type germanium samples doped with oxygen ($\approx 1.2 \times 10^{17}$ cm^{-3}) and antimony were compared and marked differences were observed in the defect energy levels produced and in the annealing behaviors of the two samples, emphasizing the important role of dopant impurities. In the 325°K irradiations the n-type germanium samples were exposed to high fluxes in order to study the ultimate position of the Fermi level.

Portions of the results obtained in the research program have been given in various presentations and papers during the period 15 March 1965 to 15 September 1965 and are listed below.

1. "Annealing of Infrared Defect Absorption Bands in 40 Mev Electron-Irradiated Silicon", J. C. Corelli, G. Oehler, J. F. Becker and K. J. Eisentraut, Jour.Appl.Phys.,36, 1787 (1965).

2. "Recombination, Trapping and Annealing in 10-50 Mev Electron-Irradiated Germanium", J. E. Fischer and J. C. Corelli, Bull. Am. Phys. Soc., 10, 600 (1965).

3. "Studies of Radiation Effects in 30-60 Mev Electron-Irradiated Silicon and Germanium", J. C. Corelli, presented at the IEEE Annual Conf. on Nuclear and Space Radiation Effects, Univ. of Michigan, Ann Arbor, Michigan, July 12-15, 1965.

4. Members of our group were also invited to give talks on our research work as follows:

Dr. John C. Corelli:

Knolls Atomic Power Laboratory, General Electric Company, Schenectady, New York, March 26, 1965.

Harpur College, Binghamton, New York, March 29, 1965.

U. S. Naval Research Laboratory, Washington, D. C., May 3, 1965.

Providence College, Providence, R. I., May 6, 1965.

State University of New York at Albany, Albany, New York, May 18, 1965.

NASA Goddard Space Flight Center, Greenbelt, Maryland, August 11, 1965.

Mr. John E. Fischer:

Aerospace Corporation, ElSegundo, California, August 10, 1965.

Spargue Electric Company, North Adams, Massachusetts, May 5, 1965.

Mr. Li-Jen Cheng:

Chalk River Laboratory, Ontario,Canada, June 26, 1965.

NASA Goddard Space Flight Center, Greenbelt, Maryland, August 11, 1965.

II. A Study on Infrared Absorption Bands in Silicon Induced by ≈ 45 Mev Electrons - Part I. The 1.8 Micron Band

L. J. Cheng and M. Gaerttner

Introduction

Measurement of infrared absorption is a very useful tool for studying the nature of radiation-induced defects in semiconductors. For irradiated Si, there have been many infrared absorption bands observed. These are the 1.8 μ[1-7], 3.3 μ[3,7,8], 3.9 μ[3,8], 5.5 μ[3,8], 8 μ[8], 12 μ[7,8,9,10,11], 20.5 μ[3,12], 27 μ[3,12], 30.1 μ[3,12], and some bands between 9 μ to 12 μ[7,8,10,11]. A schematic diagram of the bands in the wavelength range from 1 to 15 microns for silicon is shown in Fig. 1. Among these bands, only the 12 μ band has been identified as a specific defect configuration and is due to the vibration of the oxygen atom in the vacancy-oxygen complex (i.e. the A-center)[9]. Also the bands between 9 μ and 12 μ have been found to be associated with oxygen impurities in samples[7,8,10].

The goal of this work was to try to find out detailed information concerning the defect center causing the 1.8 μ band by measuring stress-induced alignments of the defect. Similar studies are currently underway on the 3.3 μ and 3.9 μ band and will be reported in the near future. Investigation of stress-induced ordering of point defects in oriented single crystals is a very fruitful tool to study the properties of defects, especially defect symmetries. This technique applied to electron spin resonance and infrared absorption studies has been used to study the radiation-induced defects in silicon by other workers[9,11,13,14,15,16].

Among the absorption bands introduced by irradiation, the 1.8 μ band was the first one to be observed in the neutron - and deuteron - irradiated Si samples[1], and then in electron-irradiated crystals. The 1.8 μ band was observed in both p- and n-type Si. The width at half maximum is about 0.1 ev at 80°K and 0.16 ev at 300°K.[6] The peak absorption shifts toward shorter wavelengths with decreasing temperature. Fan and Ramdas[11] studied the effect of unixial stress on the 1.8 μ band at room temperature and liquid nitrogen temperature. Their result was consistent with the model of a defect with an axis of symmetry in the $\langle 110 \rangle$ direction. The effect was as strong at 78°K as at room temperature, indicating that change in electronic distribution rather than rearrangement of the defect is involved. The 1.8 μ band anneals according to monomolecular kinetics with an activation energy for defect migration of about 1.2 ev*[3].

Experimental Method

The rectangular bar samples were cut from commercially available silicon ingots (pulled and floating zone crystals). The resistivities of the samples before irradiation for most cases were about 100 Ω-cm, except for those mentioned especially. The surfaces of the samples for passing of infrared light were polished with diamond compound and then 0.3 micron alumina abrasive in order to achieve good transmission. A Perkin-Elmer Model 21 Infrared Spectrometer was used to measure the infrared spectra. A pair of AgCl polarizers were mounted in the spectrometer at a fixed position, and the samples were rotated through 90° in order to perform the absorption measurement with polarized light. A hydraulic press capable of being mounted on the spectrometer was

*The original value of E_A=0.8 eV is not correct. We reestimated the value from the Fan and Ramdas data as about 1.2 eV.

used for the stressing experiments at room temperature. The same equipment also was used for the stressing experiments at higher temperature by introducing a small oil bath around the sample in the setup. The magnitude of the stress was measured by a pressure gauge. The isochronal and isothermal annealing experiments were carried out in a temperature controlled furnace with or without an oil bath. The samples were irradiated with $\approx$45 Mev electrons from the R.P.I. Linear Accelerator. The samples were immersed in a cold water bath during irradiation which maintained a sample temperature of $\lesssim 40^{\circ}C$.

Experimental Results

The production rates of the 1.8 μ band in pulled and floating zone (FZ) samples by $\approx$45 Mev electrons at room temperature are plotted in Fig. 2. The absorption increases linearly with irradiation. A similar result was reported by Fan and Ramdas[11]. The production rate of the 1.8 μ band in pulled crystals is about 1.5 times larger than in FZ samples. The oxygen concentration is of the order of $\lesssim 10^{16}$ atoms/cm^3 in the FZ samples and of the order of 10^{17} to 10^{18} atoms/cm^3 in the pulled crystals. Therefore the presence of oxygen in the sample plays a role in the formation of the defect. It will be shown later that oxygen is not actually a part of the defect center. Fan and Ramdas[11] also reported that neutron irradiation produced the 1.8 μ band irrespective of the content of any known impurity in the samples.

The isochronal annealing of the 1.8 μ band for three samples is shown in Fig. 3. The annealing of the band shows two stages. The magnitude of the lower temperature stage ($\sim 180^{\circ}C$) was found to increase approximately with the initial carrier concentration

of the sample. It appears that this first stage may be due to the recovery of free carriers in the sample. This would cause an increase of background absorption accompanied by a decrease in the intensity of the 1.8 μ band since a double beam spectrometer was used. For the time being, the first stage of the annealing will be neglected, since we believe it is not the real annealing of the defect causing the 1.8 μ absorption band. We will only examine the last stage.

There is a very important feature which should be pointed out. The annealing temperature for the band is higher in the floating zone than in the pulled crystal. This means that the annealing temperature of the band depends on the oxygen concentration of the sample. Watkins and Corbett[16] reported that the annealing of the divacancy in irradiated silicon exhibited similar dependence on the presence of oxygen. They also showed that the distribution of the paramagnetic electrons from spin resonance measurements had a preferental direction close to the $\langle 110 \rangle$ direction. As mentioned above, Fan and Ramdas[11] reported that the defect causing the 1.8 μ band has a symmetry in $\langle 110 \rangle$ direction. The above mentioned similarities between the divacancy and the defect causing the 1.8 μ band and discussions with Drs. Watkins and Corbett led us to suspect that we were observing the infrared absorption due to the divacancy.

In Fig. 4, a model of the divacancy is shown which was first given by Corbett and Watkins[19]. For each divacancy, there are three equivalent electronic configurations (see Fig. 5). Under a uniaxial stress in the $[100]$ direction, the energy of the two equivalent electronic configurations b and c would become lower

than that of the electronic configuration a. Then, a local electronic reorientation occurs. The distribution of electrons among these three configurations follows Boltzmann statistics. If the transition dipole moment of the 1.8 μ band is assumed to be along the $\langle 110 \rangle$ direction in the plane perpendicular to the covalent bands, the dichoric ratio of the band for $[100]$ stressing during the measurement should be

$$D \equiv \frac{\alpha_{E_\perp}}{\alpha_{E_{11}}} = \frac{1 + e^{-\frac{rS}{kT}}}{2}$$

where S is the strength of the applied stress, r, the component of the elastic dipole in the stress direction; T, the temperature of the measurement; in ^{o}K and k, the Boltzmann constant. The value of D is smaller than unity for the $\langle 100 \rangle$ stressing which agrees with the experimental results shown in Fig. 6 and Table I.

TABLE I

Dichroic Ratio on the 1.8 μ Band of the Samples During Stressing at ~25° C

Stress Direction	Magnitude of Stress Kg/cm^2	Infrared Beam Direction	$\frac{\alpha_{E_\perp}}{\alpha_{E_{11}}}$
$[100]$	2000	$[011]$	0.8
$[110]$	2000	$[001]$	1.25
$[111]$	2000	$[011]$	1.3

Also, in Table I, the dichroic ratios due to the $[110]$ and $[111]$ stressings are listed. The result is the same as that obtained by Fan and Ramdas[11] and yields a fair fit to the model of a defect with a transition dipole moment in the $\langle 110 \rangle$ direction. It will

be shown later that the measured direction of the transition dipole mement is about 6^{o} off the $\langle 110 \rangle$ direction. In addition the experiment also shows that the 1.8 μ band is unsymmetric with respect to the absorption peak.

If one examines the model of the divacancy in silicon more closely, one can observe that there is another "degree of freedom" amenable to study which is the reorientation of the vacancy-vacancy axis. Watkins and Corbett[16] reported that the divacancy can be reoriented under the application of a high-temperature stress. Hence, a study of the reorientation of the defect under high-temperature stressing should yield more evidence as to whether or not the defect causing the 1.8 μ band is the divacancy.

The vacancy-vacancy axis reorientation is not acheived as easily as the electronic reorientation, since the vacancy-vacancy reorientation must take place by a process in which one of the two vacancies makes a jump to separate it from the other vacancy by one lattice spacing and then the other vacancy "pops" in. However this reorientation can be made to occur by stress alignment at elevated temperature. In this experiment we* first compressed a set of samples along a [110] axis at a pressure of 3000 kg/cm^2 with the sample temperature kept at $\sim 160^{o}$C for 15 minutes. Then the samples were cooled down to room temperature while still under stress. After cooling to room temperature the samples were removed from the stressing apparatus and inserted in the infrared spectrometer equipped with a AgCl polarizer. A significant dichorism was observed in the 1.8 μ band at room temperature, when

---

*We would like to acknowledge the help of Dr. G. D. Watkins who did the stressing for our first two samples.

the infrared beam was in $[1\bar{1}0]$ and $[001]$ directions (shown in Fig. 7). From this result, we are able to conclude that the defect has an atomic symmetry lower than the symmetry of silicon crystal. Also the stress response of the defect in the $\langle 110 \rangle$ direction is similar to the stress response of the divacancy reported by Watkins and Corbett[16]. Under the assumptions that the defect is a divacancy and the dipole transition of the divacancy is roughly along the $\langle 110 \rangle$ axis in the plane perpendicular to the two covalent bonds we estimate that the ratio between the number of the divacancies in the plane perpendicular to the stress axis and the number of the divacancies parallel to the stress axis, $n_\perp / n_{//}$ is about 2. Using the divacancy data of Watkins and Corbett[16] and assuming $\frac{n_\perp}{n_{//}} = e^{-\frac{rS}{kT}}$, we also estimate the value $n_\perp / n_{//}$ of the divacancy for 1 hour stressing under 3000 kg/cm^2 pressure to be about 2, which is in good agreement with our data. It will be seen later in the annealing experiment that there is no difference between stressings of 15 minutes and one hour, since the relaxation time of the reorientation process is about 15 minutes or less.

Since the vacancy-vacancy axis of the divacancy is in a $\langle 111 \rangle$ direction (if we neglect the small shift of the axis due to Jahn-Teller distortion), stressing in a $\langle 100 \rangle$ direction at high temperature should not produce any energy splitting among all the orientations of the divacancies in the sample. In other words, no dichrosim should be observed after a high-temperature stress along a $\langle 100 \rangle$ direction. Our experimental data have shown no significant dichrosim is observed for the 1.8 μ band after

stressing along a $\langle 100 \rangle$ direction at a temperature of 160°C for 15 minutes (see Table II).

TABLE II

Dichroic Ratio on the 1.8 μ Band of the Samples After Stressing at ~160° C for 15 Minutes

Stress Direction	Magnitude Of Stress Kg/cm^2	Infrared Beam Direction	$\frac{\alpha_{E_\perp}}{\alpha_{E_\parallel}}$
$[1\bar{1}0]$	3000	$[001]$	1.45
$[1\bar{1}0]$	3000	$[110]$	1.3
$[111]$	2100	$[\bar{1}10]$	1.33
$[100]$	2100	$[110]$	1.0

The above results demonstrate that the defect causing the 1.8 μ band has an atomic symmetry axis along a $\langle 111 \rangle$ direction, which fits very well with the model of the divacancy.

Isochronal annealing experiments were carried out on the recovery of the stress-induced dichroism. Figure 8 shows the isochronal annealing of the stress-induced dichroism in the 1.8 μ band and the spin resonance data on the divacancy given by Watkins and Corbett[16]. Our annealing experiments were run using the same annealing times (15 minutes) as Watkins and Corbett.[16]

The polarization defined as $\frac{n_\perp - n_\parallel}{n_\perp + n_\parallel}$ has been calculated from the experimental data by using the fact that the defect has electronic symmetry along the $\langle 110 \rangle$ direction and atomic symmetry along the $\langle 111 \rangle$ direction as is the case for the divacancy. From Fig. 8 it can be seen that the polarization of the defect causing the 1.8 μ band is isochronally annealed out in the same

manner as the annealing of the polarization of the divacancy reported by Watkins and Corbett[16].

Isothermal annealings of the dichroism and of the normal absorption of the 1.8 μ band both anneal out exponentially with time, i.e., follow first order kinetics (see Figs. 9 and 10). The activation energy for annealing out of the dichroism and of the normal absorption band is the same $\approx$1.2 ev, see Fig. 11. The annealing experiments demonstrate that the defect causing the 1.8 μ band is annealed out through a process of diffusion in the crystal. Watkins and Corbett[16] have mentioned in their paper that the divacancy has this similar property for annealing. From experimental data, we estimate the frequency factor of reorientation of the defect causing the 1.8 μ band to be $\approx 6 \times 10^{11}$/sec. Also the frequency factors of the annealings of the defect causing the 1.8 μ band in pulled and F.Z. samples are $\approx 8 \times 10^{8}$/sec and $\approx 4 \times 10^{7}$/sec respectively. The ratio of the frequency factor in FZ to pulled crystals may be representative of the ratio of the concentrations of the defect sinks in both crystals. The concentration of oxygen impurities in a pulled crystal is higher than that in a FZ crystal by a factor of ~100. The difference between the two frequency factors shows that the oxygen impurity is one of the major traps for the divacancy defect, but not necessarily the only one.

Discussion and Conclusions

The close similarity in the results of our infrared studies and the spin resonance results of Watkins and Corbett[16] present a substantial body of evidence which leads us to conclude that the defect involved in the 1.8 μ micron band is in fact the

divacancy. However there are a few minor experimental facts requiring further explanation in support of this conclusion, the most important of which is that the production rate of the divacancy in pulled crystals is higher than in FZ samples. A plausible explanation for the differences in production rate is that the interstitial oxygen atoms may have a comparably larger displacement cross section than the silicon atoms in the crystal lattice. If this is true, the scattered energetic oxygen atoms will produce more divacancies that recoiling silicon atoms through their collisions with stationary silicon atoms in the lattice. However, more investigations are needed to ascertain the precise role which the oxygen atoms play in the formation of the divacancy in silicon during irradiation.

A simple molecular orbital treatment of the divacancy by the method of linear combination of atomic orbitals (LCAO) was given by Watkins and Corbett in their divacancy paper[16]. A divacancy in the undistorted silicon lattice has D_{3d} symmetry. After a Jahn-Teller distortion the symmetry of the defect becomes C_{2h}. A simple LCAO molecular-orbital model of the electronic structure of the divacancy after Jahn-Teller distortion is shown in Fig. 12 with the possible transitions due to the dipole moments in z-direction and x-y plane. The possible transitions* occur due to the fact that the transition probability is proportional to the square of the matrix element $\langle f|I|i\rangle$, where $|i\rangle$ is the initial state of the system, $\langle f|$ is the final state, and I is the Hamiltonian of the interaction between the dipole of the system and the electro-

*We thank Dr. G. D. Watkins for very valuable discussions on this subject.

magnetic field of the light ($I \propto e\bar{R}$). The matrix element will vanish, unless the compositions of the direct product of the irreducible representations of i and I, $D^i \times D^I$, contain the same irreducible representations of D^f, according to group theory. From our experimental result on the dichroism after high temperature stressing, we deduce that the transition dipole moment is not in the z-direction, otherwise we would get an opposite dichroism. So we shall consider the transitions with the dipoles in x-y plane. The transition, d, in Fig. 12 should be neglected, since it exists only for the triple negatively-charged divacancy which is not present in irradiated silicon.

Some rough estimations are made for the angle between the dipole and the y axis, θ, which is defined as $\theta = \tan^{-1} \frac{\langle |x| \rangle}{\langle |y| \rangle}$ The result is that $\theta_a \cong 65^\circ$, $\theta_b \cong 20^\circ$, and $\theta_c \cong 6^\circ$ for the transitions, a, b, and c respectively. In the estimation, we have used the following simplifications; 1) ignore the overlap of the wavefunctions, i.e. $\langle a | b \rangle = 0$ etc.; 2) assume $\langle a | x | a \rangle = X_a \langle a | a \rangle$, where X_a is the x-component of the position vector of the a atom, and so on. Also we have estimated the relative intensities for the transitions, a, b, and c, to be 0.3 a^2, 1.3 a^2, and 1.7 a^2 respectively.

Now we shall check which transition best fits our experimental data. For a sample orientated in such a way that the stress direction at $\sim 160^\circ C$ was applied in [110] direction and the observations made in [110] and [001] directions, the calculated dichroic ratios are;

$$\left(\frac{\alpha_{E_\perp}}{\alpha_{E_{//}}} \right)_{\langle 001 \rangle} = \frac{\frac{n_\perp}{n_{//}} \left[\cos^2 (45^\circ - \theta) \right] + \cos^2 \theta + \cos^2 (45^\circ + \theta)}{\frac{n_\perp}{n_{//}} \left[\cos^2 \theta + \cos^2 (45^\circ + \theta) \right] + \cos^2 (45^\circ - \theta)}$$

and

$$\left.\frac{\alpha_{E_\perp}}{\alpha_{E_{//}}}\right)_{\langle 1\bar{1}0\rangle} = \frac{1}{\left\{\cos^2[45^\circ+\tan^{-1}(\sqrt{2}\tan\theta)]+\cos^2[45^\circ-\tan^{-1}(\sqrt{2}\tan\theta)]\right\}\left(1-\frac{\cos^2\theta}{2}\right)+\frac{\cos^2\theta}{1+\frac{n_\perp}{n_{//}}}}$$

for the infrared beam in the $[001]$ and $[1\bar{1}0]$ directions respectively. The calculated ratios of

$$\frac{\left.\alpha_{E_\perp}/\alpha_{E_{//}}\right)_{[001]}}{\left.\alpha_{E_\perp}/\alpha_{E_{//}}\right)_{[1\bar{1}0]}}$$

from the above formulas are plotted as a function of θ in Fig. 13 for various values of $\frac{n_\perp}{n_{//}}$. Also the experimental value of the ratio for $\frac{n_\perp}{n_{//}} \approx 2$ is shown in the figure, from which we have $\theta \sim 6^\circ$.

This experimental result yields a good fit with transition c. Therefore we would like to suggest the conclusion that the 1.8 μ band is due to the transition c as shown in Fig. 12, as resulting from an application of the simple model of Watkins and Corbett[16]. This transition c can exist in the single negative, neutral, and single positive charged state of the divacancy defect. Unfortunately, our experimental result cannot give any direct information concerning the charged state of the defect which gives rise to the 1.8 μ band.

However, we can use some indirect evidence on the Fermi level dependence of the 1.8 μ band to deduce the charge state of the defect. From the known charge states of the divacancy (see Fig. 14 in reference 16), it is quite possible that the charge state of the divacancy causing the 1.8 μ band is neutral. However, no matter what the charge state of the defect is, one would like to observe some infrared absorptions due to two other charge states

of the divacancy defect. Due to the electrostatic interactions between electrons, the energies required to make the transitions will be expected to be different from that of the 1.8 μ band. There are two good candidates for these among all other infrared absorption bands in irradiated silicon, which are the 3.3 μ band in n-type silicon and the 3.9 μ band in p-type silicon, we have observed both bands. In a future paper, we shall report on some studies relating to the 3.3 and 3.9 μ bands, at which time we shall be able to conclude whether or not they are due to the other charge states of the divacancy.

References

1. M. Becker, H. Y. Fan, and K. Lark-Horovitz, Phys. Rev., 85, 730 (1952).

2. H. Y. Fan, Repts. Progr. in Phys., 19, 107 (1956).

3. H. Y. Fan and A. K. Ramdas, J. Appl. Phys., 30, 1127 (1959).

4. V. S. Vavilov, A. F. Poltnikov, and G. V. Zakhvatkin, Soviet Physics - Solid State 1, 894 (1959).

5. E. N. Lotkova, V. S. Vavilov, and N. N. Sobolev, Opt. i Spektroskopia, 13, 216 (1962).

6. E. N. Lotkova, Soviet Physics - Solid State 6, 1500, 1964.

7. J. C. Corelli, G. Oehler, J. F. Becker and K. J. Eisentraut, J. Appl. Phys., 36, 1787 (1965).

8. J. C. Corelli, "Radiation Damage to Semiconductors by High Energy Electron and Proton Radiation", NASA, NsG-290, Progress Report (1965), Rensselaer Polytechnic Institute.

9. J. W. Corbett, G. D. Watkins, R. M. Chrenko, and R. S. McDonald, Phys. Rev.,121, 1015 (1961).

10. J. W. Corbett, G. D. Watkins, and R. S. McDonald, Phys. Rev., 135A, 1381 (1964).

11. H. Y. Fan and A. K. Ramdas, Proc. Intern. Conf. on Semicond. Phys., Prague (1960) p. 309.

12. M. Balkanski and W. Nazarewicz, J. of Phys. Soc. of Japan, 18, Suppl. II, 37 (1963).

13. G. D. Watkins and J. W. Corbett, Phys. Rev., 121, 1001 (1961).

14. G. D. Watkins, J. Phys. Soc. Japan, 18, Suppl. II, 22 (1963).

15. G. D. Watkins and J. W. Corbett, Phys. Rev., 134A, 1359 (1964).

16. G. D. Watkins and J. W. Corbett, Phys. Rev.,138A, 543 (1965).

17. H. Y. Fan and A. K. Ramdas, Bull. Am. Phys. Soc., Series II, 129 (1958); J. Phys. Chem. Solids, 8, 272 (1959).

18. A. K. Ramdas and H. Y. Fan, Bull. Am. Phys. Soc., Ser II, 159 (1959).

19. J. W. Corbett and G. D. Watkins, Phys. Rev. Letters, 7, 314 (1961).

III. Infrared Studies of 48 Mev Electron-Irradiated (at 125°K) Oxygen-Doped Germanium

M. Gaerttner

Introduction

We have recently reported[1] infrared studies on oxygen-doped germanium irradiated at 25°C by 40-60 Mev electrons. Isochronal annealing experiments were performed from about 70°C up to 400°C (20 minute time pulses) and during the course of annealing 14 radiation-induced defect absorption bands in the wavelength range 11 to 18 microns were observed and studied. No radiation-induced bands from 9 to 16 microns are observed in irradiated oxygen-free germanium. In the room temperature irradiation the results yielded strong evidence that one of the oxygen vibrational bands induced in oxygen-doped germanium (at 618 cm^{-1}) was a defect complex consisting of a single oxygen atom plus a vacancy which corresponds to the comparable defect found in silicon, namely the silicon A-center. If the 618 cm^{-1} band in germanium was an A-center (relatively simple oxygen defect complex) then it should appear at lower irradiation temperature, since the defect is formed most easily by a primary vacancy capturing an oxygen atom. In order to check this point we decided to perform a "cold temperature" irradiation (125°K).

Experimental Procedure

The sample was cut from the same oxygen-doped single crystal germanium ingot* used in the room temperature irradiations. The

*Purchased from Semi-Elements Inc., Saxonburg, Pennsylvania.

two faces corresponding to a ⟨111⟩ plane, measuring 7mm x 18mm, were ground, polished, and etched. A complete description of the pre-irradiation sample is presented below.

N-type germanium

Oxygen doped - 1.2×10^{17} $0/cm^3$

Dimensions - 7mm x 7mm x 18mm

Resistivity - 1.0 ohm-cm

Carrier Concentration - 4.8×10^{15} e/cm^3 at $300^{o}K$

The sample was irradiated at 48 Mev to a total integrated flux of 3×10^{17} e/cm^2. In order to obtain this dose it was necessary to set the beam current at 3 $\mu amp/cm^2$ for approximately 8 hours. (The electrons were incident on the sample in a ⟨111⟩ direction.) The temperature of the sample during irradiation never exceeded $127^{o}K$. The vacuum around the sample was less than 1 micron except during irradiation, when it reached a couple of microns. Note, this difference in vacuum may or may not be significant since a thermocouple gage was used to monitor pressure during irradiation.

To keep the temperature of the sample as low as possible during the irradiation it was necessary to design and build a new cryostat. The four window bottom of the cryostat could be rotated enabling the infrared beam to be incident on the sample through NaCl windows perpendicular to the ⟨111⟩ plane. The sodium chloride windows, although not directly in the beam, were opaque to visible light after irradiation. However in the region from 2 to 16 microns, the transmission of the windows was high and flat. In a separate experiment the radiation damage effects in NaCl were studied and it was found that no radiation-induced defect bands

were produced in the 2 to 16 micron range. Copper-constantan thermocouples mounted at the top and bottom of the sample indicated that the temperature variation in the sample during the irradiation was less than $3^{o}C$. Because of the possible danger of a violent chemical reaction involved in producing an accumulation of ozone inside the liquid nitrogen cryostat, the coolant used during the irradiation was liquid argon (BP $88^{o}K$). After irradiation the liquid argon was replaced by liquid nitrogen.

The radioactivity level of the cryostat after irradiation was approximately 1 R per hour and two days passed before annealing was attempted. Spectrum measurements were taken on Perkin Elmer Model 421 dual beam grating infrared spectrometer located in the Materials Research Building. A special ringstand was built for holding the cryostat rigidly on the spectrometer. The same spectrometer settings were used to take spectra and the time required to take a complete scan was around one hour. The isochronal anneals were of 20 minute duration separated by roughly 20 degree temperature intervals. All spectrum measurements were made at liquid nitrogen temperature ($78^{o}K$).

Between 150 and $300^{o}K$ the sample was warmed inside the cryostat. To facilitate warming, the liquid nitrogen above the sample was removed by inserting a plunger with a ground glass tapered joint at the end. The temperature was controlled manually using a 0-110V AC power supply and observing the thermocouple voltages on a Leeds and Northrup type H AZAR recorder. The exact thermocouple voltages were measured with a precision potentiometer. After the $323^{o}K$ anneal the sample was removed from the cryostat

and annealed in an oven containing a flask of silicone oil. After each of these anneals, the sample was polished and placed in a cold cell (smaller liquid nitrogen cryostat), which was then evacuated to 10^{-5} mm Hg. The temperatures of all the anneals were controlled with an accuracy of $\pm$ 1°C.

A convenient way of displaying the growth and decay modes of bands is to plot the area of the absorption band (appropriately normalized) versus frequency. The areas were taken from the spectra using a polar planimeter; and we make the reasonable assumption that the area under the absorption peak is directly proportional to the defect concentration since the infrared spectrometer settings were kept constant during the entire annealing experiment.

Results, Discussion and Conclusions

After the 376°K anneal a room temperature spectrum was taken from 1 to 14 μ on a Perkin-Elmer Model 21 prism dual beam infrared spectrometer. The resulting spectrum was found to be similar to that observed in p-type germanium. The conversion from n-type to p-type in heavily irradiated germanium is expected. The conversion results from free electrons being trapped on defects induced by the irradiation.

A striking and unexpected feature of the annealing experiments is the large changes in the background transmission. A very wide absorption band centered about the 860 cm^{-1} oxygen interstitial band appeared after the 154°K anneal and disappeared after the 193°K anneal and is shown in Fig. 14. The wide absorption could be some broadening effect of the 860 cm^{-1} band. A similar but more widespread absorption occurred after the 223°K anneal and

lasted until the 304°K anneal (see Fig. 15). This absorption resulted in no transmission below 650-700 cm^{-1} and consequently no band data in this temperature region could be taken. It is possible that vapors condensed on the sample or alternatively by some mechanism electrons were freed and later recaptured. The same type of effect was seen in electrical measurements performed with heavily irradiated n-type germanium and was recently reported by Gerasimov and Konovalenko[2]. They found regions where the conductivity first fell, then rose sharply, and finally fell again. They did not supply adequate data however to indicate how good a correlation there was. Similar effects were not observed in the electrical measurements undertaken at the Linear Accelerator Lab with the same oxygen-doped germanium as used here. This is due to the relatively lower flux of electrons used in the electrical property studies. The sample was not converted to p-type.

The only band present in unirradiated oxygen doped germanium is the conspicuous 860 cm^{-1} band. This is caused by interstitial oxygen atoms and is not present in oxygen free germanium. Irradiation has been seen[1,3] to reduce the intensity of this band, which indicates a decrease in the concentration of interstitial oxygen atoms. This effect was also observed here. Irradiation of oxygen-doped germanium produces many oxygen-associated vibration bands (10-16 micron region), none of which are present in irradiated oxygen-free germanium.

The pre-anneal spectrum had absorption bands at 1380, 715, 673, and 618 cm^{-1}. The 618 cm^{-1} band, which anneals out at 150°C, has previously been detected in room temperature irradiations of

oxygen-doped germanium[1]. Paramagnetic resonance and infrared absorption experiments on irradiated oxygen-doped silicon have directly proved that a "similar" band in silicon results from a silicon A-center (meaning a substitutional atom-oxygen vacancy complex)[4]. By "similar" it is meant that both bands have 1) the same decay modes, 2) they have the same frequency ratios between them and the corresponding interstitial bands and 3) similar annealing properties. From this it is concluded that the defect responsible for the 618 cm^{-1} band could be the germanium A-center. Also, because it appears after 100-120°K anneal (10°K irradiation)[5], we have further evidence that the 618 band is not a primary defect band. In addition the results strongly suggest that the vacancy moves at ~60-80°K and then captures an oxygen atom to form the A-center similar to the case of silicon. The verification that the 618 cm^{-1} band is the Ge A-center has been suggested in some recent spin resonance work by Baldwin[6].

After the first anneal, the 715 cm^{-1} band is nearly gone and the 618 cm^{-1} band has shown considerable growth. The results are shown in Fig. 16. Therefore the 715 band is probably associated with the same defect as the 618 cm^{-1}. It has been proposed by Whan that the 715 cm^{-1} results possibly from a different charge or configuration state of the A-center[5]. A liquid helium temperature irradiation shows that the 715 cm^{-1} band initially appears at 50°K[5].

As yet the 1380 and 673 cm^{-1} bands have not been mentioned in publications. These bands display roughly the same decay modes (the 673 cm^{-1} anneals out a little faster). This suggests that they are different vibrational modes of the same defect. These

bands, which were not observed in Whan's 2 Mev liquid helium temperature irradiation[5], may be produced by a different primary defect and oxygen complex since the temperature at which they anneal out is different from the temperatures at which the 618 and 715 cm^{-1} bands anneal out.

After the 303 and 323°K anneals, small bands at 630, 711, 729, 778, 801, and 816 cm^{-1} appeared for the first time. All of these bands except the 630 (a very small one) have been seen after room temperature irradiations[1,3], although not all were present in the room temperature irradiated sample cut from the same ingot. An inspection of Fig. 16 will reveal that J. Becker's bands do not pick up where mine stopped. Only the 816 cm^{-1} band has the slightest tendency to do so. The sample is presently in a freezer and the complete anneal (say, to 650°K), may shed further light on what is happening to these bands.

For a while it was not known which of these small bands resulted from primary defects. Low temperature irradiations have served to partially clarify the picture. Because of the high annealing temperature required to produce them, R. Whan[3,5] concluded that they do not originate from primary defects, but from defects formed by migrating vacancies.

An observation that should be pointed out is that high temperatures tend to complicate the infrared bnad structure. At low temperatures there were 3 to 4 bands. At high temperatures (250°C) a dozen bands have been seen (some of J. Becker's smaller bands were not included in Fig. 3b).

Many answers will be obtained through more refined experiments. Liquid helium temperature irradiations are called for. Additional detail can be found by observing the anisotropic nature of defects using polarized infrared and stress techniques, and it is possible we may perform such experiments within the next year.

References

1. "Infrared Properties of 40-60 Mev Electron-Irradiated Germanium", by J. F. Becker and J. C. Corelli, "Progress Report Covering period 15 September 1964 - 15 March 1965", Rensselaer Polytechnic Institute and to be published in J. Appl. Phys., (Nov. 1965).

2. A. B. Gerasimov and B. M. Konovalenko, Soviet Physics - Solid State, Vol. 6, No. 10, (1965).

3. R. E. Whan and H. J. Stein, Appl. Phys. Letters, 3, 187, (1963).

4. J. W. Corbett, G. D. Watkins, R. M. Chrenko and R. S. McDonald, Phys. Rev., 121, 1015 (1961) and G. D. Watkins and J. W. Corbett, Phys. Rev., 121, 1001 (1961).

5. R. E. Whan, Appl. Phys. Letters, 6, 221 (1965).

6. J. A. Baldwin,Jr., Jour. Appl. Phys.,36, (Part I), 793 (1965).

IV. Lifetime and Trapping in 6-50 Mev Electron - Irradiated Germanium

John E. Fischer

Introduction

The time decay of excess carriers in semiconductors is a sensitive probe of lattice imperfections. Defects introduced by high-energy radiation fall into two main classes: recombination centers and trapping centers.

Several workers have used this type of measurement to assess radiation damage. In particular, Curtis and Crawford[1] found significant differences in the defect level structure and recovery behavior of arsenic- and antimony-doped germanium irradiated near room temperature with cobalt-60 gamma rays. Namely, they obtained different positions in the gap for the dominant radiation-induced recombination levels. They cited the respective atom sizes as a possible cause of the dissimilar behavior: arsenic and germanium are similar in size (1.21 and 1.22 angstroms, respectively), whereas antimony is substantially larger (1.41 angstroms); the positive lattice strain surrounding the Sb atom may be expected to influence the stable defect configuration and annealing behavior.

We felt that it would be interesting to pursue this problem further, by going to low-temperature irradiations and also by attempting to correlate the temporary trapping levels with the defect acceptor levels which are also produced by radiation (6-50 Mev electrons). This phase of our program has been underway for the past several years.

Experimental

Figure 17 shows a very schematic diagram of the experimental apparatus. The samples are cooled to 85°K by helium exchange gas in contact with a tube filled with liquid nitrogen. The main body of the cryostat is a standard 5 liter nitrogen dewar. The bridge sample is used to monitor DC conductivity and Hall coefficient voltage, using a 950 gauss permanent magnet. The rectangular sample is used for trapping and recombination studies. The two samples are cut from adjacent portions of the same ingot. The electron irradiations are performed at the RPI microwave Linac, with the electron beam first traversing the thinner bridge sample. The cryostat is removed from the target room to an adjacent laboratory for the lengthy annealing runs.

Excess carriers are introduced by 50 nanosecond bursts of 150 KVP x-rays from a Field Emission Corporation Model 845 flash x-ray machine. The use of this device for performing lifetime measurements was suggested to us by Dr. O. L. Curtis*. The samples are warmed to successively higher temperatures in 5-10 degree steps for 15 minutes at each temperature. All measurements are made at 85°K unless otherwise noted.

We are dealing with minority carrier traps in n-type material, so if the excess hole denisty produced by the x-ray burst is large compared to the trap density, all the traps will be initially filled and the amplitude of the trapping portion of the decay curve is a direct measure of the trap density, independent of energy position in the gap and minority carrier capture cross-section. Furthermore, Baicker[2] has solved the nonlinear equations that

*Northrup Nortronics, Newbury Park, California.

govern the decay under conditions of large injection, and the solutions are such that one can obtain the trap density and energy from the shape of a single decay curve taken at one temperature.

Recovery of τ in P-type Ge Irradiated at 85°K

Before discussing n-type germanium, we would like to present results on a 4Ω-cm p-type In-doped specimen. This sample was irradiated by 48 Mev electrons at 85°K to a integrated flux of 1.3×10^{13} e/cm^2 in an attempt to establish the existence or absence of trapping levels. No traps were observed upon irradiation. The lifetime was reduced to less than 100 ns so that it could not be resolved, due to the 50 ns x-ray pulse. The isochronal annealing of the lifetime is plotted in Fig. 18, along with that of an identical sample irradiated to 1×10^{12} e/cm^2 (see Progress Report 15 March 1964 - 15 September 1964). The pre-anneal value of τ for SMIn 4.0-2 is obtained by a linear extrapolation of τ^{-1} vs flux. Note that the annealing for the 2 samples is identical (after τ of SMIn 4.0-2 has recovered enough to be measurable), indicating that the annealing rate is independent of defect concentration, i.e., first order kinetics. On the other hand, the complex shape of the annealing curve (especially the broad range of annealing temperature) would indicate a higher order reaction process. We will not speculate on the causes of this apparent contradiction at this time.

85°K Irradiation of N-Type Ge

We turn now to the study of traps in n-type material. The large-injection method used here has the advantage that the number of traps is uniquely determined by the signal voltage at the

trapping plateau, in contrast to the low-injection method[3], in which the trap density cannot be determined without prior knowledge of the trapping cross-section. Some typical data obtained by this large injection method are shown in Fig. 19. In this example, we are looking at the time decay of excess carriers in 20 Ω-cm arsenic-doped germanium irradiated at 85°K after annealing for 15 minutes at the temperatures shown in Fig. 19. As mentioned before, the measurements are made at 85°K. Each curve in Fig. 19 is a composite of several photographs taken at overlapping oscilloscope sweep speeds. Each photograph represents the response of the sample to a single x-ray pulse. The intensity of the pulses are reproducible enough so that normalization among the several sweeps making up one complete decay curve is a minor problem.

The initial decay, on the order of microseconds, is a recombination process which eliminates the holes that were not trapped. The slower stage represents trapped holes finally boiling out and recombining with electrons.

Figures 20 and 21 show the isochronal recovery of hole trapping levels and defect acceptor levels in 20 ohm-cm As- and Sb-doped germanium irradiated at 85°K with 1.5×10^{13} e/cm^2 of 47 Mev. Trapping levels are introduced at roughly the same rate with both dopants, and the trap density is about the same as the density of defect acceptors for both dopants. These facts, plus the gross similarity in annealing behavior of the two types of defect levels, suggest that the same defect is responsible for both property changes. It is reasonable to ascribe both property

changes to the same defect, since in the temperature range in which we observe trapping, electrons are frozen onto the defect acceptors, so that the ensemble may be more attractive to holes than to further electron capture.

The recovery of both property changes for both dopants can be described as occurring in two main temperature regions. The fractional recovery of carrier concentration in the region below room temperature, in which an acceptor level deeper than 0.20 ev from the conduction band disappears, has been found by Wikner[4] to decrease with increasing bombarding energy in the range 10-35 Mev, whereas Brown[5] et al observe no annealing in this region using 0.7 Mev electrons. In the higher temperature region, Corelli[6] et al find the 0.20 level disappearing. Saito and Pigg[7] have observed annealing of $1/\mu$ but not carrier concentration below room temperature in n-type samples irradiated with Co-60 photons, whereas in Wikner's and our experiments, n and σ recover together in this region. Apparently the defect responsible for anneal of carrier concentration in this temperature region requires a recoil energy in excess of 700 kev for its formation.

The high-temperature annealing stage has been investigated by many workers[6,8] and is by no means well-understood. It seems certain, however, that defect-impurity and defect-defect interactions should control the behavior here, since the motion of simple defects occurs at much lower temperatures ($70^{\circ}K$)[9]. Thus the annealing behavior in this region is expected to be very complex, with perhaps several reactions occurring simultaneously, which cannot be resolved using macroscopic techniques.

Another experiment of this type was performed on 9 Ω-cm Sb-doped germanium. Figure 22 demonstrates the linearity of trap introduction and carrier removal (mobility changes are less than 10%). At this point, a word on traps in unirradiated material is in order. In most ingots, trap densities of the order of 10^{10} cm^{-3} exist; this can be reduced by an order of magnitude by heating in air to 300°C for 5 minutes. However, in some cases (notably 3 Ω cm As-doped), the trap density exceeds the excess hole density ($\sim 10^{13}$ cm^{-3}) and is not reduced by heating. Shulman[10] has demonstrated that copper introduces hole traps in germanium, so the offending ingots may contain large concentrations of copper impurities.

This sample (SM Sb 9.0-1) was studied in more detail than the others. Both the sensitivity and low-frequency response of the measuring system was improved in order to study small densities of long lived traps. The decay of excess carriers after irradiation is shown in Fig. 23. The lifetime is too short to be resolved. Note the existence of the long-lived trap which accounts for about 9% of the trapped holes. In addition, there is a "permanent" trap (the trapped carriers do not recombine unless the sample is heated above 85°K) which accounts for less than 1% of the trapped holes. It was hoped that the trap energies could be determined by illuminating with filtered infrared light; both bandpass interference filters and long wave pass filters made from some III-V semiconductor compounds were used. The wavelengths of the former did not correspond to any of the trap energies, and the resolution of the latter did not permit this determination to be made. An attempt

was made to fill all of the long-lived and "permanent" traps with white light in order to study the dominant level, but this also was not possible, as shown.

Figure 24 shows the isochronal annealing of (all) traps and acceptors. Here again, the gross similarity in introduction rates and annealing behavior strongly suggests that the same defect is responsible for both effects.

Figure 25 presents the anneal of the long-lived traps (> 1 sec). The broad anneal from $100^{\circ}K$ to $300^{\circ}K$ corresponds well to the two curves in Fig. 24. The growth of long-lived traps centered at $480^{\circ}K$ corresponds to the high-temperature decay of (all) traps and acceptors. Finally, the recovery of the lifetime at $85^{\circ}K$ is plotted in Fig. 26, where we have again determined a pre-anneal value of τ from a linear extrapolation of τ^{-1} vs. flux. We conclude from this plot that the dominant recombination center at $85^{\circ}K$ is not related to the trapping levels or the defect acceptors.

Further evidence for the correspondence between the trapping levels and defect acceptors is obtained by comparing Fig. 23 with the temperature dependence of the Hall coefficient. The dominant trap (first decay stage in Fig. 23) is fairly well represented by Baicker's[2] calculation; it lies roughly .16 ev above the valence band. This trap energy remains the same throughout the annealing process. The long-lived trap (second decay stage) is not well-represented by Baicker's model, probably because the assumption of quasi-thermal equilibrium is violated (this assumption is tantamount to requiring many round trips to occur between the trap and the valence band before recombination occurs), but this trap is

almost certainly higher in the gap than .16 ev, such that the small probability for thermal release of a trapped hole leads to a long lifetime. We conclude, then, that about 90% of the traps are .16 ev above the valence band, the remaining 10% being considerably higher in the gap. The Hall coefficient is observed to be independent of temperature above 1000/T = 5.5, from which we can estimate that about 86% of the total carrier removal is accounted for by an unresolved acceptor level more than 0.4 ev below the conduction band, whereas only 14% of the carriers are trapped by the well-known level .20 ev below the conduction band. These results are summarized in Fig. 27. As in the case of the previously discussed samples, the total carrier removal rate is roughly equal to the total trap introduction rate. These results strongly suggest that the deep acceptor lies 0.16 ev above the valence band.

From the temperature dependence of the Hall coefficient, we observe the .20 level annealing between 220°K and 430°K, which accounts for 17% of the carrier recovery in Fig. 24, whereas the deep acceptor anneals in the 2 major stages shown. Most of the trap annealing is accounted for by the 0.16 ev trapping levels, which would correspond to the deep acceptor. We conclude, then, that we have fairly good evidence that the hole trapping levels and the net acceptors are identical. The occurrence of 2 well-separated annealing stages for what is apparently one defect is not known; the .16 ev trap may actually be several closely-spaced levels which anneal at different temperatures.

We are planning 2 additional runs of this type, namely 3 Ω-cm Sb-doped and 5 Ω-cm As-doped, in a further effort to determine

differences between arsenic and antimony.

Room Temperature Irradiation of N-Type Ge

We are concurrently performing a series of 300°K runs to determine the energy dependence of the trap introduction rate. In our previous progress report, the suggestion was made that the formation of traps is enhanced by higher energy in the range 10-55 Mev. On the other hand, the carrier removal rate is not a strong function of energy in this range[11], which casts doubt on the conclusion drawn in the last section. For this reason, we are repeating the experiment rather carefully, over as broad an energy range as possible. Additional motivation is provided by the question of the role of the dopant atom in trap formation[1]; we are irradiating As- and Sb-doped samples from 1 Ω-cm to 20Ω-cm to examine this aspect of the problem. Preliminary results are shown in Fig. 28, where we plot the trap introduction rate vs. initial resistivity for As- and Sb-doped samples irradiated at 300°K with 6 Mev and 47 Mev electrons. The 6 Mev irradiations were carried out by Mr. R. G. Schonberg of Varian Associates; we sincerely thank him for his assistance. We note first of all that, with the exception of 2 stray points, the increase in trap introduction rate from 6 to 47 Mev is roughly a factor of 2, in general accord with the carrier removal results[11]. Furthermore, the trap introduction at both energies is not a dramatic function of donor type or concentration. The two samples showing very large introduction rates are questionable; the 3Ω-cm 6 Mev sample is from an ingot having pre-irradiation trap density larger than the density of radiation-induced traps, and the two cannot be separated easily.

The 11Ω-cm 47 Mev sample may have developed a large contact resistance; the resistance after irradiation was twice that expected.

We plan another series of this type at $\sim$85 Mev. We are also studying the possibility of using bridge samples to eliminate contact effects and also to increase the accuracy of determining trap densities (recall that the trap density depends upon the conduction electron concentration, which cannot be determined accurately from a rectangular parallelopiped sample shape). It is fairly clear, however, that our previous suggestion that trap formation is greatly enhanced by high energy (which was based on only 2 samples) is not borne out.

References

1. O. L. Curtis, Jr. and J. H. Crawford, Jr., Proceeding of Symposium on Radiation Damage in Semiconductors, Royaumont 1964, p. 143, Dunod, Paris, 1965.

2. J. A. Baicker, Phys. Rev., 129, 1174 (1963).

3. G. K. Wertheim, Phys. Rev., 109, 1086, (1958).

4. E. G. Wikner, Phys. Rev., 138A, 294 (1965).

5. W. L. Brown, et.al., Jour. Appl. Phys., 30, 1269 (1959).

6. J. C. Corelli,et.al., Bull. Am. Phys. Soc. II, 9, 48, (1964).

7. Saito and Pigg, ORNL, Solid State Division Report, 1965.

8. J. C. Pigg and J. H. Crawford, Jr., Phys. Rev., 135A, 1141, (1964). (Earlier references cited in this paper.)

9. R. Whan, App. Phys. Letters, 6, 221 (1965).

10. R. G. Shulman and B. J. Wyluda, Phys. Rev., 102, 1455, (1956).

11. J. C. Corelli and H. B. Huntington, NASA CR-62 (1964).

V. Electrical Properties of ~50 Mev Electron-Irradiated Germanium

Arne H. Kalma

High Flux Experiment

This experiment was performed to find out whether high flux irradiation of germanium causes the Fermi level to reach an ultimate value or if it continues to drop to the valence band. If an ultimate Fermi level exists, its position and the amount of flux necessary to reach it was to be determined.

Several one ohm-cm, and tenth ohm-cm, n-type germanium, antimony-doped samples were irradiated at about 50°C with 50 Mev electrons to different total integrated fluxes ranging from 0.9 x 10^{18} electrons/cm^2 to 2.9 x 10^{18} electrons/cm^2. All the samples converted to p-type early in the irradiation at integrated fluxes $\lesssim 10^{16}$ electrons/cm^2 as expected. The initial and final Fermi levels are shown in Fig. 29 for the most heavily irradiated sample of each resistivity. The ten ohm-cm sample is from a previous experiment and will be explained later. The solid curves are the preirradiation values and the dashed ones are postirradiation values after integrated fluxes of 2.9 x 10^{18} electrons/cm^2 for the one ohm-cm and tenth ohm-cm samples and 5.7 x 10^{16} electrons/cm^2 for the ten ohm-cm sample. The Fermi level for all samples having the same concentration of dopant was the same in all cases after irradiation and thus only one of each resistivity is illustrated in Fig. 29.

The temperature dependence of carrier concentration of the samples having the highest antimony concentration is shown in Fig. 30. The unlabeled curve is the preirradiation temperature

dependence. The curve labeled 1 is for a sample irradiated to 0.9×10^{18} electrons/cm^2, 2 is for one irradiated to 1.7×10^{18} electrons/cm^2, and 3 is for one irradiated to 2.9×10^{18} electrons/cm^2. The Fermi level for sample 3 is shown in Fig. 29. The material doped to 1Ω-cm exhibits the same behavior in temperature dependence of carrier concentration and need not be shown. It can be seen from the carrier concentration curves of Fig. 30 that only the samples which received the lowest amount of integrated flux have not reached saturation and even these are quite close to saturation. Comparison of the ultimate Fermi levels of the two samples having different doping concentration shows that a different value was reached in each case (see Fig. 29). At room temperature, the Fermi level winds up closer to the valence band for more highly doped samples, and is at E_v + 0.20 eV for the 0.1Ω-cm samples and is at E_v + 0.23 eV for the 1Ω-cm samples. This difference of 0.03 eV is much larger than the variation in the value for samples of the same resistivity which is of the order of .005 eV. At low temperatures, 80 to 120°K, the Fermi levels for both 0.1 and 1Ω-cm material come closer together and, when extrapolated to 0°K, both end at .006 - .010 eV below the top of the valence band. The Fermi level is relatively insensitive to the carrier concentration at low temperatures and this explains why in the samples irradiated to lowest integrated fluxes the Fermi levels are the same as for the samples irradiated to higher integrated fluxes even though the carrier concentrations are a bit different.

From experiments on 10 and 30Ω-cm n-type Ge reported on in previous progress reports[1], it was observed that the Fermi level

extrapolated to $0^{o}K$ is down to $\approx .01$ eV below the top of the valence band after 50 Mev electron irradiations to integrated fluxes as low as 1-5 x 10^{16} electrons/cm^2. The room temperature Fermi level for these samples is still dropping toward the ultimate value even after integrated fluxes $\lesssim 10^{17}$ electrons/cm^2. At $300^{o}K$, the Fermi levels of the 10 and 30 Ω-cm samples after irradiation to $\lesssim 10^{17}$ e/cm^2 are around 0.28 eV above the top of the valence band.

Since the doping concentration in the 10 and 30 Ω-cm samples is less than in the 0.1 and 1 Ω-cm samples the ultimate Fermi level after irradiation should be further from the valence band in the lightly doped material (10 and 30 Ω-cm), based on results given here. But even taking this into account, the 10 and 30 Ω-cm samples did not reach an ultimate Fermi level value. One example of 10 Ω-cm material is shown in Fig. 29. From this it can be seen that even at the lowest temperatures, at which measurements were made the Fermi level of the 10 Ω-cm sample is still well above the two ultimate Fermi levels of the 0.1 and 1 Ω-cm samples from this experiment and the latter two coincide in this range. Thus, it is obvious that in the previous experiments the samples were not irradiated to sufficiently high integrated fluxes to drive the samples to ultimate Fermi levels.

The conclusion to be drawn from the present experiment is that the Fermi level reaches an ultimate value after about 10^{18} electrons/cm^2 and that the original doping of the sample affects the location of the Fermi level. The ultimate Fermi level is higher the lower the doping concentration in the sample. It takes about 10^{18} electrons/cm^2 to reach this ultimate level along the

entire temperature range from liquid nitrogen to room temperature. But fluxes of $\sim 10^{16}$ electrons/cm^2 lower the low temperature end of the Fermi level enough that, when extrapolated to 0°K, it falls below the top of the valence band and is the same value as that of the more highly irradiated samples.

P-type germanium samples of about thirty ohm-cm were irradiated in a previous experiment to integrated fluxes from about 10^{16} to 5×10^{16} electrons/cm^2. The Fermi levels of these samples have not reached the ultimate value of the samples studied in this experiment and are even higher than the Fermi levels of the irradiated ten ohm-cm n-type material previously mentioned. It is not clear whether this higher value is the ultimate Fermi level for p-type material or if it will continue to fall upon further irradiation. Further irradiation on this p-type material has been performed but the results were not available to include in this progress report.

Oxygen-Doped Germanium Experiment

This experiment was performed to obtain electrical measurements to compare with infrared measurements on oxygen-doped germanium obtained in previously reported[1] room temperature irradiations and especially in a 125°K irradiation reported on in the third section of this report. The purpose behind these experiments was to see if there were any similarities between oxygen-doped germanium and oxygen-doped silicon radiation damage, the latter of which is fairly well understood.

Two samples were irradiated simultaneously with 45 Mev electrons to an integrated flux of 2.7×10^{14} electrons/cm^2 at about 82°K. One was oxygen doped and the other antimony doped to

resistivities of about one ohm-cm. The latter was used as a check to observe correlations and differences between oxygen-doped and oxygen-free germanium. After irradiation the samples were annealed isochronally using 20 minute pulses at various temperatures from $\sim 100^{o}K$ up to $380^{o}K$.

The flux dependence of the conductivities and carrier concentrations of both samples are shown in Fig. 31. The initial slopes are given in Table I.

TABLE I

	Oxygen Doped	Antimony Doped
Carrier Concentration	11.6/cm	12.4/cm
Conductivity	2.08×10^{-14} cm^3/electron	2.76×10^{-14} cm^3/electron

The carrier concentration change occurs at about the same rate for both samples but the antimony-doped sample has a faster rate of decrease of conductivity.

The temperature dependences of the carrier concentrations for the oxygen- and the antimony-doped samples after each anneal are shown in Figs. 32 and 33 respectively. The conductivity of the antimony-doped sample is shown in Fig. 34. The fraction of the carrier concentration damage remaining as a function of the annealing temperature is shown in Fig. 35. The annealing of the conductivity of the antimony-doped sample using as a reference the value at $1000/T = 12.0$ $(^{o}K)^{-1}$ is shown in Fig. 36.

In the oxygen-doped sample, there is a donor level at E_c-0.20eV in unirradiated material due probably to two oxygen atoms and has been studied previously by Fuller and Doleiden[2]. A level introduced

by irradiation that acts as an acceptor is at about the same energy as the original level or deeper, making the energy determination difficult. From Fig. 32 and taking into account the position of the Fermi level defect energy levels appear to be deeper than 0.14 eV below the conduction band. No single level is resolvable for the oxygen-doped sample (Fig. 32). There are no shallow levels introduced by irradiation that can be seen from this experiment. The annealing of the carrier concentration does not correspond to the annealing of any of the infrared absorption bands reported on in Section III of this report. The carrier concentration annealing has a broad annealing peak from 120°K to 240°K in which about 50% of the damage annealed out. From 240°K up to the highest annealing temperature, 380°K, less than 10% more damage annealed out so there is still 40% of the damage remaining at 380°K.

In the antimony-doped sample, surely one and possible three defect levels are introduced by irradiation. Most of the carriers, about 75%, are trapped on a level located at .20 eV ± .03 eV below the conduction band. The 0.2 eV level has been observed by many workers. It is the annealing of this level that is shown in Fig. 35 along with the annealing of all levels. The high temperature level off of the carrier concentration could not be reached due to the elevated temperature* so the concentration of defects associated with the 0.2 eV level could not be obtained exactly. It appears that the carrier concentration curves level off below the pre-irradiation value so that there must be a level deeper than ~0.2 eV below conduction band produced by the irradiation that is responsible

*The solder used to make the ohmic contacts would have melted before reaching the elevated temperatures.

for trapping about 25% of the carriers. Nothing can be said about this deeper level as its existance is only inferred from what appears to be carriers still trapped after the 0.2 eV level is ionized. Actually, the deeper level concentration may be considerably less than 25% of the removed carriers. It is fairly definite that there is a shallow level, or levels ($<$0.08 eV from conduction band) introduced by the radiation but so many of the other levels are introduced that few electrons are trapped on the shallow level and when it is being ionized, the carrier concentration is so low that little meaning can be gotten from the measurement. The conductivity shows up the shallow level in a much clearer fashion. From Fig. 34, it can be seen that, upon annealing, the conductivity first drops at about 220^{o}K and then rises until the level is gone at about 290^{o}K. The 0.2 eV level begins going out at about 280^{o}K so that it is still trapping almost all of the carriers until the shallow level is gone. The shallow level annealing peak is fairly sharp, occurring between 220^{o}K to 290^{o}K (see Fig. 36). This shallow level is what causes the large changes in conductivity around 240^{o}K in Fig. 36. These large changes cannot be observed in the carrier concentration percentage change curve Fig. 35 as the total carrier concentration change due to irradiation is too large. This is why the conductivity results have been plotted as shown in Fig. 36. The 0.2 eV level also has a fairly sharp annealing stage that starts at about 280^{o}K and is still recovering at the highest anneal temperature 360^{o}K. The solder on the leads melted on the next anneal. At this point, less than 30% of the level was left although about 45% of the total damage was left.

Comparing the oxygen and antimony doped samples, it can be seen that both the energy levels and annealing behaviors of the radiation induced defects are different. Thus, it is concluded that the defects introduced depend on the dopant in the sample. It therefore appears to be a coincidence that the introduction rates are close to the same. The fact that the conductivities change at a different rate reinforces this conclusion as the defects formed in the antimony doped sample lower the mobility more per defect than those in the oxygen doped sample, showing that the antimony defects are more efficient scatterers.

References

1. Progress Reports covering periods 15 September 1964 - 15 March 1965 and 15 March 1964 - 15 September 1964.

2. C. A. Fuller and F. H. Doleiden, J. Phys. Chem. Solids, 19, 251 (1961).

VI. Photoconductivity Studies in 10-50 Mev Electron-Irradiated Silicon*

L. J. Cheng and A. H. Kalma

A low-noise, high impedence amplifier capable of measuring a very small photoconductivity signal (about order of 10^{-7} to 10^{-8} volt) at 13 cycle/sec frequency, has been constructed. The pre-amplifier consists of two nuvistor tubes with open grid at the first stage. The sensitivity of the amplifier is very high. Precise photoconductivity spectra cannot be obtained, unless the absorption of infrared light due to water vapor and carbon dioxide in the system can be completely eliminated. We have tried to use a method of flushing the system by dry nitrogen gas, but the result was still unsatisfactory. In order to completely eliminate the water and CO_2 effects, an evacuable Model 1500 3/4 meter Czerny-Turner monochromator utilizing Bausch and Lomb gratings has been ordered from Spex Industries, Inc. and is expected to be delivered to us by December 1965. This evacuable monochromator will have energy resolution superior to our present system and will greatly facilitate our photoconductivity experiments.

In our recent studies on the uniaxial stress effects on the radiation-induced 1.8 μ infrared absorption band, we have concluded that the 1.8 μ absorption band is due to the electronic excitation of the silicon divacancy in one of its charged states. It would be very interesting to study the dichroism in the photoconductivity of irradiated silicon under various stressing conditions. Now we know quite well the symmetry of the divacancy from infrared

---

* In view of the improvements and modifications of the equipment currently underway, we shall give only a brief discussion of this work.

absorption and electron spin resonance experiments. We shall look into what kind of photoconductivity is caused by the divacancy and determine the electronic levels of the divacancy located in the forbidden gap in silicon. The studies of the dichroism in photoconductivity would be able to give us some microscopic information concerning defect energy levels and charged state.

We have irradiated several oriented samples of 100 Ω-cm floating zone silicon doped with phosphorus with neutrons at room temperature. The neutron flux was obtained from (γ,n) reactions of bremsstrahlung radiation caused by an electron beam incident on a tungsten target during the use of Linac by another group. This irradiation was just to obtain samples to check out the experimental method of measuring photoconductive dichroism. Eventually we plan to irradiate samples with 10-50 Mev electrons in order to study photoconductivity due to specific defects, such as the divacancy. A special AgCl polarizer was built in order to achieve polarized light.

Figure Captions

Fig. 1 Schematic diagram of radiation-induced defect infrared absorption bands in silicon (both n- and p-type) in the wavelength region 1 to 13 μ.

Fig. 2 Production rate of the 1.8 μ absorption band in floating-zone and in pulled silicon irradiated by $\approx$45 Mev electrons at $\approx$300°K.

Fig. 3 Isochronal annealing (20 minutes at each temperature) of the 1.8 μ defect absorption band in pulled and in floating-zone silicon irradiated by $\approx$45 Mev electrons at $\approx$300°K.

Fig. 4 A model of the divacancy defect in silicon according to G. D. Watkins and J. W. Corbett (see text).

Fig. 5 Diagrams showing the three equivalent electronic distributions of the divacancy defect in silicon.

Fig. 6 Dichroism of the 1.8 μ absorption band in silicon resulting from room temperature stressing in the $\langle 100 \rangle$ direction. Note infrared beam (IR) is in the $\langle 011 \rangle$ direction. (See Table I and text).

Fig. 7 Dichroism exhibited by the 1.8 μ absorption band in silicon (irradiated at 300°K) resulting from 15 minute stress at $\sim$160°C (see Table II and text).

Fig. 8 Comparison of the recovery of stress-induced divacancy axis polarization in silicon from infrared measurements (Dichroism) and from spin resonance measurements (ESR) by Watkins and Corbett. Both isochronal anneals used 15 minute temperature pulses (see text).

Fig. 9 Isothermal anneals of the 1.8 μ defect absorption band at 248°C and at 198°C for 45 Mev electron-irradiated (at $\sim$300°K) floating-zone silicon.

Fig.10 Isothermal anneal of the dichroism exhibited by the 1.8 μ absorption band at 122°C, 106°C and 100°C. The stress was applied in the $\langle 110 \rangle$ direction and the infrared beam passed through the sample in the $\langle 1\bar{1}0 \rangle$ direction (see text).

Fig.11 Time for 50% anneal plotted as a function of $\frac{1000}{T}$ for (1) anneal of 1.8 μ band in floating-zone silicon, (2) annealing data on the 1.8 μ band of Fan and Ramdas (see text) and (3) annealing of the dichroism of the 1.8 μ band.

Fig. 12 Simple LCAO molecular orbital model of the electronic structure of the silicon divacancy after Jahn-Teller distortion showing the possible electronic transitions.

Fig. 13 Ratio of the dichroism of 1.8 μ band with the infrared beam in the $\langle 001 \rangle$ direction to the $\langle 1\bar{1}0 \rangle$ direction (after stressing in $\langle 110 \rangle$ direction) plotted as a function of θ, (direction off any $\langle 110 \rangle$ axis) for various values of $n_\perp/n_\parallel$. The measured value is shown on the graph.

Fig. 14 Infrared spectra for irradiated oxygen-doped germanium in the wavelength region 2.5 microns (4000 cm^{-1}) to 20 microns (500 cm^{-1}) after 48 Mev electron irradiation at 125°K before anneal and after 20 minute anneals at the indicated temperatures. All spectra were measured at 80°K.

Fig. 15 Infrared spectra for irradiated oxygen-doped germanium showing in detail the wavelength region 11.4 microns (880 cm^{-1}) to 16.7 microns (600 cm^{-1}) after 48 Mev electron irradiation at 125°K before anneal and after 20 minute anneals at the indicated temperatures. All spectra were measured at 80°K.

Fig. 16 Isochronal annealing of oxygen-associated defect absorption bands (from 50°K up to 600°K) in irradiated oxygen-doped germanium. See text of Section III for detailed explanation.

Fig. 17 Schematic of experimental arrangement for 85°K irradiations.

Fig. 18 Isochronal annealing of lifetime in 4 Ω-cm indium-doped Ge irradiated at 85°K with 10^{12} and 1.3×10^{13} e/cm^2 of 47 Mev.

Fig. 19 Typical response of an irradiated sample to a burst of x-rays, exhibiting minority carrier trapping. Measurement made at 85°K.

Fig. 20 Isochronal annealing of traps and acceptors in 20 Ω-cm As-doped Ge.

Fig. 21 Isochronal annealing of traps and acceptors in 20 Ω-cm Sb-doped Ge.

Fig. 22 Introduction of traps and removal of conduction electrons in 9 Ω-cm Sb-doped Ge.

Fig. 23 Response of 9 Ω-cm Sb-doped Ge at 85°K to a burst of x-rays.

Fig. 24 Isochronal annealing of traps and acceptors in 9 Ω-cm Sb-doped Ge.

Fig. 25 Isochronal annealing of long-lived traps in 9Ω-cm Sb-doped Ge.

Fig. 26 Isochronal annealing of recombination centers in 9Ω-cm Sb-doped Ge.

Fig. 27 Defect level scheme of 9Ω-cm Sb-doped Ge.

Fig. 28 Trap introduction at 300°K vs. donor content and type for 6 Mev and 47 Mev irradiation.

Fig. 29 Temperature dependence of Fermi levels for 0.1, 1.0 and 10Ω-cm Sb-doped germanium before irradiation (solid curves at top of figure) and after irradiation of the 0.1 and 1.0 Ω-cm samples to integrated fluxes of 2.9 x 10^{18} e/cm^2 and the 10 Ω-cm sample to an integrated flux of 5.7 x 10^{16} e/cm^2 with $\approx$50 Mev electrons at $\approx$325°K (dashed curves at bottom of figure are for post-irradiation temperature dependences).

Fig. 30 Temperature dependence of carrier concentration 0.1Ω-cm antimony-doped germanium after 50 Mev electron irradiation (at 325°K) to total integrated fluxes of 0.9 x 10^{18} e/cm^2 curve 1, 1.7 x 10^{18} e/cm^2 curve 2, and 2.9 x 10^{18} e/cm^2 curve 3, the unmarked curve is the carrier concentration temperature dependence before irradiation.

Fig. 31 Flux dependence of carrier concentration and conductivity for an oxygen- and an antimony-doped germanium sample irradiated simultaneously by $\approx$45 Mev electrons at $\approx$82°K.

Fig. 32 Temperature dependence of carrier concentration of oxygen-doped germanium before and after irradiation and annealing for 20 minutes at the temperatures indicated on the figure.

Fig. 33 Temperature dependence of carrier concentration of antimony-doped germanium before and after irradiation and annealing for 20 minutes at the temperatures indicated on the figure.

Fig. 34 Temperature dependence of the conductivity of antimony-doped germanium before and after irradiation and annealing for 20 minutes at each of the temperatures indicated on the figure.

Fig. 35 The percent of carrier concentration damage remaining as a function of annealing temperature (20 minute pulses) for irradiated oxygen- and antimony-doped germanium. Note: for the antimony-doped sample isochronal a curve is given for all defects and the 0.2 eV level separately.

Fig. 36 Annealing of conductivity of irradiated antimony-doped germanium. In each case the conductivity values shown were measured at 83.5°K after 20 minute anneals at temperatures given in the figure.

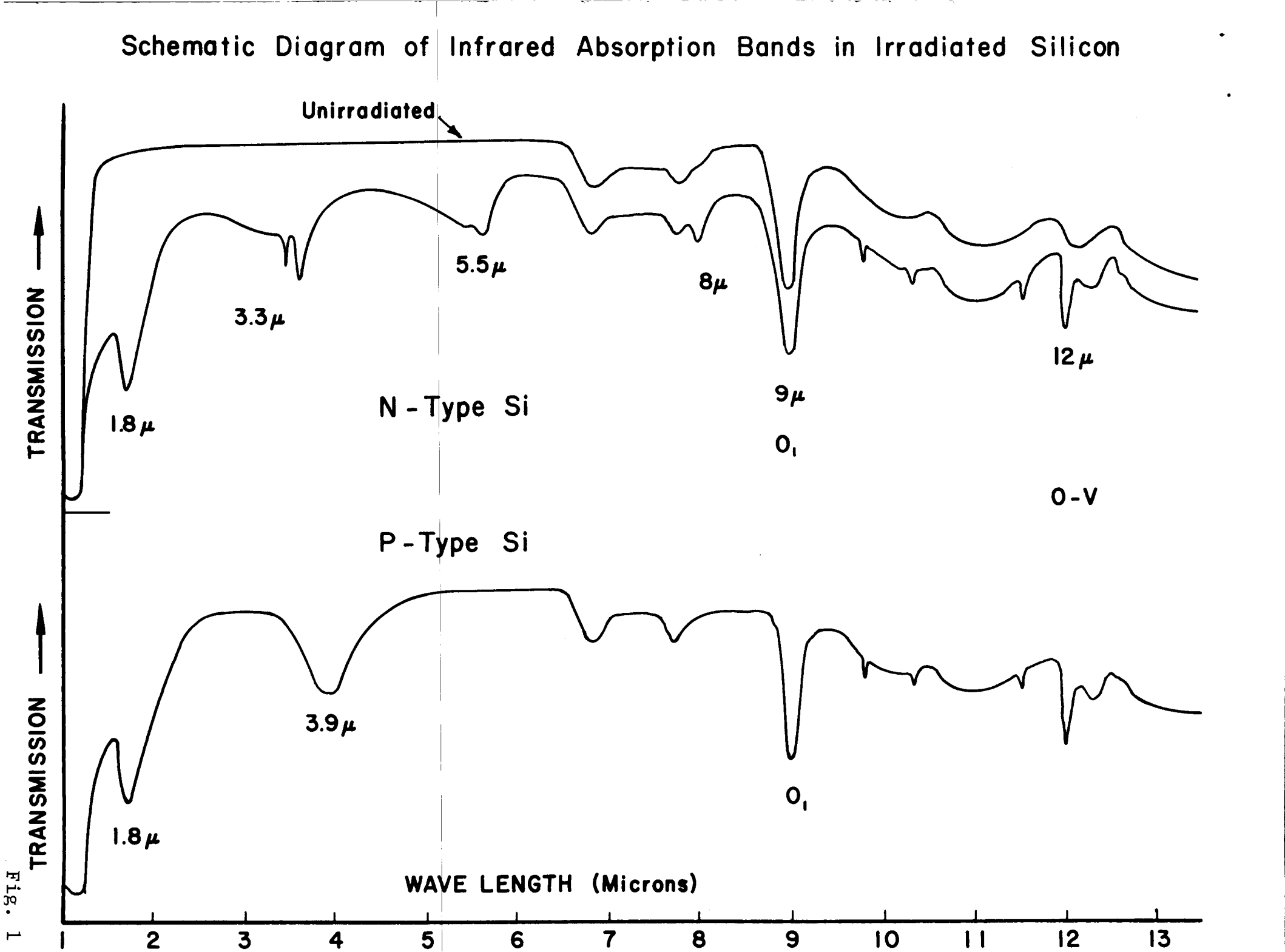
Schematic Diagram of Infrared Absorption Bands in Irradiated Silicon
Unirradiated
TRANSMISSION
1.8μ
3.3μ
5.5μ
8μ
9μ
12μ
N - Type Si
O1
O - V
P - Type Si
TRANSMISSION
1.8μ
3.9μ
O1
WAVE LENGTH (Microns)
1
2
3
4
5
6
7
8
9
10
11
12
13

Fig. 1

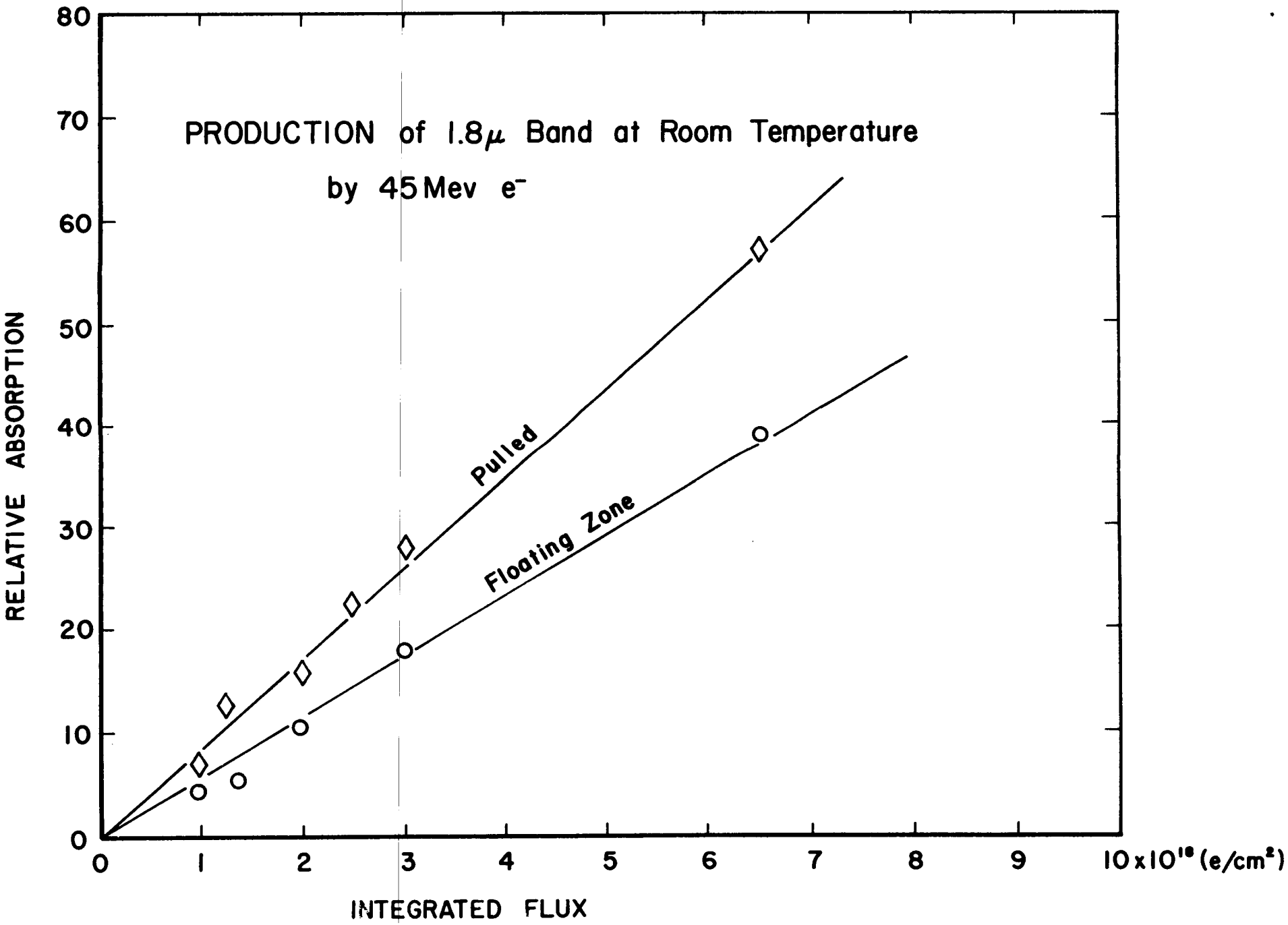
PRODUCTION of 1.8μ Band at Room Temperature
by 45 Mev e⁻
RELATIVE ABSORPTION
INTEGRATED FLUX
Pulled
Floating Zone
0
10
20
30
40
50
60
70
80
1
2
3
4
5
6
7
8
9
10 x 10¹⁸ (e/cm²)

Fig. 2

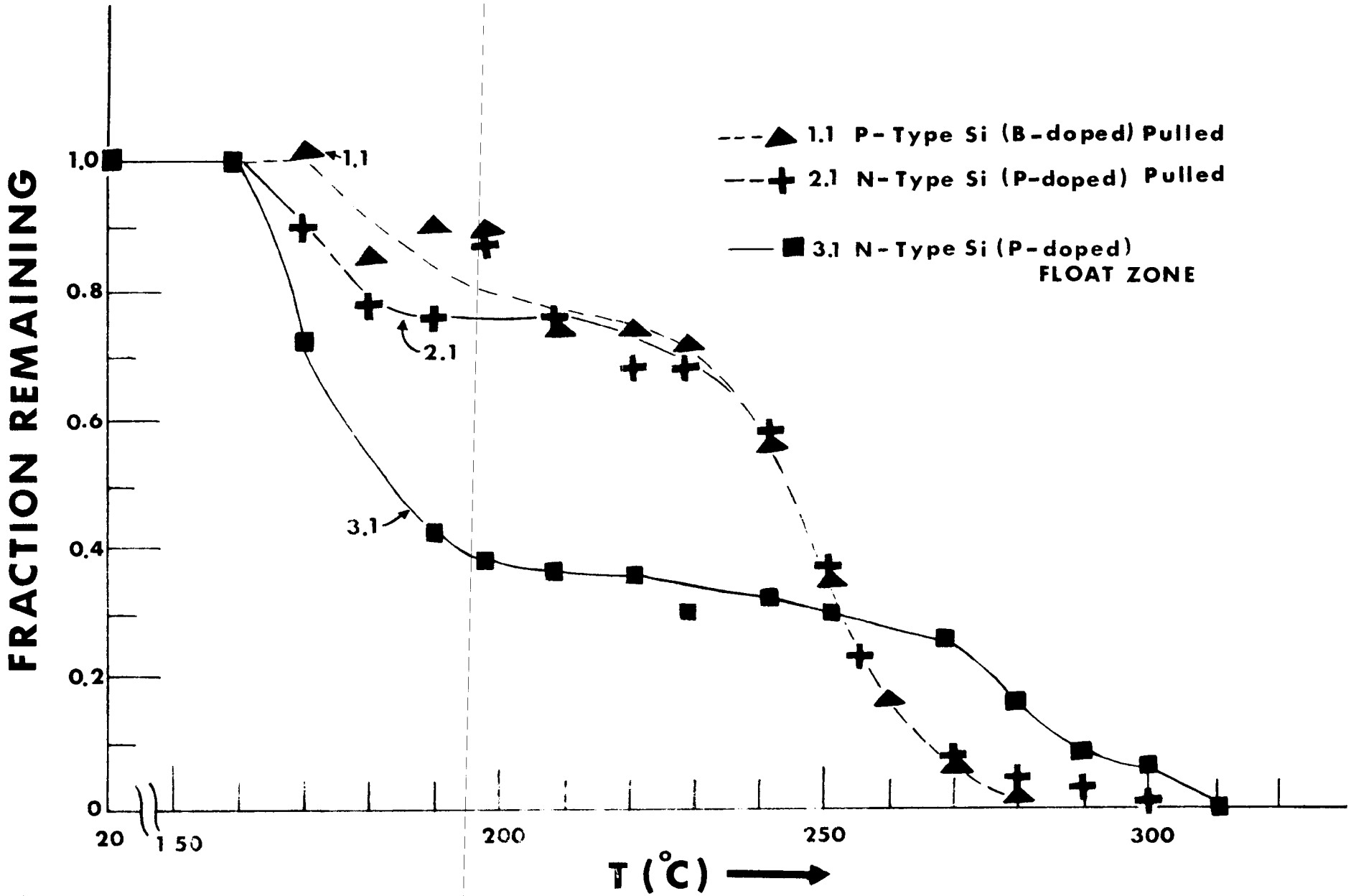
1.1 P-Type Si (B-doped) Pulled
2.1 N-Type Si (P-doped) Pulled
3.1 N-Type Si (P-doped) FLOAT ZONE
FRACTION REMAINING
1.0
0.8
0.6
0.4
0.2
0
1.1
2.1
3.1
20
150
200
250
300
T (°C)

Fig. 3

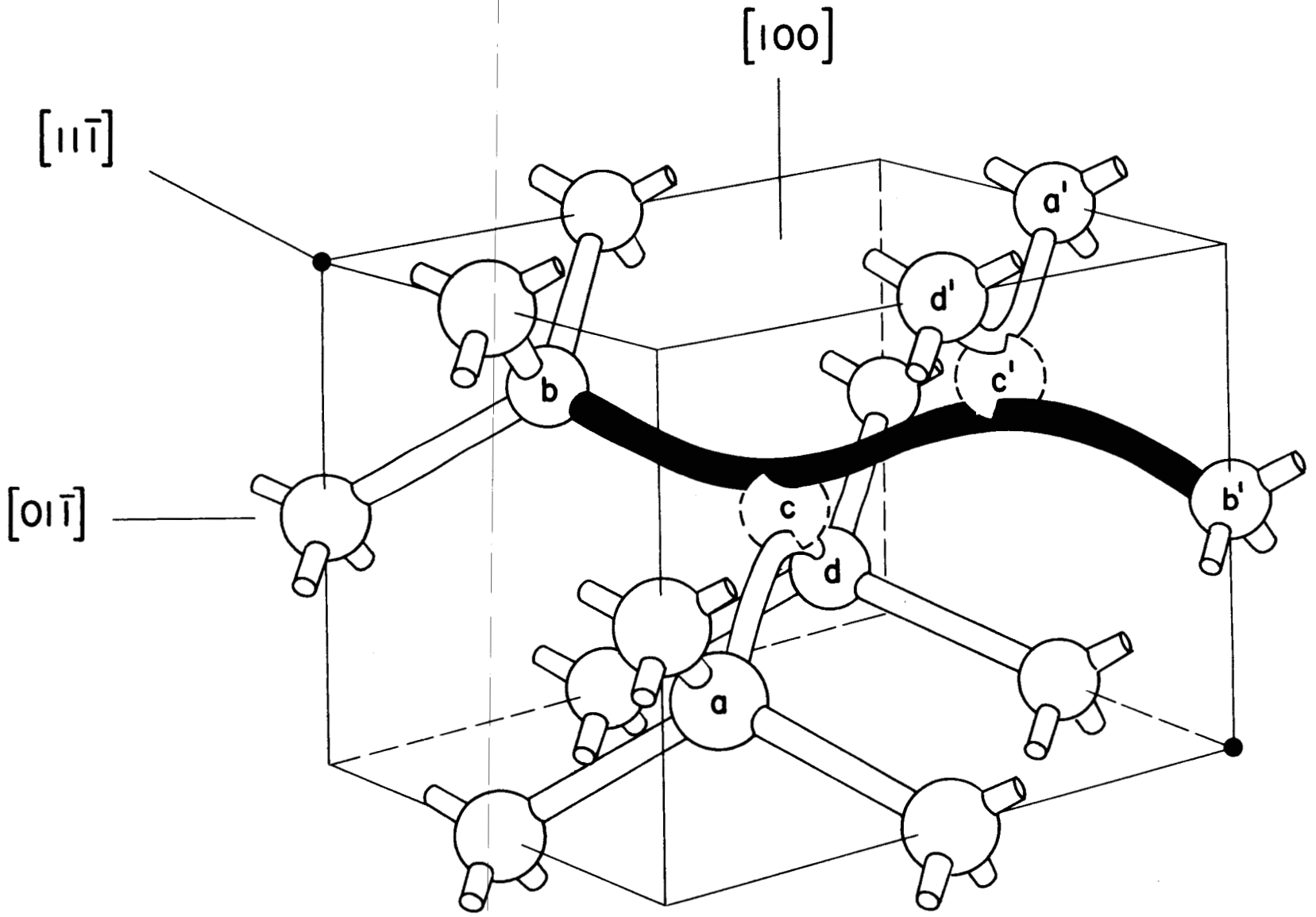

Fig. 4

A Model of Divacancy

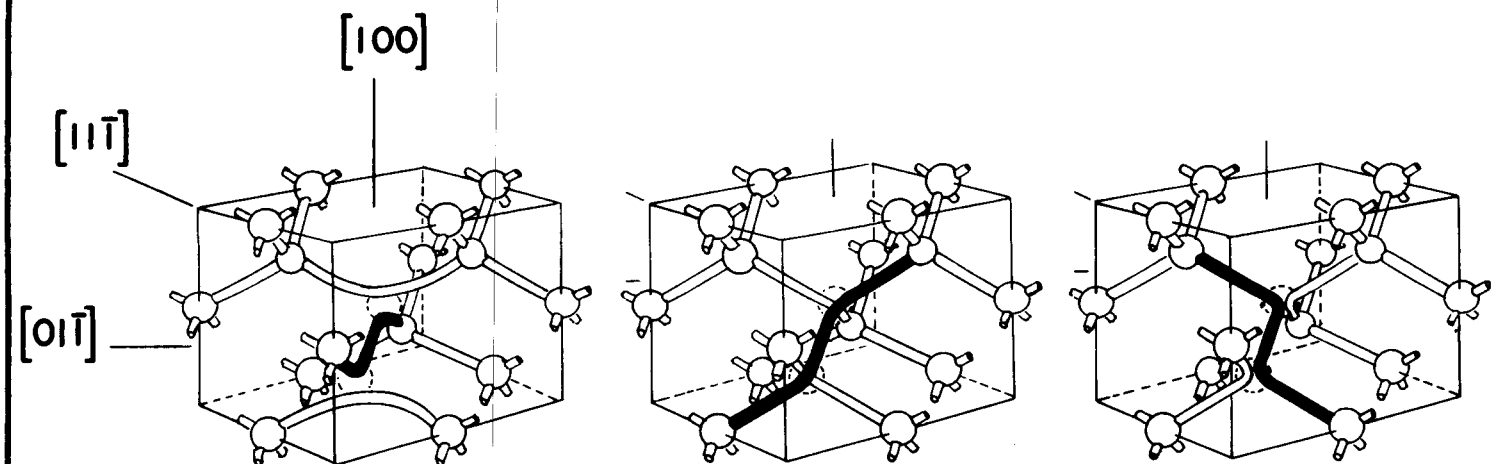

Three Equivalent Electronic Distributions
of a Divacancy

Fig. 5

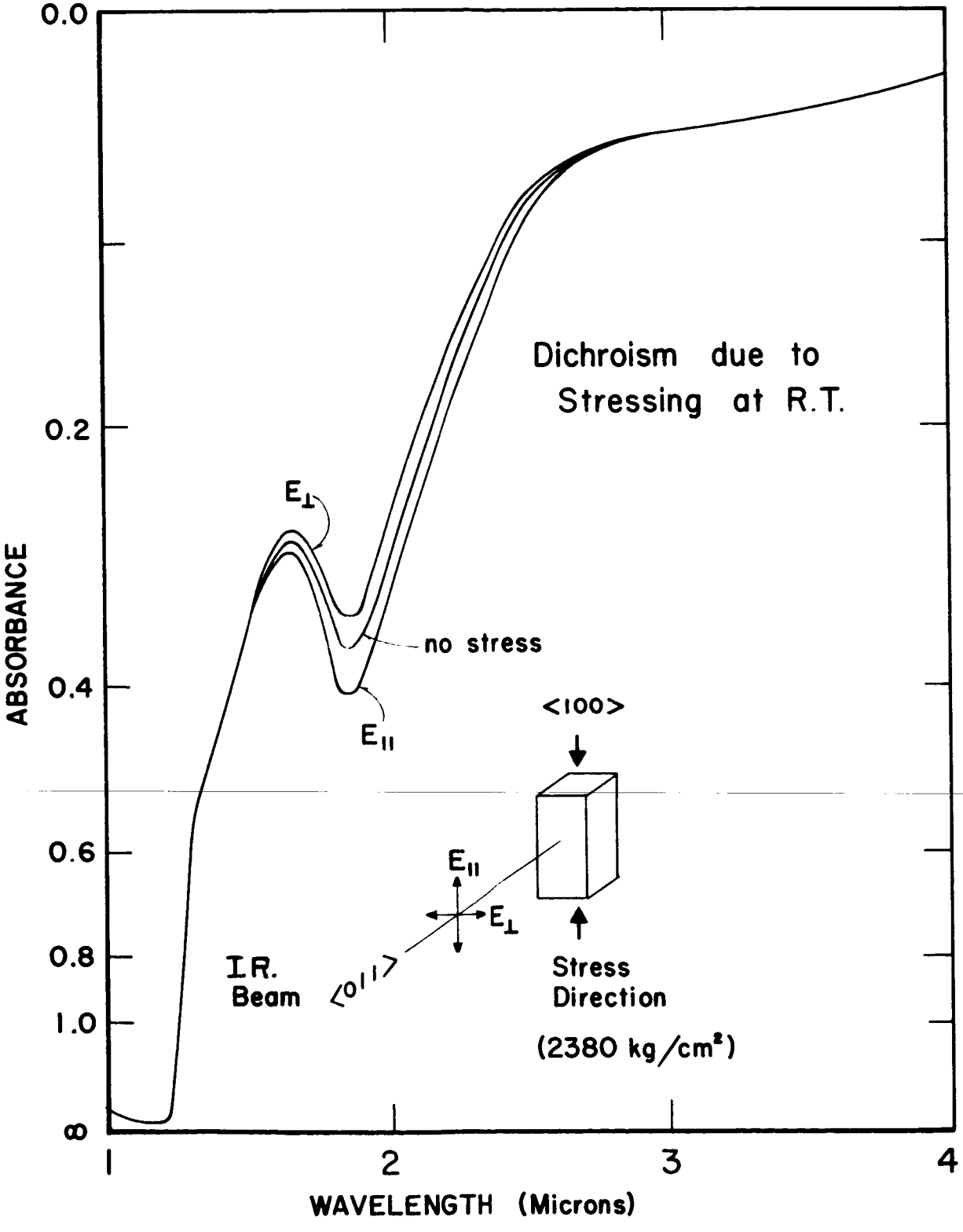
0.0
0.2
0.4
0.6
0.8
1.0
∞
ABSORBANCE
1
2
3
4
WAVELENGTH (Microns)
Dichroism due to
Stressing at R.T.
E⊥
no stress
E||
<100>
E||
E⊥
IR.
Beam
<011>
Stress
Direction
(2380 kg/cm²)

Fig. 6

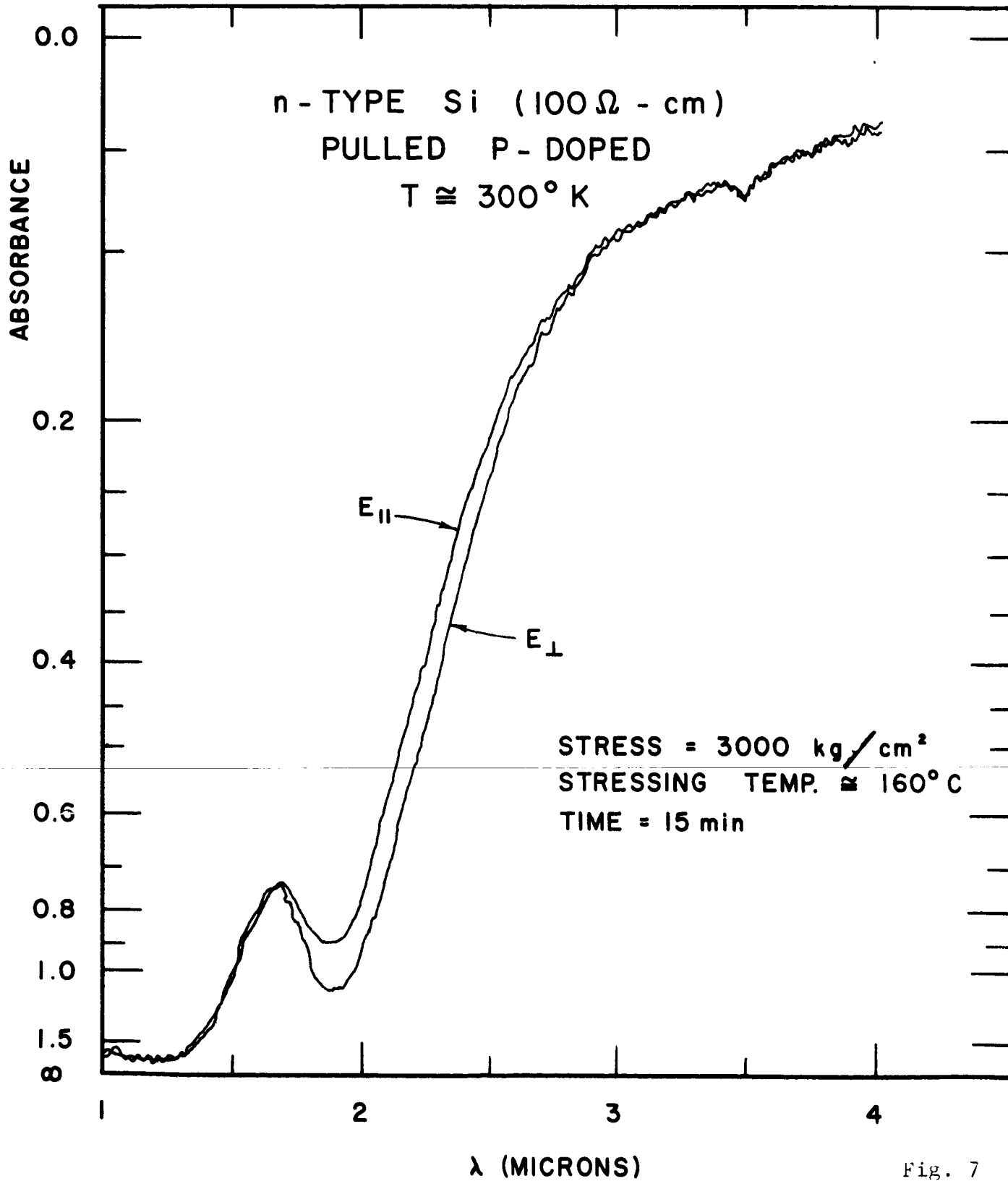
n - TYPE Si (100 Ω - cm)
PULLED P - DOPED
T ≅ 300° K
E||
E⊥
STRESS = 3000 kg/cm²
STRESSING TEMP. ≅ 160° C
TIME = 15 min
ABSORBANCE
0.0
0.2
0.4
0.6
0.8
1.0
1.5
8
1
2
3
4
λ (MICRONS)

Fig. 7

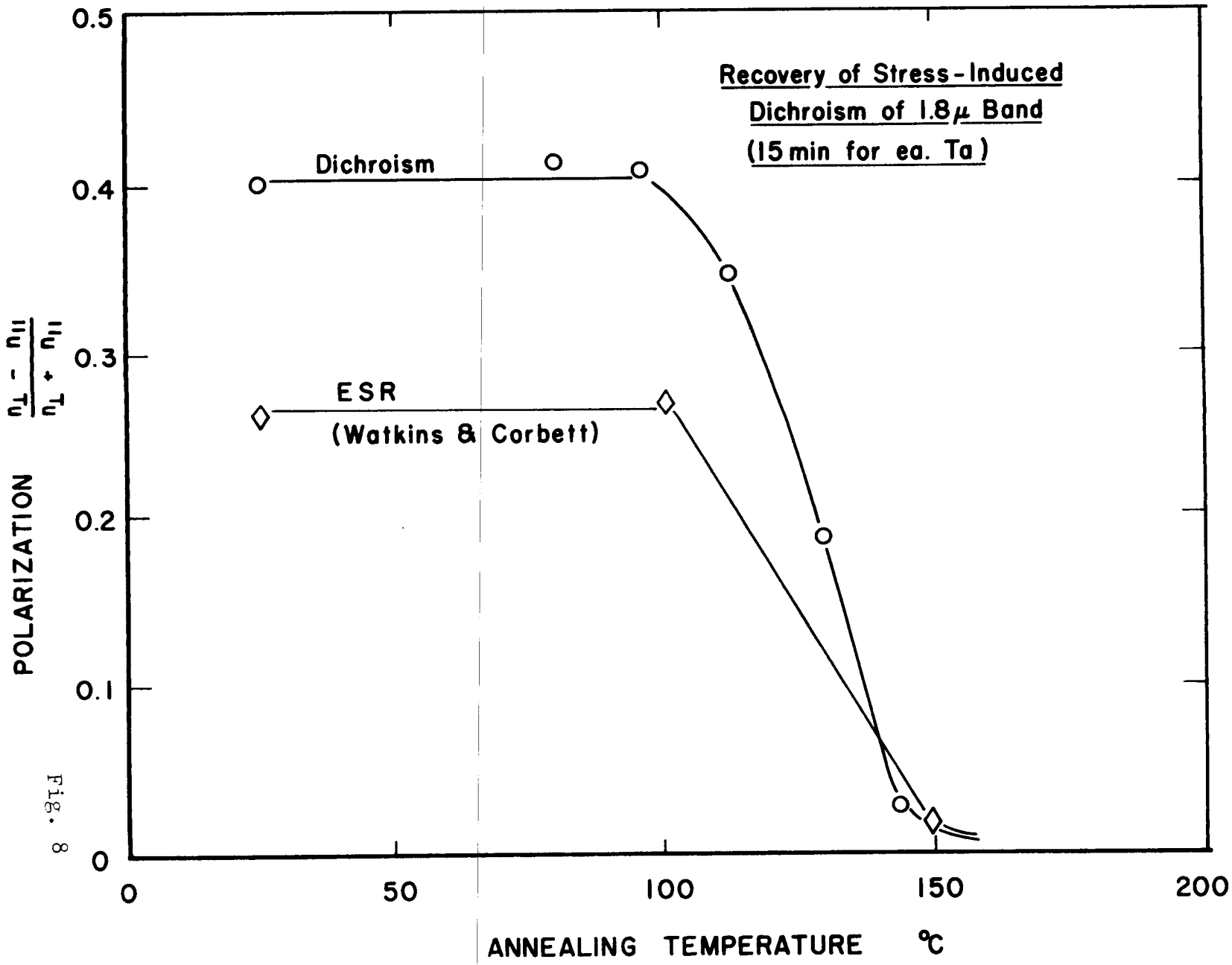
Recovery of Stress-Induced
Dichroism of 1.8μ Band
(15 min for ea. Ta)
Dichroism
ESR
(Watkins & Corbett)
POLARIZATION $\frac{n_\perp - n_{11}}{n_\perp + n_{11}}$
0.5
0.4
0.3
0.2
0.1
0
0
50
100
150
200
ANNEALING TEMPERATURE °C

Fig. 8

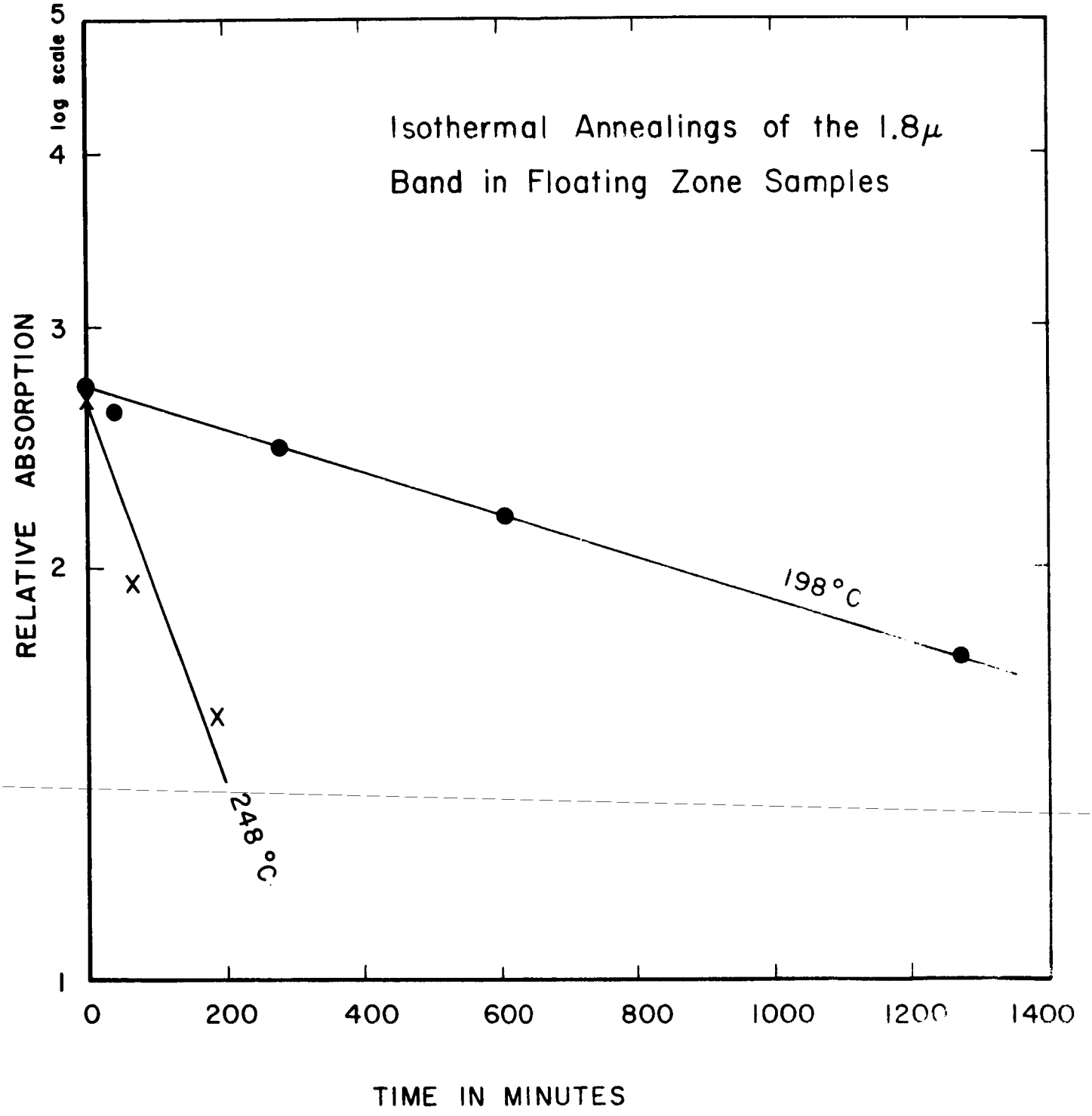
Isothermal Annealings of the 1.8μ
Band in Floating Zone Samples
RELATIVE ABSORPTION
4 log scale
5
4
3
2
1
198°C
248°C
X
X
0
200
400
600
800
1000
1200
1400
TIME IN MINUTES

Fig. 9

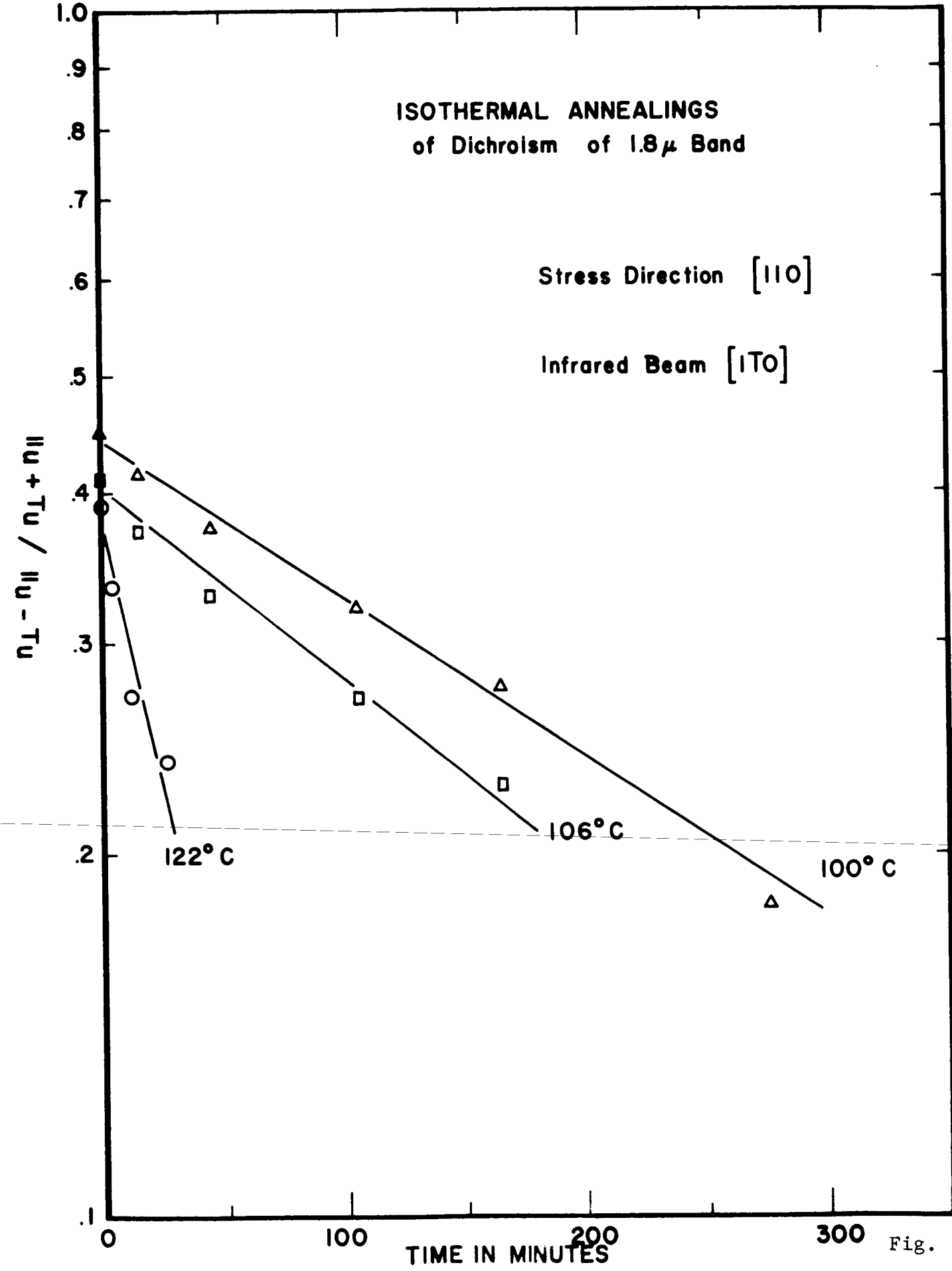
ISOTHERMAL ANNEALINGS
of Dichroism of 1.8μ Band
Stress Direction [110]
Infrared Beam [1T0]
122° C
106° C
100° C
1.0
.9
.8
.7
.6
.5
.4
.3
.2
.1
0
100
200
300
TIME IN MINUTES
$\frac{\parallel u + T u}{\parallel u - T u}$

Fig. 10

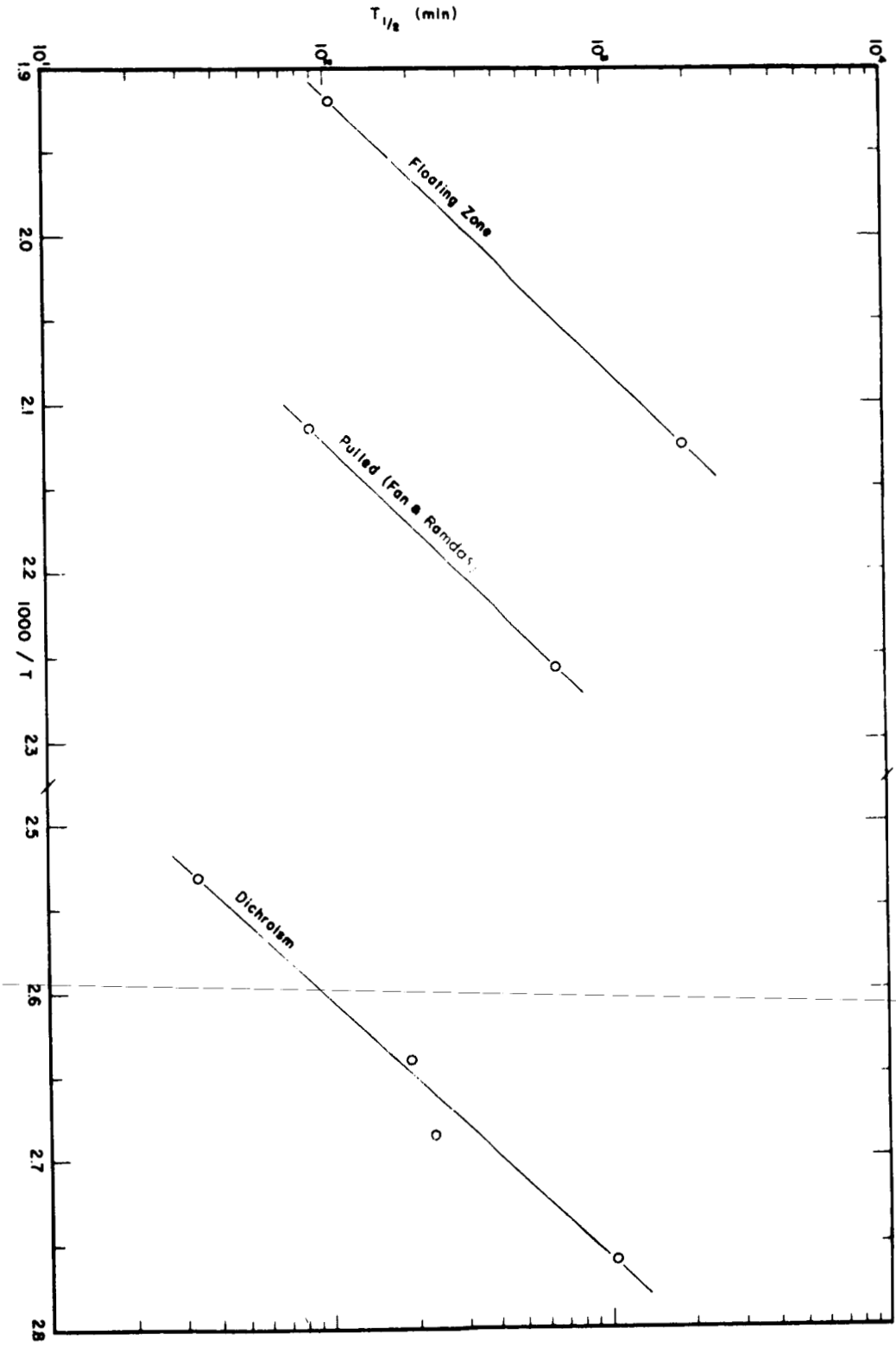
$T_{1/2}$ (min)
10^1
10^2
10^3
10^4
1.9
2.0
2.1
2.2
2.3
2.5
2.6
2.7
2.8
1000 / T
Floating Zone
Pulled (Fan & Ramdas)
Dichroism

Fig. 11

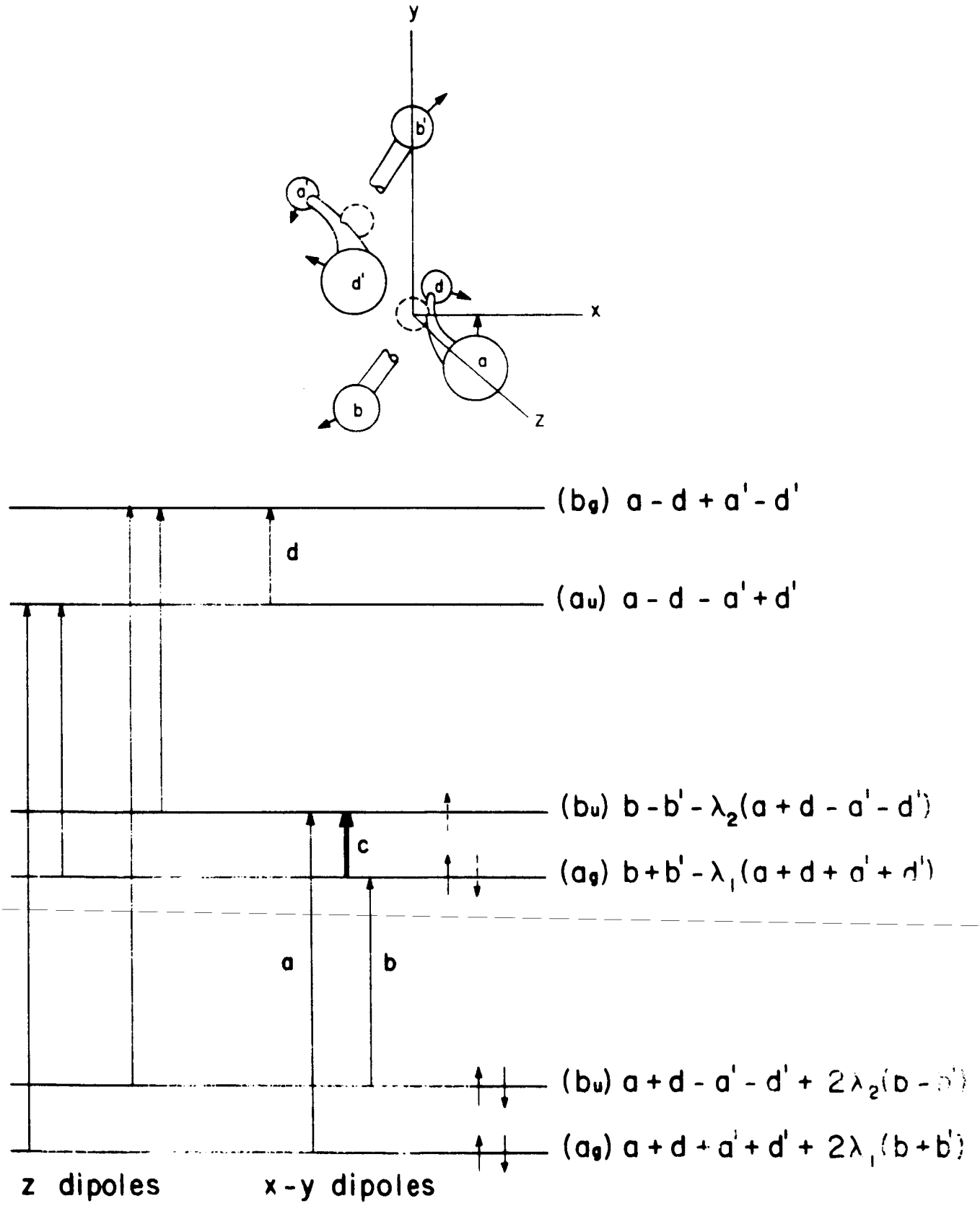
y
x
z
b'
a'
d'
d
a
b
(b_g) a - d + a' - d'
(a_u) a - d - a' + d'
(b_u) b - b' - λ_2(a + d - a' - d')
(a_g) b + b' - λ_1(a + d + a' + d')
(b_u) a + d - a' - d' + 2λ_2(b - b')
(a_g) a + d + a' + d' + 2λ_1(b + b')
d
c
a
b
z dipoles
x-y dipoles

Fig. 12

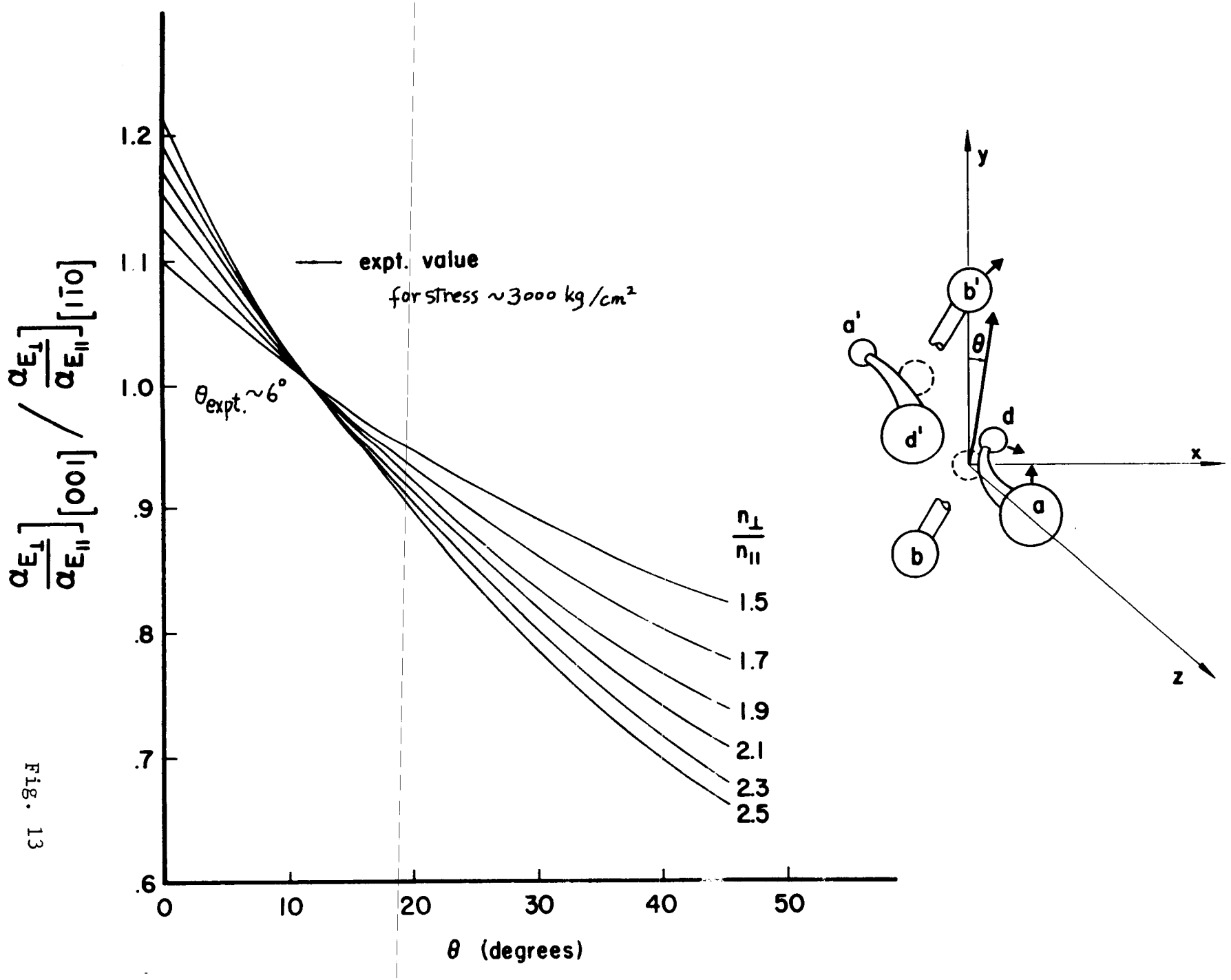
$\frac{\alpha_{E_\perp}}{\alpha_{E_{11}}}\Big]_{[001]} \Big/ \frac{\alpha_{E_\perp}}{\alpha_{E_{11}}}\Big]_{[1\bar{1}0]}$
1.2
1.1
1.0
.9
.8
.7
.6
0
10
20
30
40
50
θ (degrees)
expt. value
for stress ~3000 kg/cm²
$\theta_{expt.} \sim 6°$
$\frac{n_\perp}{n_{11}}$
1.5
1.7
1.9
2.1
2.3
2.5
y
x
z
θ
a
a'
b
b'
d
d'

Fig. 13

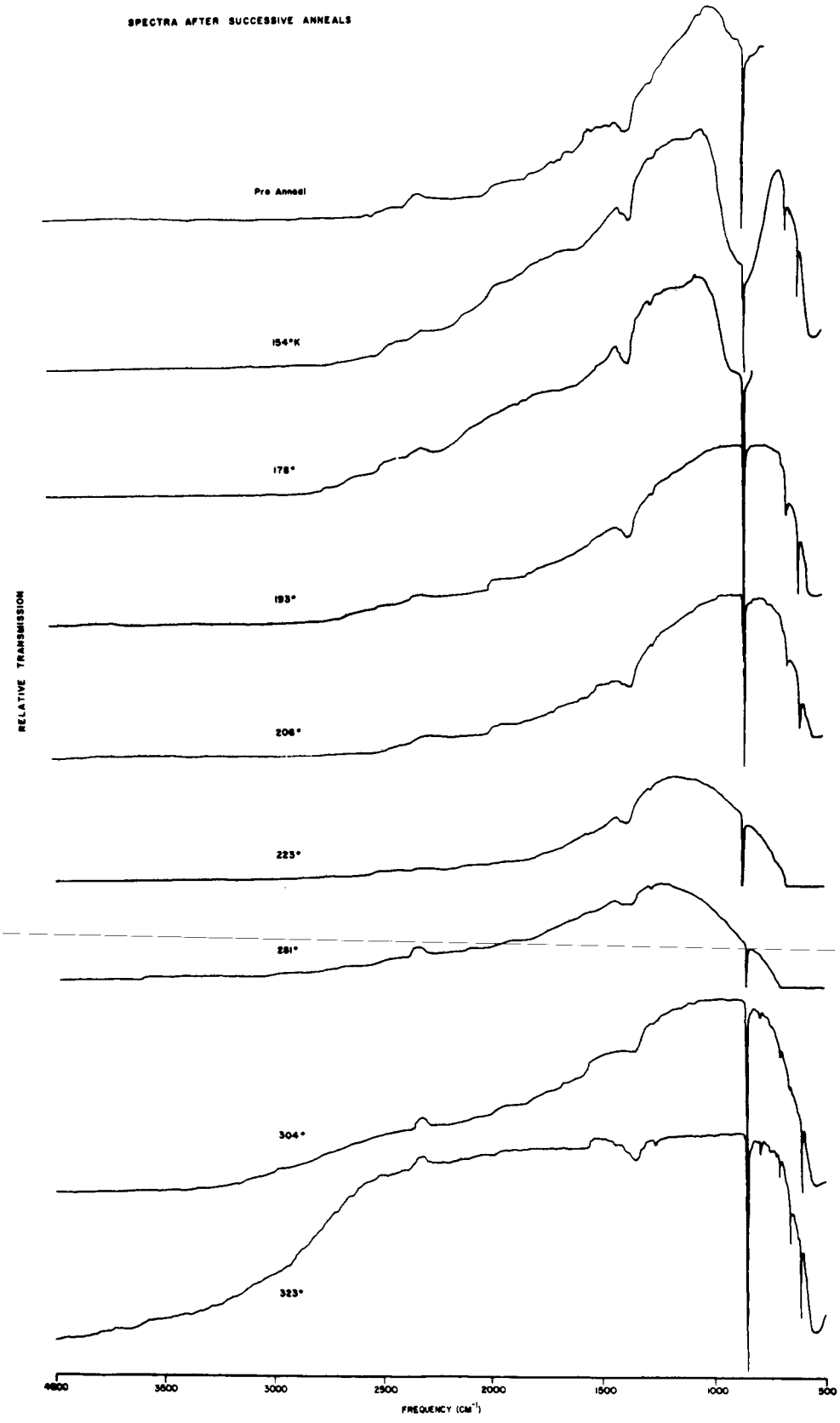
SPECTRA AFTER SUCCESSIVE ANNEALS
Pre Anneal
154°K
178°
193°
206°
223°
281°
304°
323°
RELATIVE TRANSMISSION
4000
3500
3000
2500
2000
1500
1000
500
FREQUENCY (CM⁻¹)

Fig. 14

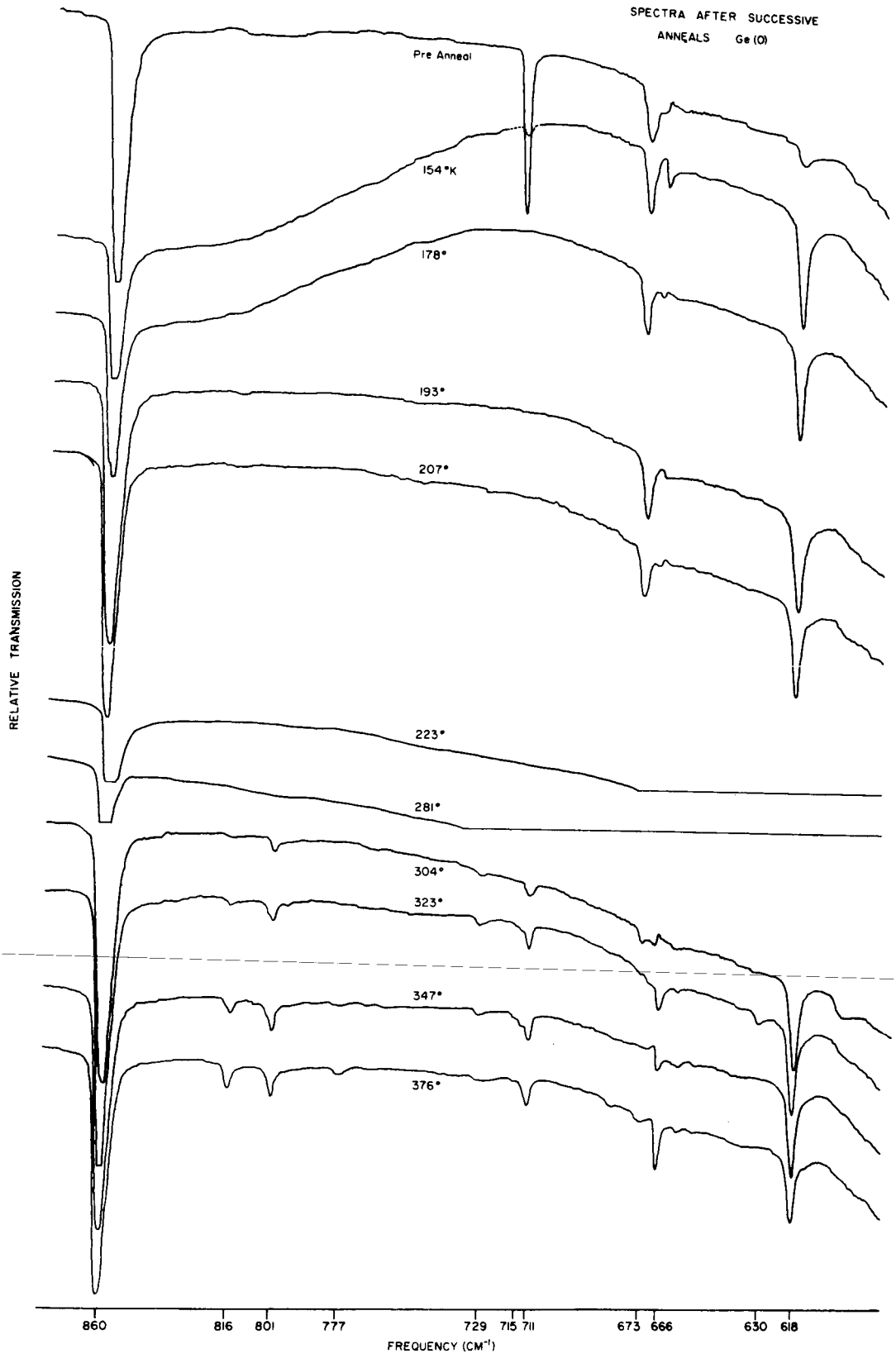
SPECTRA AFTER SUCCESSIVE
ANNEALS Ge (O)
Pre Anneal
154°K
178°
193°
207°
223°
281°
304°
323°
347°
376°
RELATIVE TRANSMISSION
860
816
801
777
729
715
711
673
666
630
618
FREQUENCY (CM⁻¹)

Fig. 15

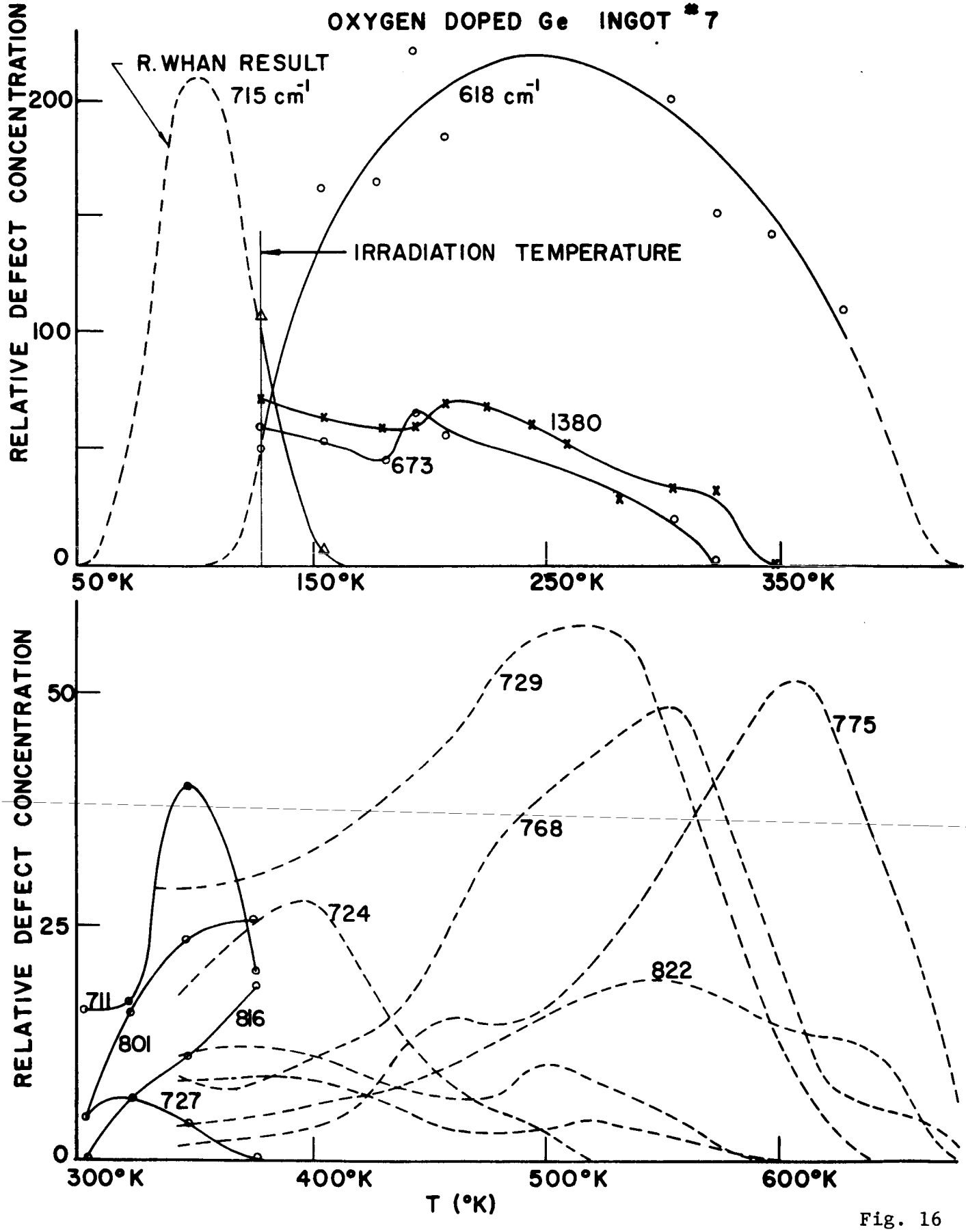
OXYGEN DOPED Ge INGOT #7
R. WHAN RESULT
715 cm⁻¹
618 cm⁻¹
IRRADIATION TEMPERATURE
1380
673
RELATIVE DEFECT CONCENTRATION
200
100
0
50°K
150°K
250°K
350°K
729
775
768
724
822
711
816
801
727
50
25
0
300°K
400°K
500°K
600°K
T (°K)

Fig. 16

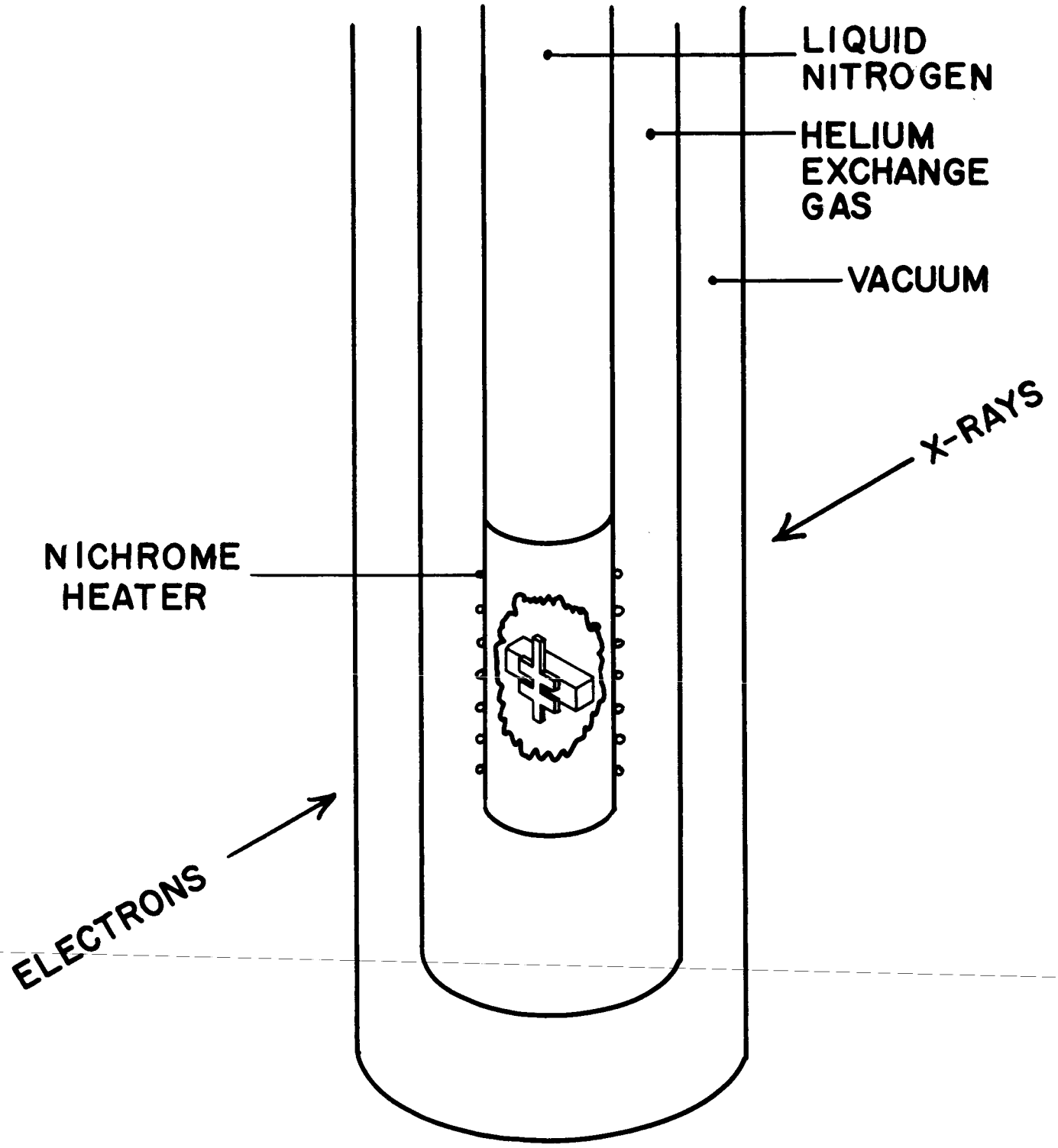
LIQUID
NITROGEN
HELIUM
EXCHANGE
GAS
VACUUM
X-RAYS
NICHROME
HEATER
ELECTRONS

Fig. 17

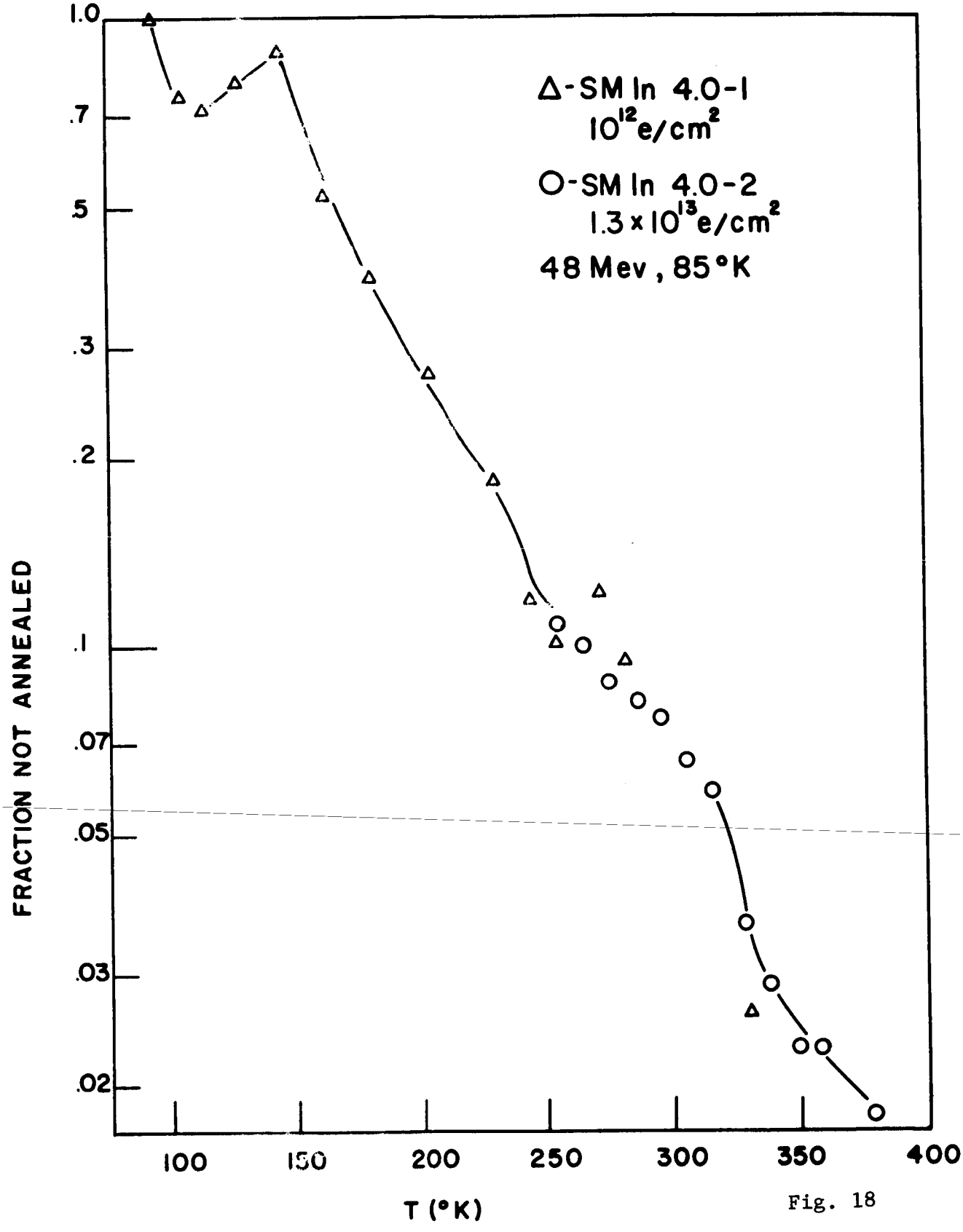
1.0
.7
.5
.3
.2
.1
.07
.05
.03
.02
FRACTION NOT ANNEALED
Δ-SM In 4.0-1
10^12 e/cm^2
O-SM In 4.0-2
1.3 x 10^13 e/cm^2
48 Mev, 85°K
100
150
200
250
300
350
400
T (°K)

Fig. 18

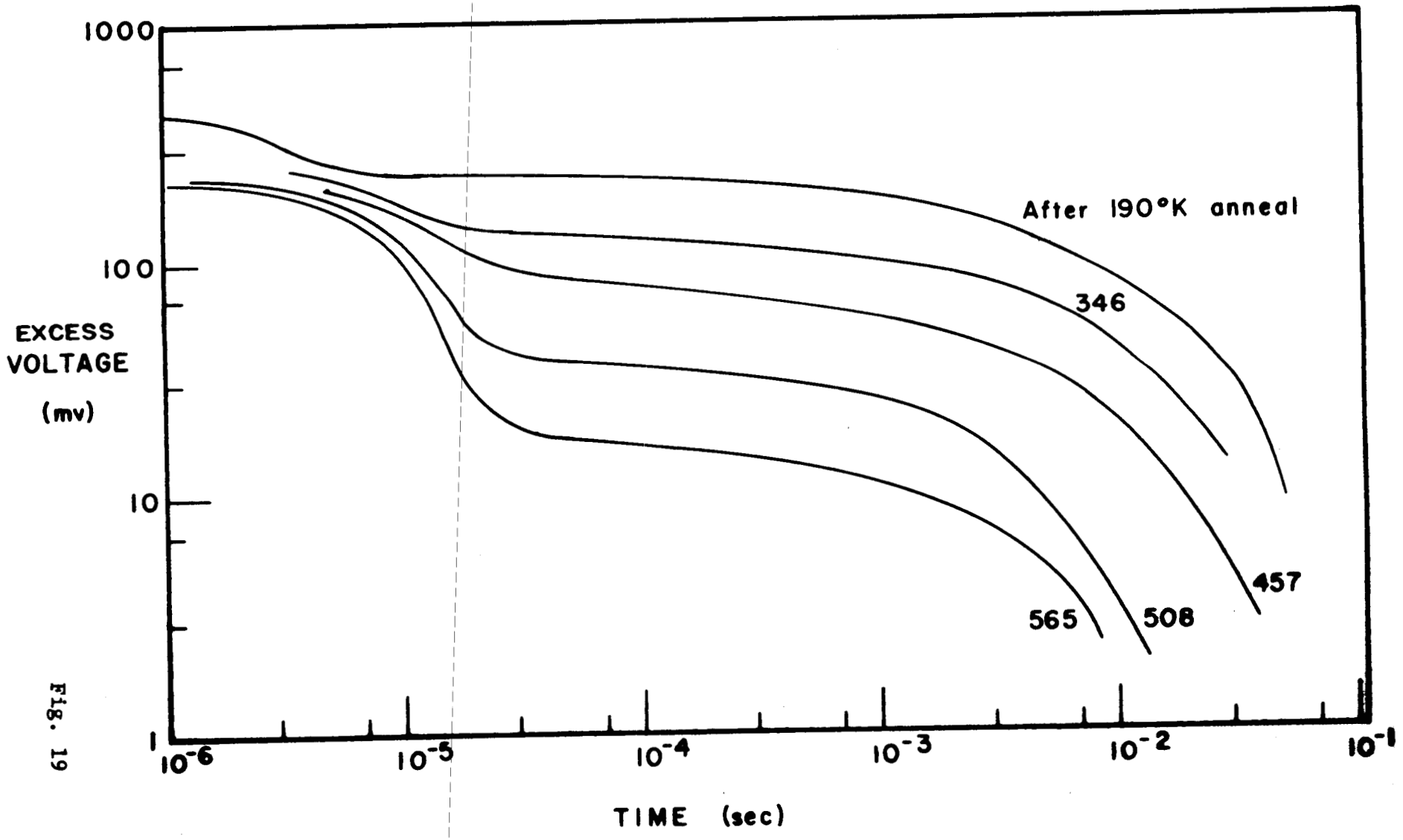
20 Ω-CM (As) Ge
1.3x 10^13 e/cm^2, 47 Mev
Tirr = 85°K
1000
100
10
1
EXCESS VOLTAGE (mv)
After 190°K anneal
346
457
508
565
10^-6
10^-5
10^-4
10^-3
10^-2
10^-1
TIME (sec)

Fig. 19

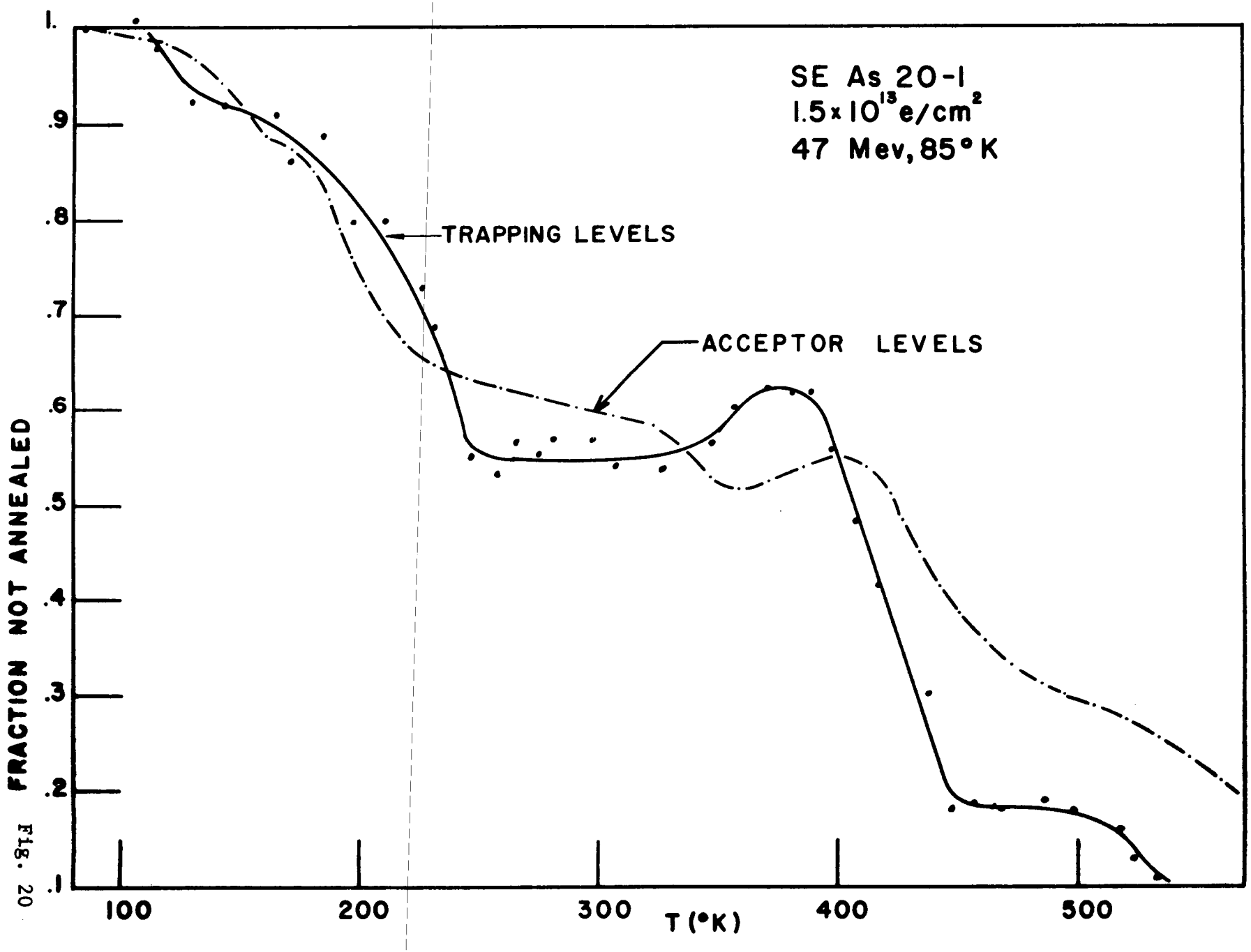
SE As 20-1
1.5 x 10^13 e/cm^2
47 Mev, 85° K
TRAPPING LEVELS
ACCEPTOR LEVELS
FRACTION NOT ANNEALED
1.
.9
.8
.7
.6
.5
.4
.3
.2
.1
100
200
300
400
500
T (°K)

Fig. 20

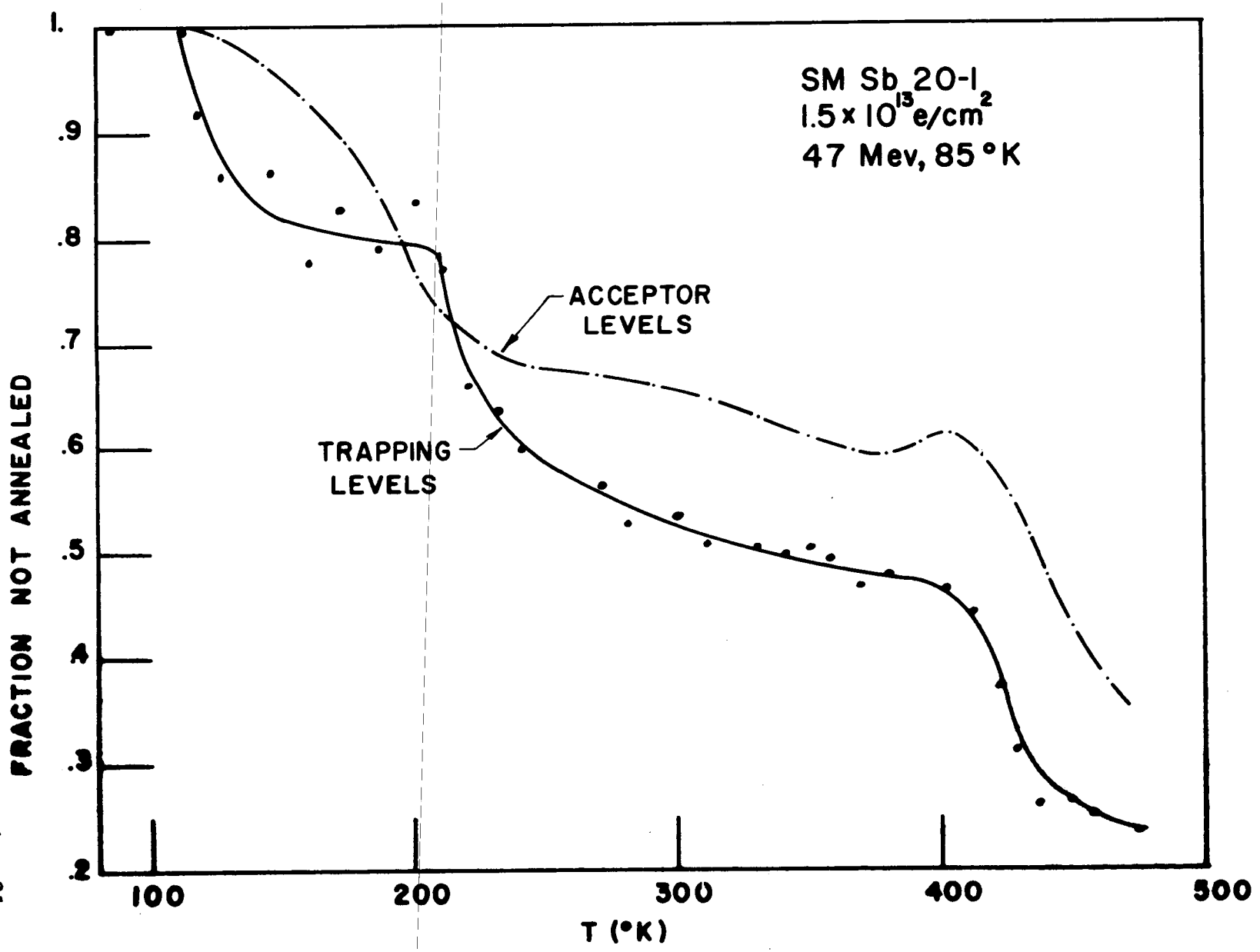
SM Sb 20-1
1.5 x 10^13 e/cm^2
47 Mev, 85 °K
ACCEPTOR LEVELS
TRAPPING LEVELS
FRACTION NOT ANNEALED
1.
.9
.8
.7
.6
.5
.4
.3
.2
100
200
300
400
500
T (°K)

Fig. 21

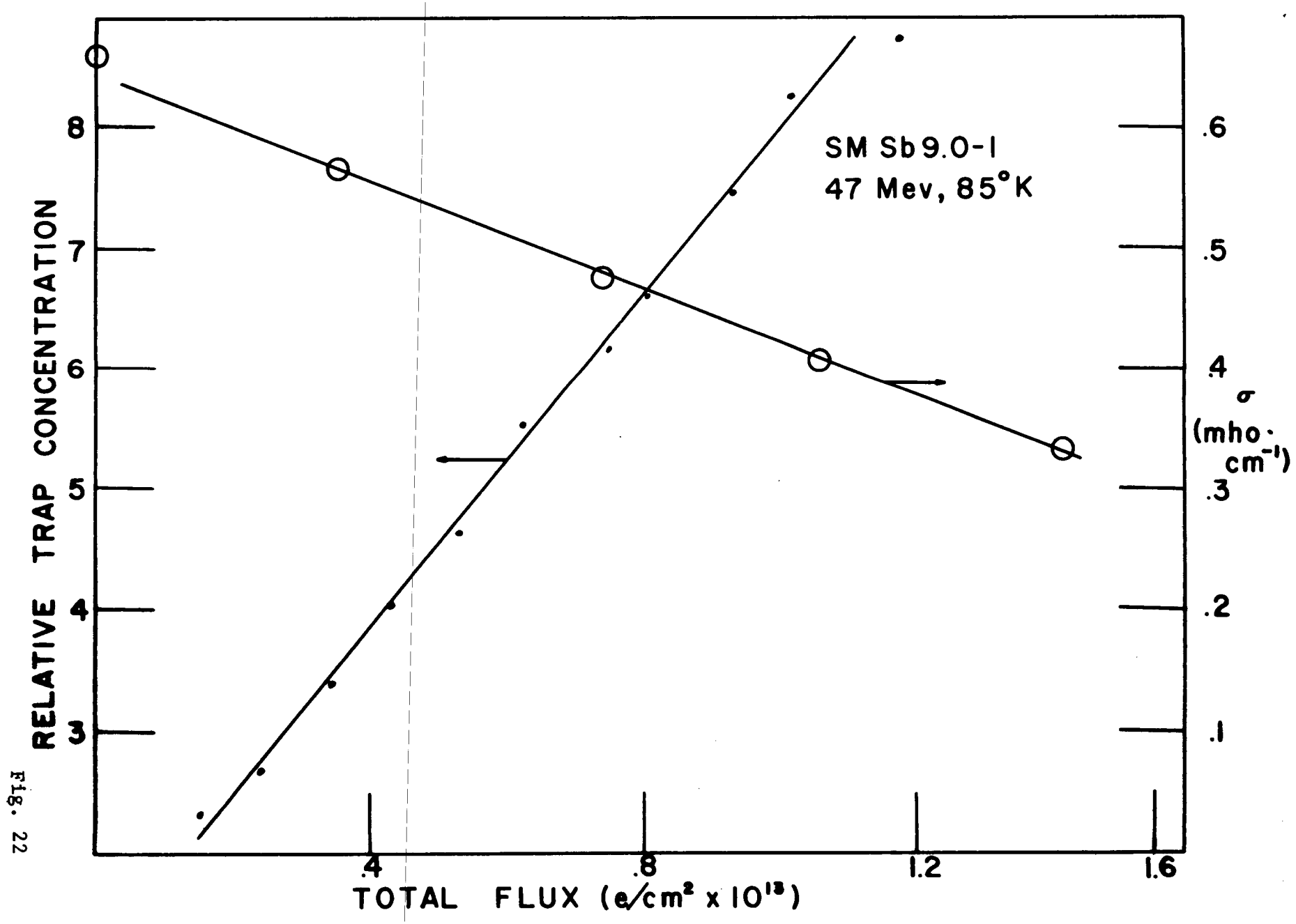
SM Sb 9.0-1
47 Mev, 85°K
RELATIVE TRAP CONCENTRATION
TOTAL FLUX (e/cm² x 10¹³)
σ (mho · cm⁻¹)
8
7
6
5
4
3
.4
.8
1.2
1.6
.6
.5
.4
.3
.2
.1

Fig. 22

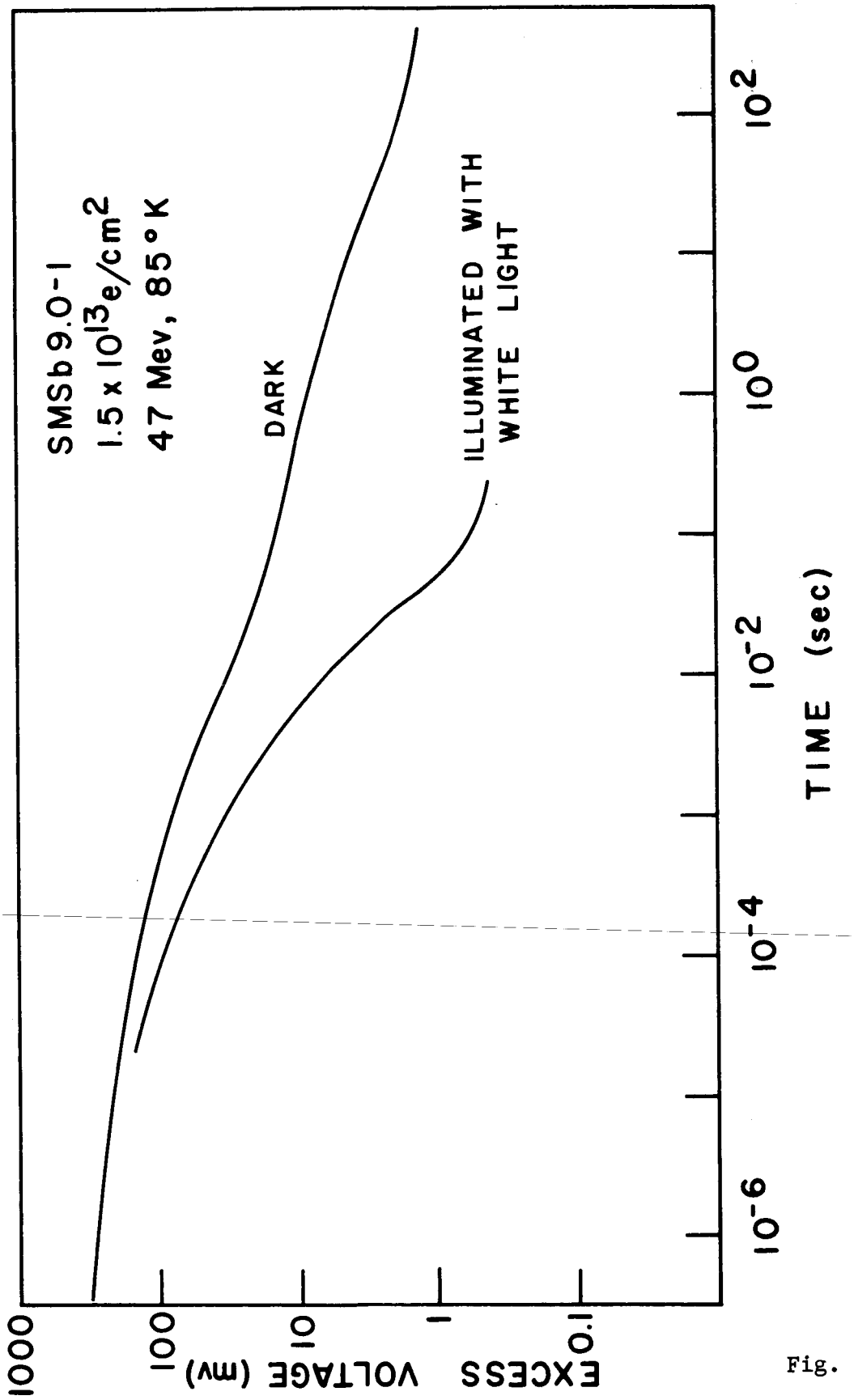
SMSb 9.0-1
1.5 x 10^13 e/cm^2
47 Mev, 85° K
DARK
ILLUMINATED WITH
WHITE LIGHT
EXCESS VOLTAGE (mv)
1000
100
10
1
0.1
10^-6
10^-4
10^-2
10^0
10^2
TIME (sec)

Fig. 23

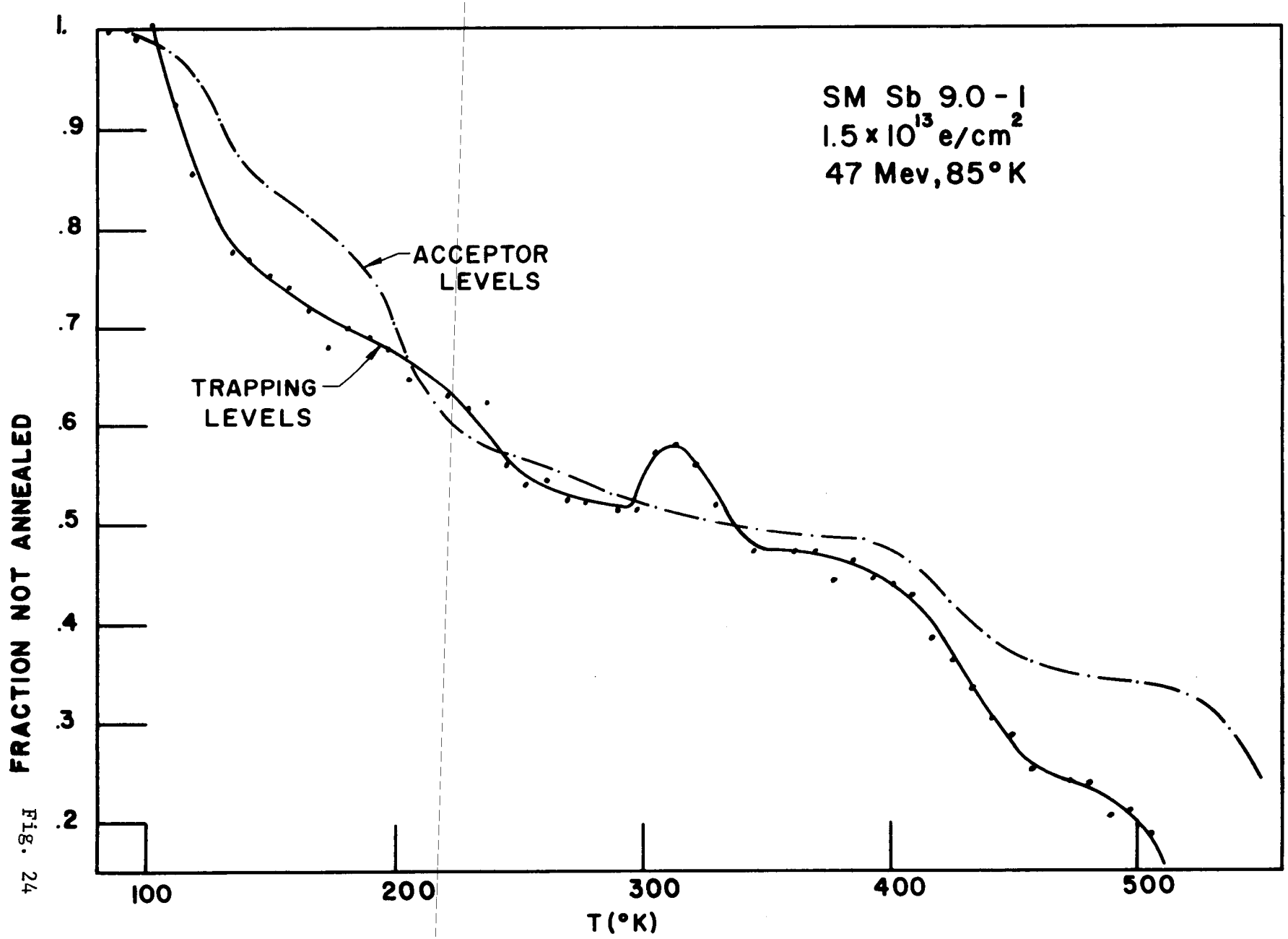
SM Sb 9.0 - 1
1.5 x 10^13 e/cm^2
47 Mev, 85° K
ACCEPTOR LEVELS
TRAPPING LEVELS
FRACTION NOT ANNEALED
1.
.9
.8
.7
.6
.5
.4
.3
.2
100
200
300
400
500
T (°K)

Fig. 24

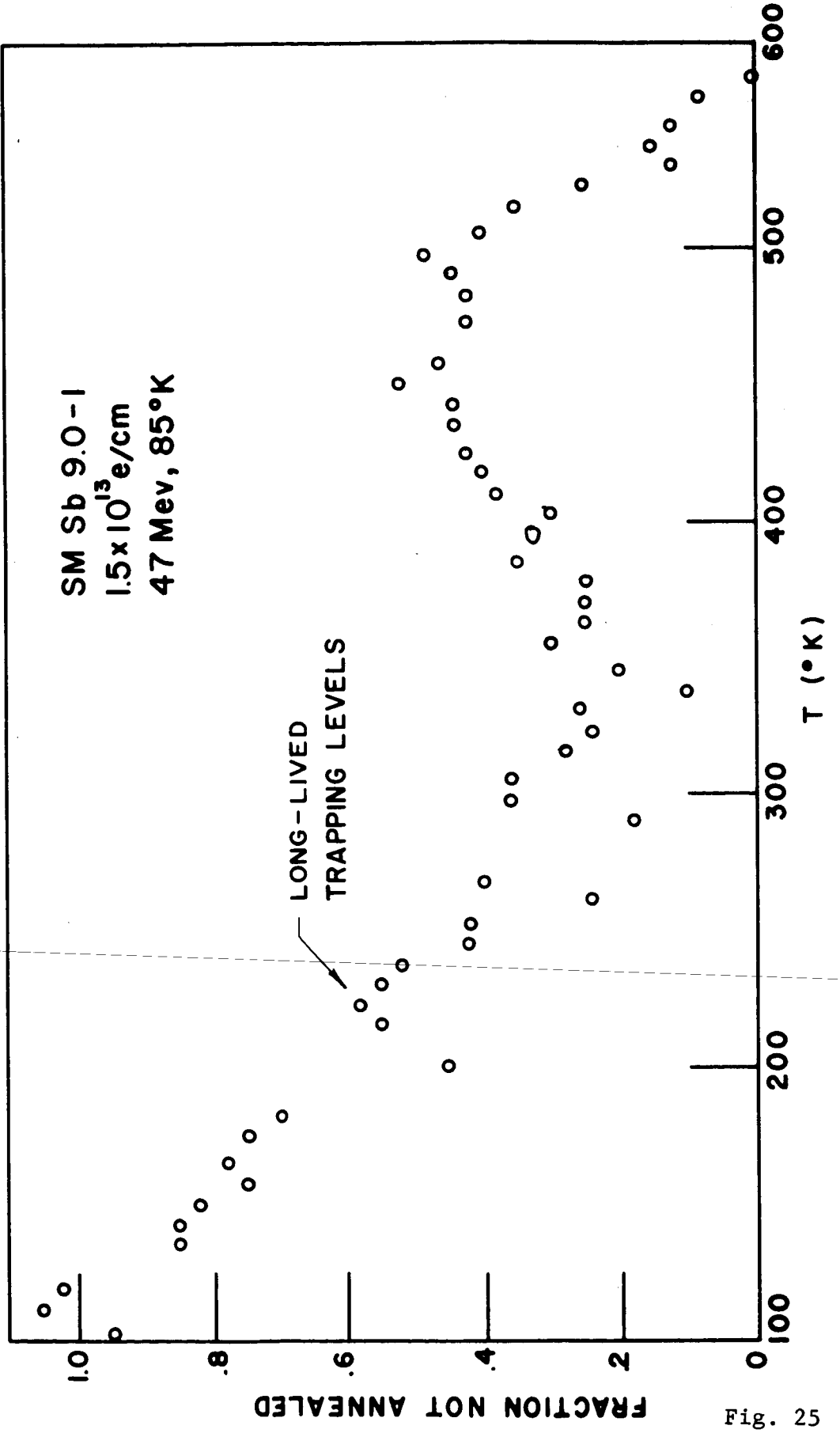
SM Sb 9.0-1
1.5x10^13 e/cm
47 Mev, 85°K
LONG-LIVED
TRAPPING LEVELS
FRACTION NOT ANNEALED
1.0
.8
.6
.4
.2
0
100
200
300
400
500
600
T (°K)

Fig. 25

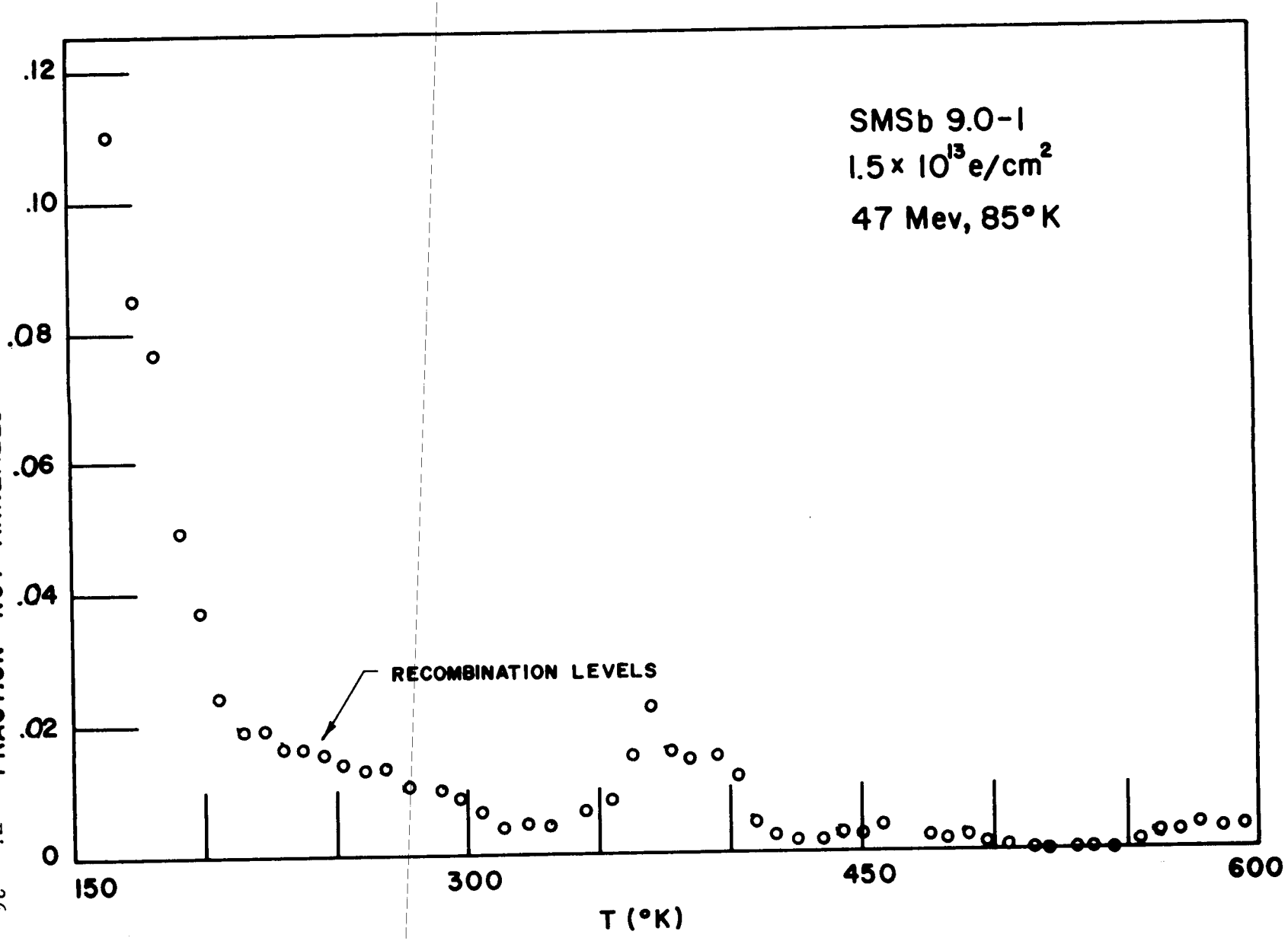
SMSb 9.0-1
1.5 x 10^13 e/cm^2
47 Mev, 85° K
RECOMBINATION LEVELS
FRACTION NOT ANNEALED
.12
.10
.08
.06
.04
.02
0
150
300
450
600
T (°K)

Fig. 26

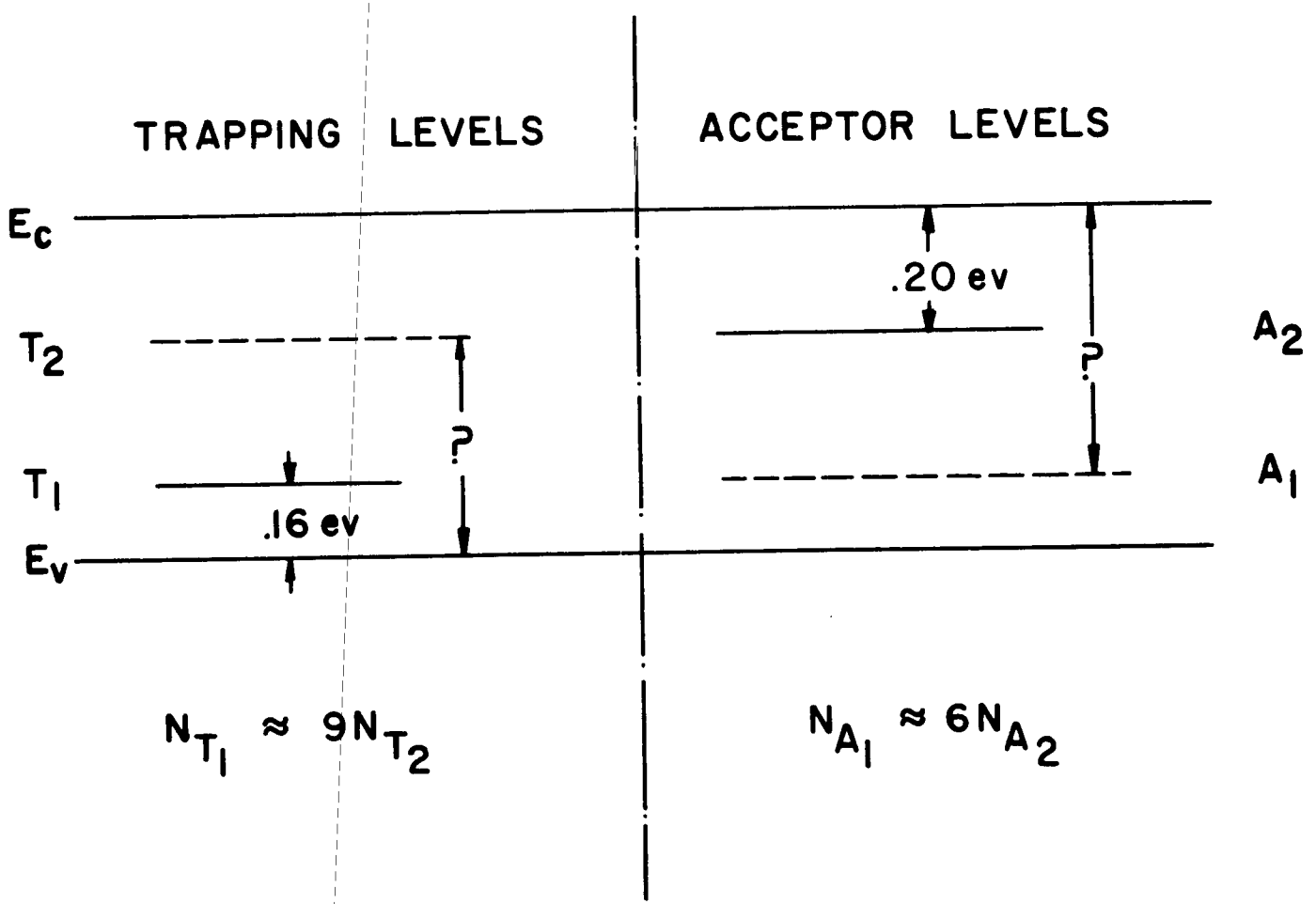
TRAPPING LEVELS
ACCEPTOR LEVELS
E_c
T_2
T_1
E_v
.16 ev
?
.20 ev
?
A_2
A_1
$N_{T_1} \approx 9N_{T_2}$
$N_{A_1} \approx 6N_{A_2}$

Fig. 27

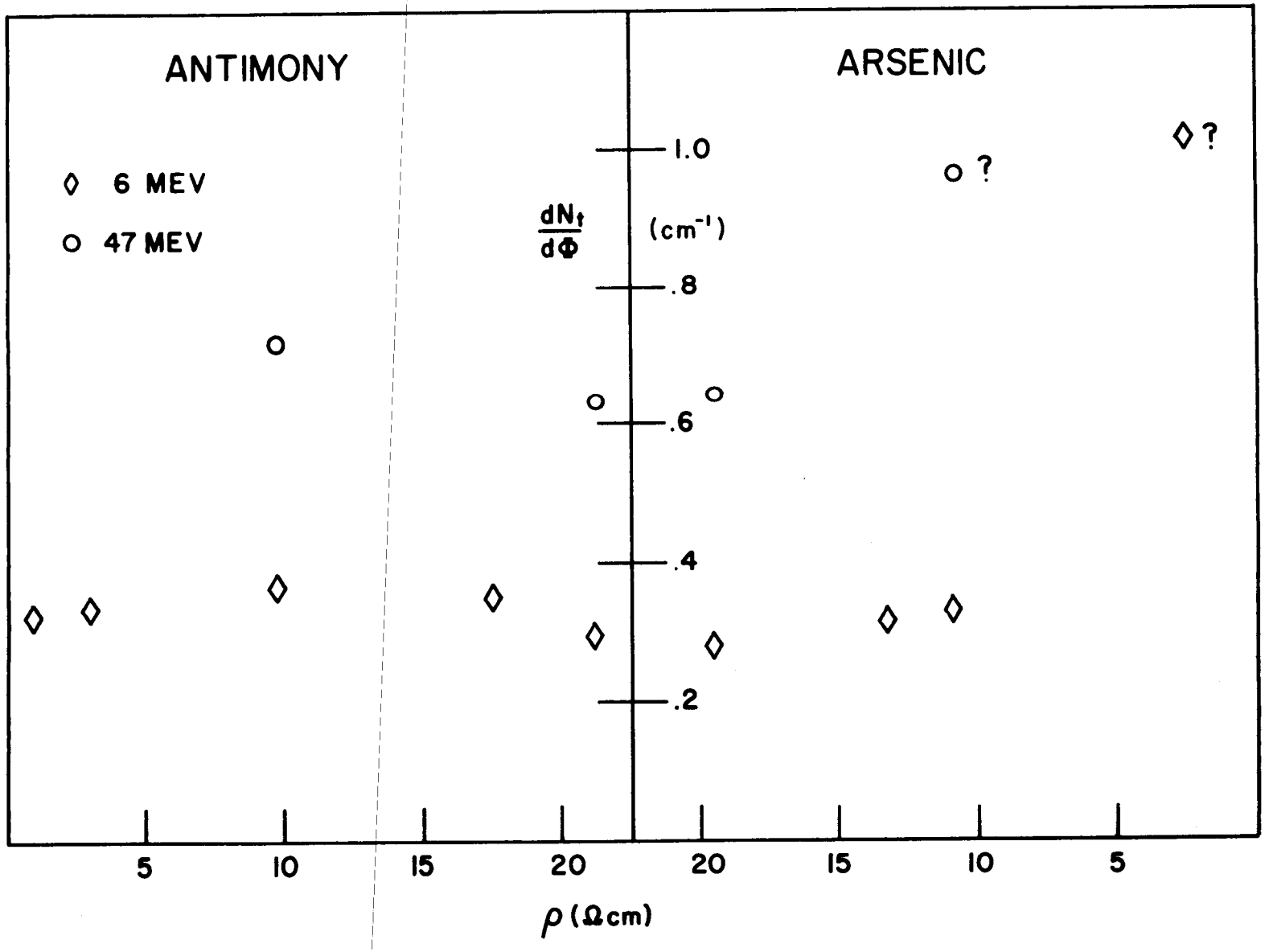
ANTIMONY
ARSENIC
◊ 6 MEV
○ 47 MEV
$\frac{dN_t}{d\Phi}$ (cm⁻¹)
1.0
.8
.6
.4
.2
○ ?
◊ ?
5
10
15
20
20
15
10
5
ρ (Ωcm)

Fig. 28

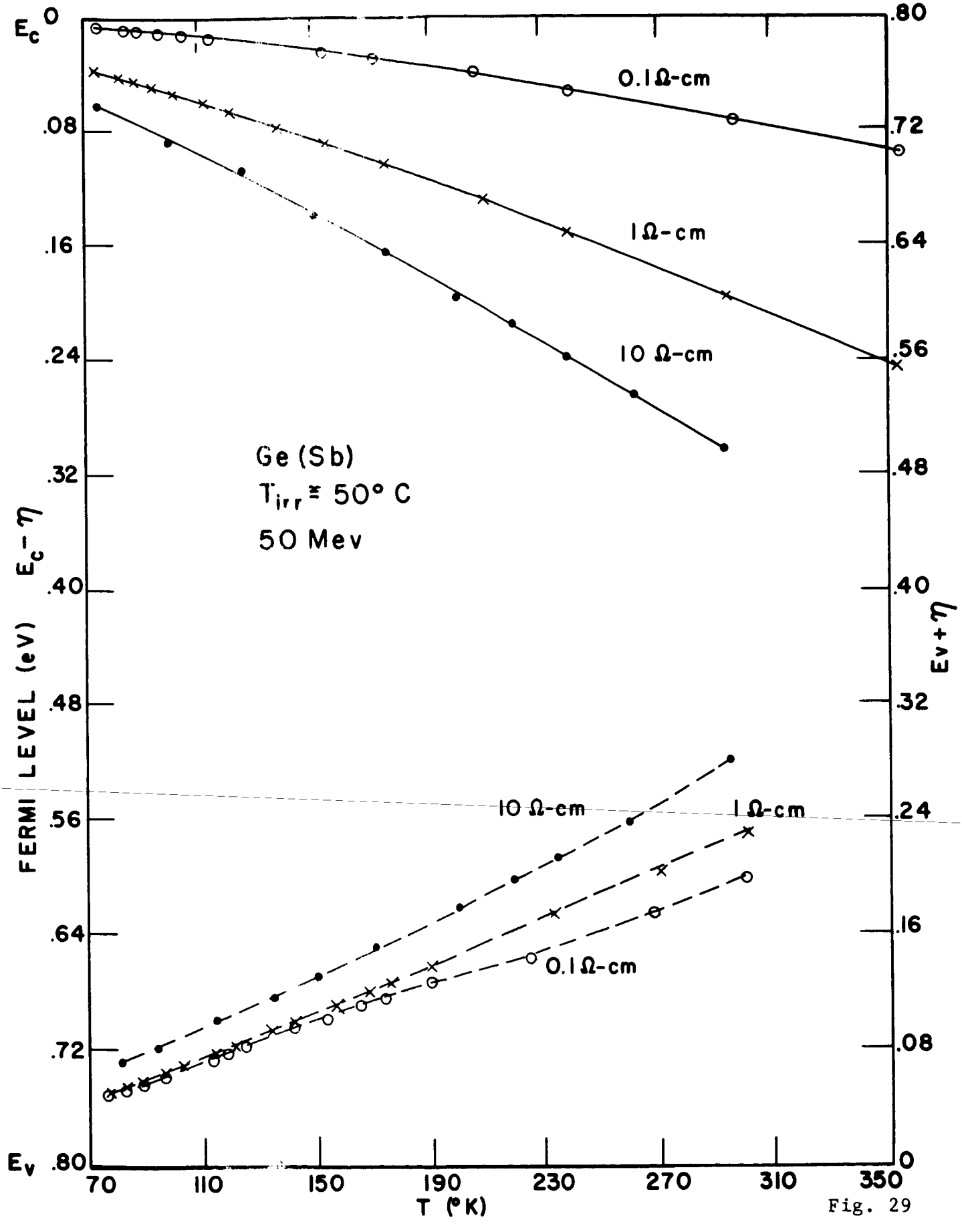
E_c 0
.08
.16
.24
.32
.40
.48
.56
.64
.72
E_v .80
.80
.72
.64
.56
.48
.40
.32
.24
.16
.08
0
0.1Ω-cm
1Ω-cm
10 Ω-cm
Ge (Sb)
T_{irr} ≅ 50° C
50 Mev
$E_c - \eta$
FERMI LEVEL (eV)
$E_v + \eta$
10 Ω-cm
1Ω-cm
0.1Ω-cm
70
110
150
190
230
270
310
350
T (°K)

Fig. 29

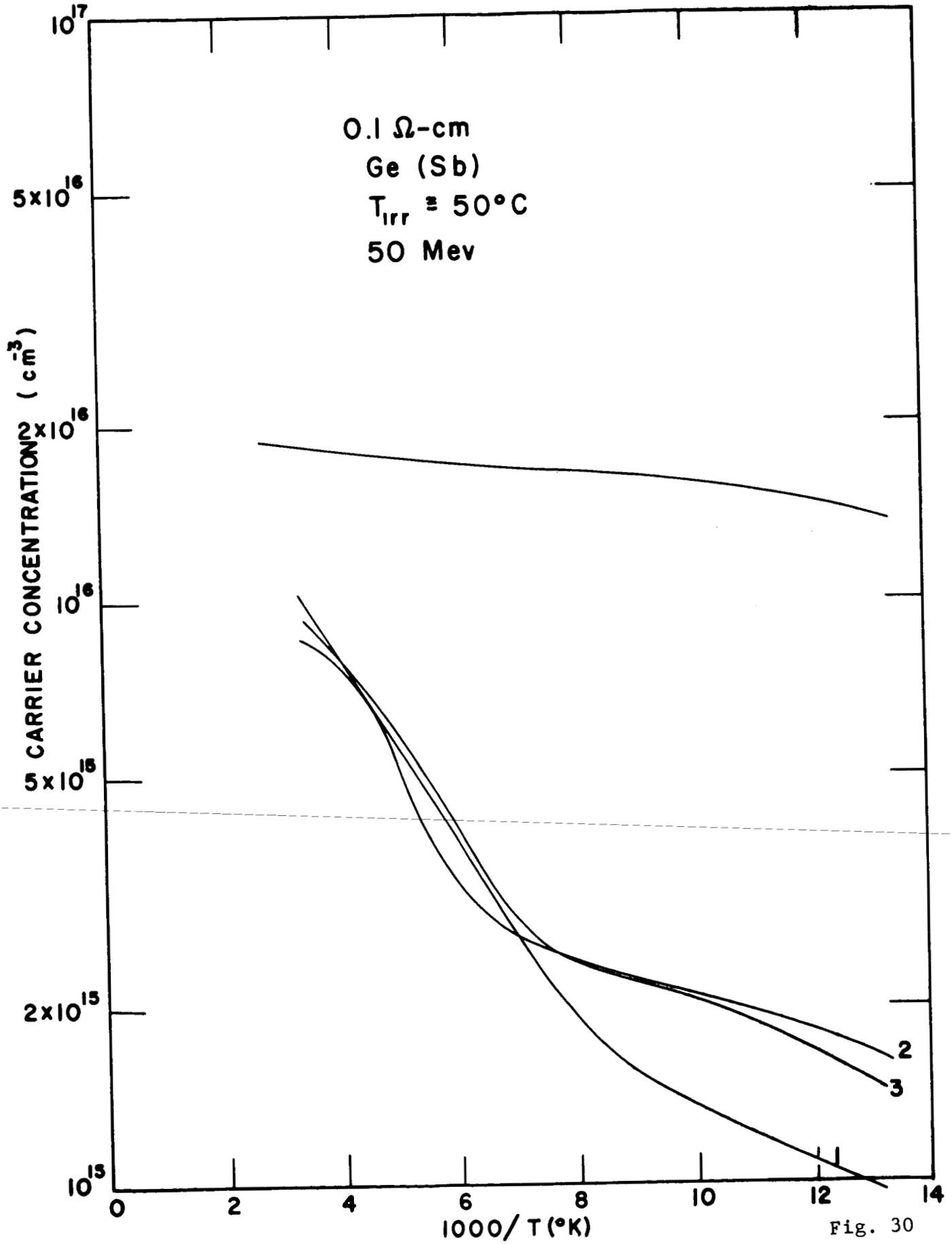
0.1 Ω-cm
Ge (Sb)
T_{irr} ≅ 50°C
50 Mev
CARRIER CONCENTRATION (cm^{-3})
10^{17}
5×10^{16}
2×10^{16}
10^{16}
5×10^{15}
2×10^{15}
10^{15}
0
2
4
6
8
10
12
14
1000/ T (°K)
2
3

Fig. 30

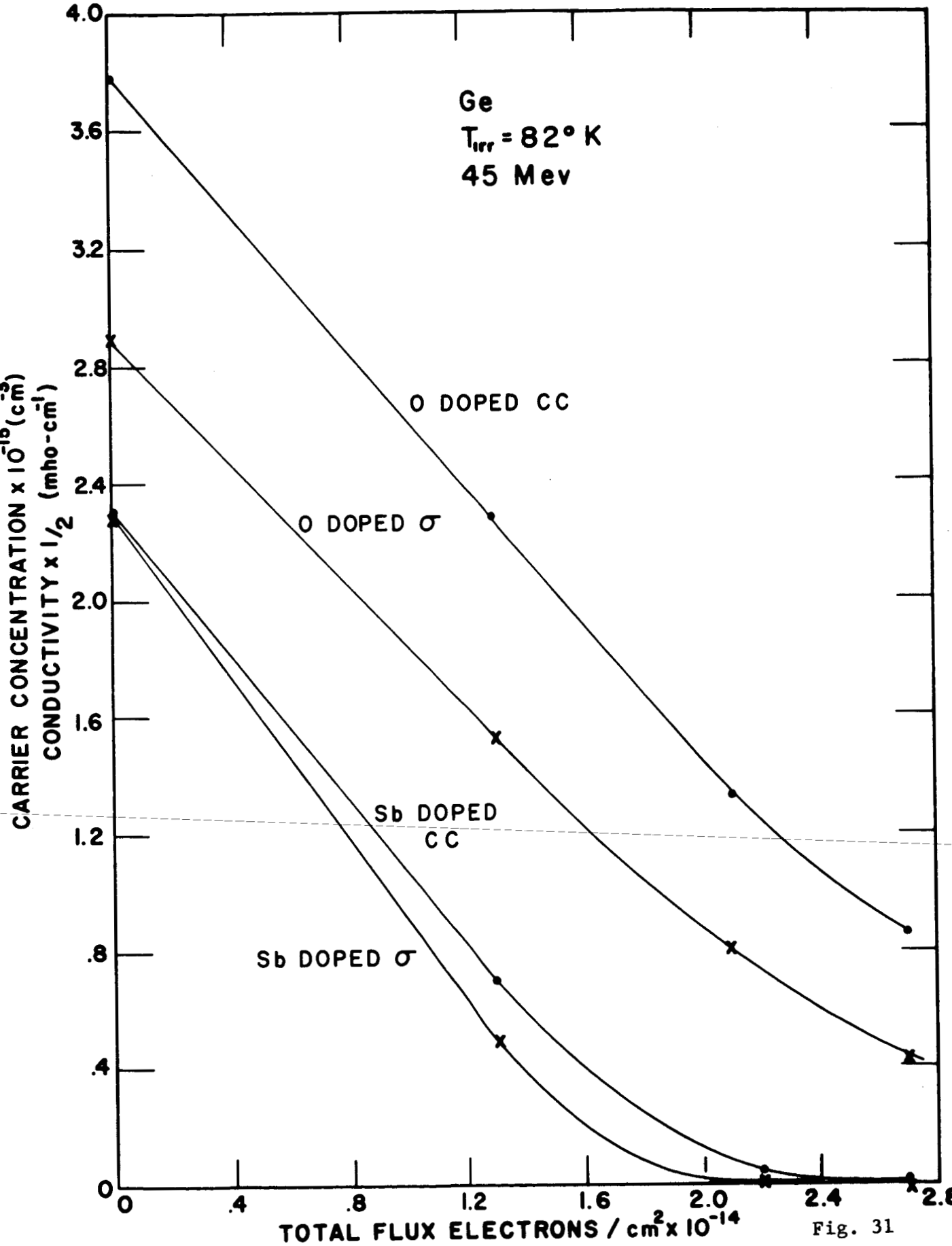
Ge
T_{irr} = 82° K
45 Mev
O DOPED CC
O DOPED σ
Sb DOPED CC
Sb DOPED σ
CARRIER CONCENTRATION x 10^{-15} (cm^{-3})
CONDUCTIVITY x 1/2 (mho-cm^{-1})
TOTAL FLUX ELECTRONS / cm^2 x 10^{-14}
4.0
3.6
3.2
2.8
2.4
2.0
1.6
1.2
.8
.4
0
0
.4
.8
1.2
1.6
2.0
2.4
2.8

Fig. 31

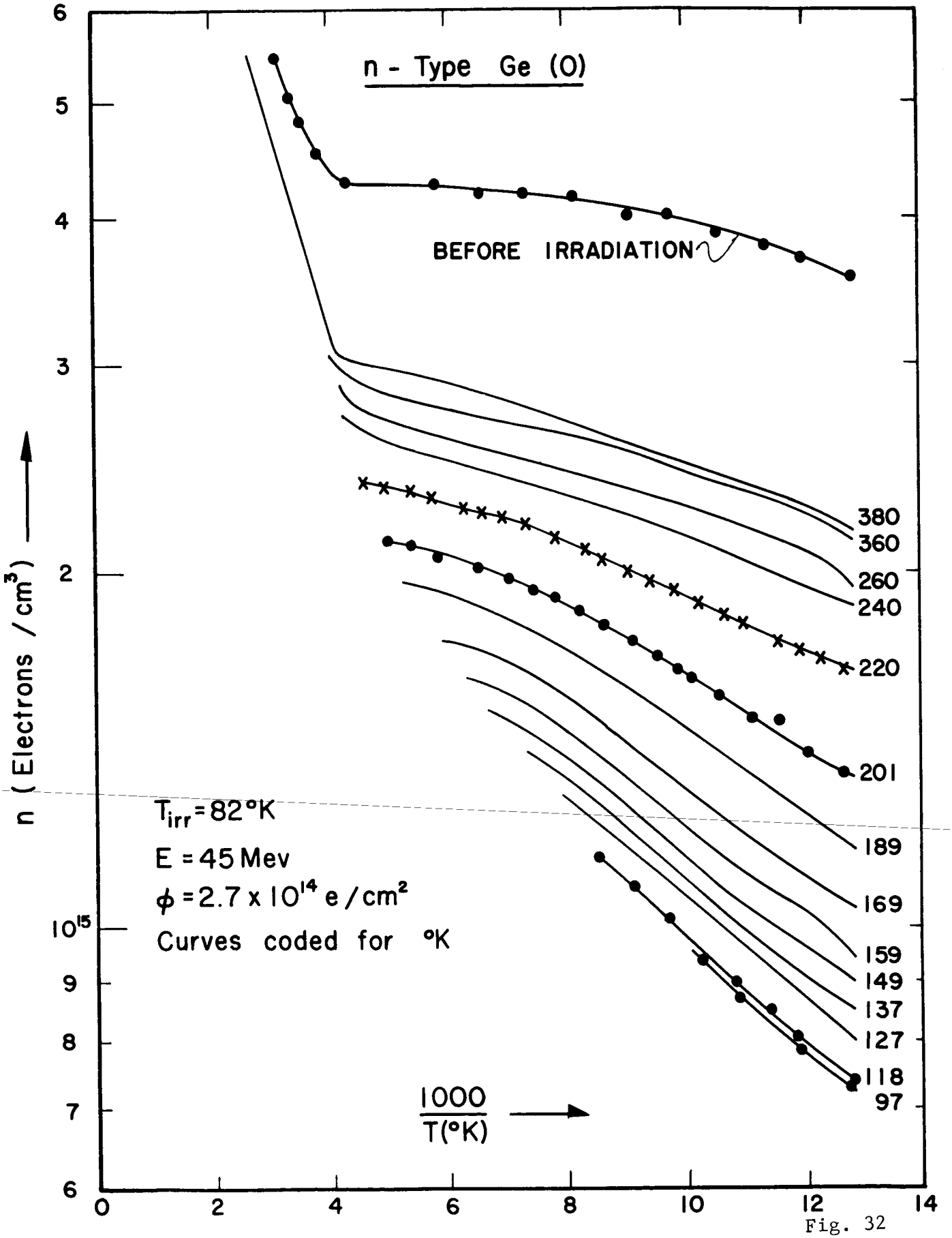
n - Type Ge (O)
BEFORE IRRADIATION
380
360
260
240
220
201
189
169
159
149
137
127
118
97
T_{irr} = 82°K
E = 45 Mev
ϕ = 2.7 x 10^{14} e / cm^2
Curves coded for °K
n (Electrons / cm^3)
10^{15}
1000 / T(°K)
6
5
4
3
2
9
8
7
6
0
2
4
6
8
10
12
14

Fig. 32

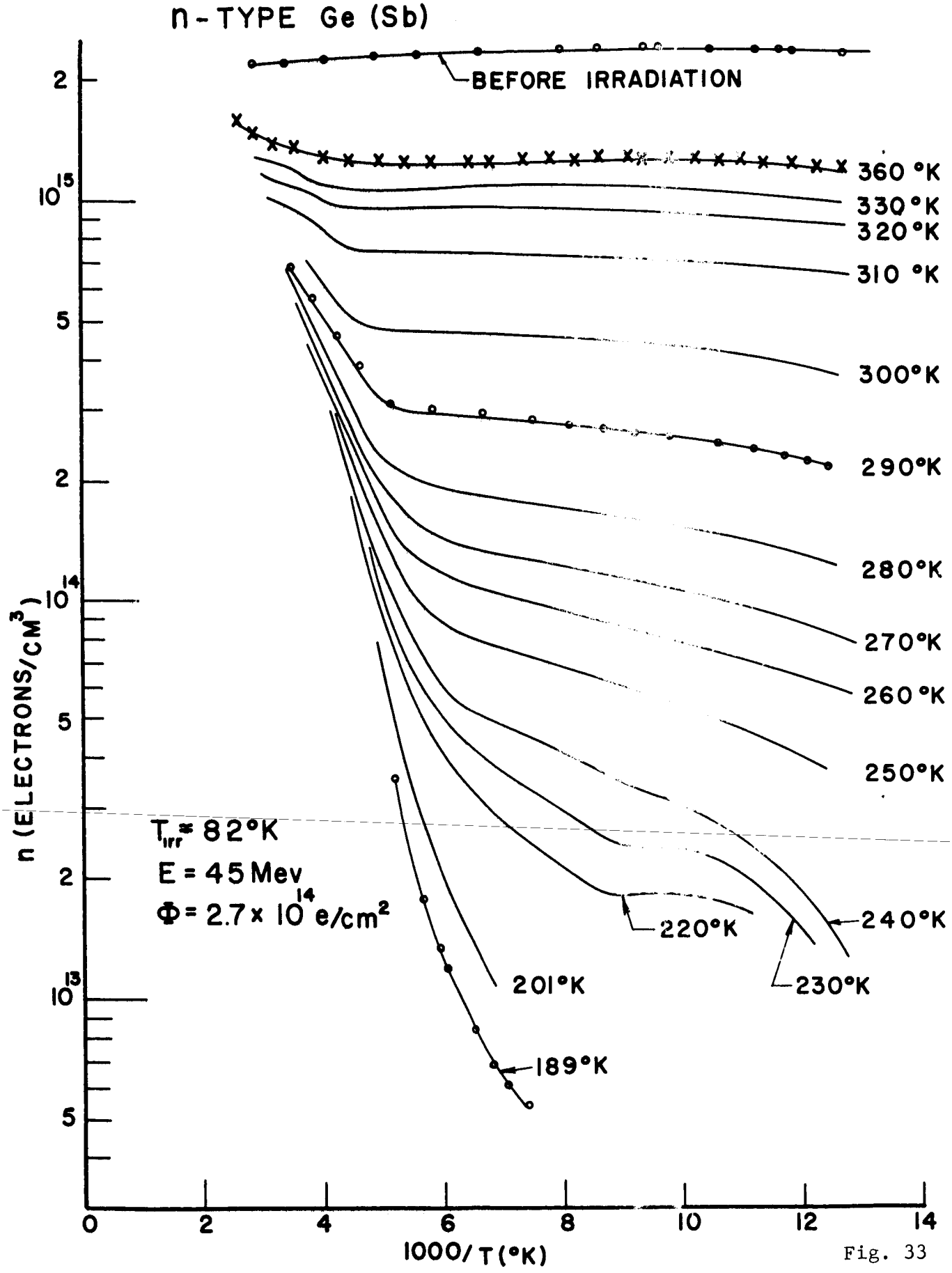
n-TYPE Ge (Sb)
BEFORE IRRADIATION
360 °K
330 °K
320 °K
310 °K
300°K
290°K
280°K
270°K
260 °K
250°K
240°K
230°K
220°K
201°K
189°K
T_{irr} = 82°K
E = 45 Mev
Φ = 2.7 x 10^{14} e/cm²
n (ELECTRONS/CM³)
1000/T (°K)
2
10^{15}
5
2
10^{14}
5
2
10^{13}
5
0
2
4
6
8
10
12
14

Fig. 33

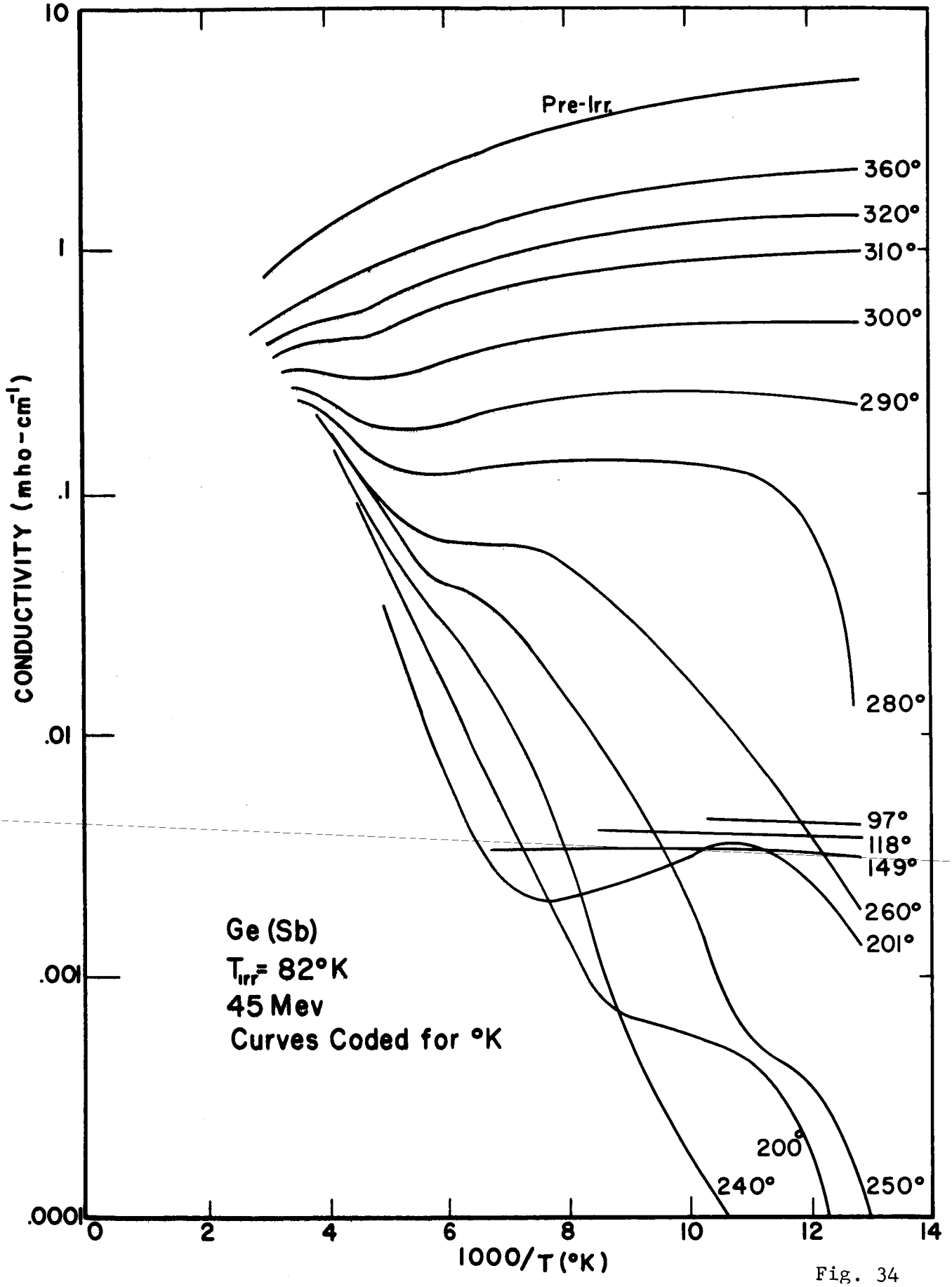
10
1
.1
.01
.001
.0001
CONDUCTIVITY (mho-cm⁻¹)
0
2
4
6
8
10
12
14
1000/T (°K)
Pre-Irr.
360°
320°
310°
300°
290°
280°
97°
118°
149°
260°
201°
200°
240°
250°
Ge (Sb)
T_irr = 82°K
45 Mev
Curves Coded for °K

Fig. 34

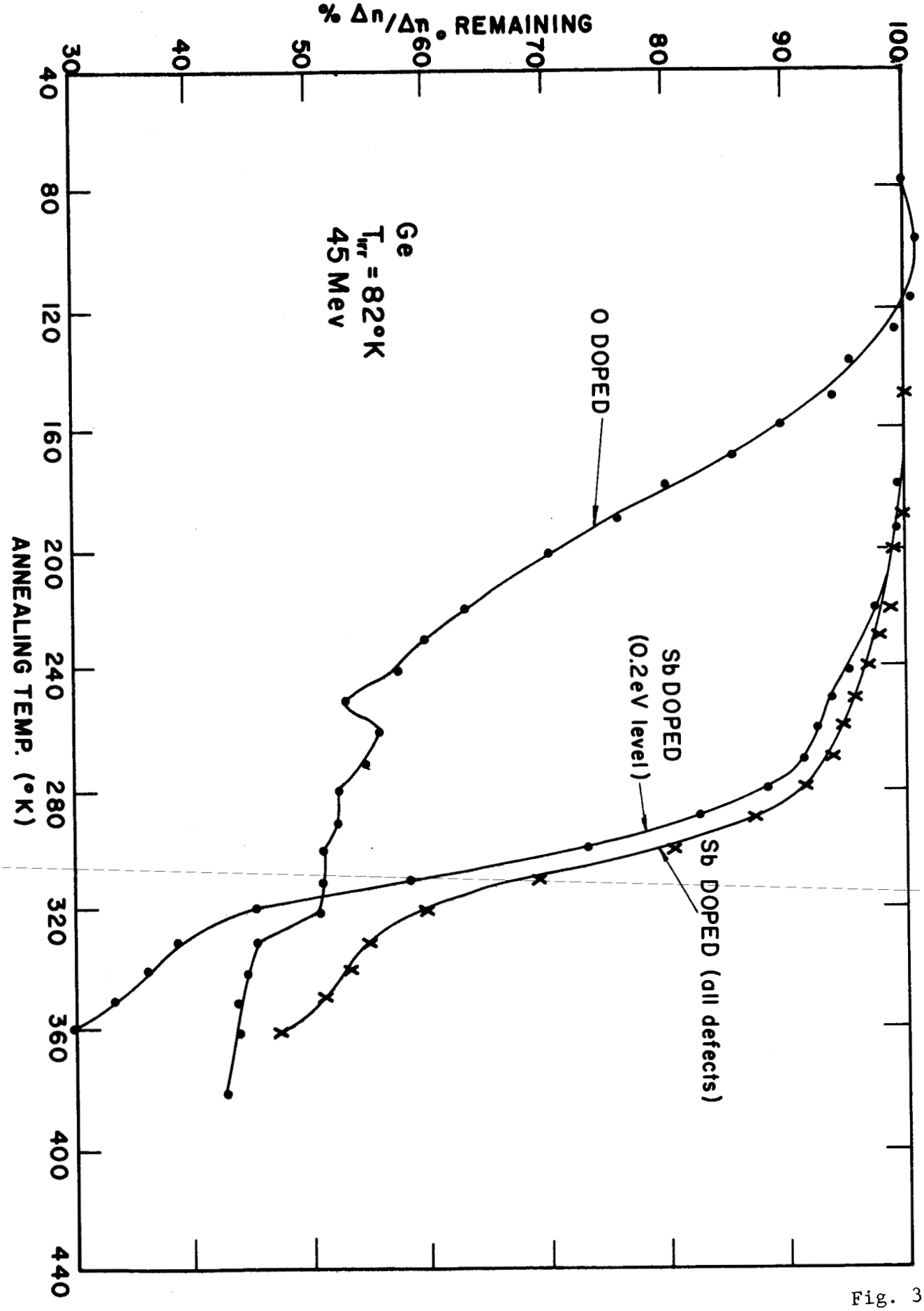
% Δn/Δn₀ REMAINING
30
40
50
60
70
80
90
100
ANNEALING TEMP. (°K)
40
80
120
160
200
240
280
320
360
400
440
Ge
T_irr = 82°K
45 Mev
O DOPED
Sb DOPED
(0.2eV level)
Sb DOPED (all defects)

Fig. 35

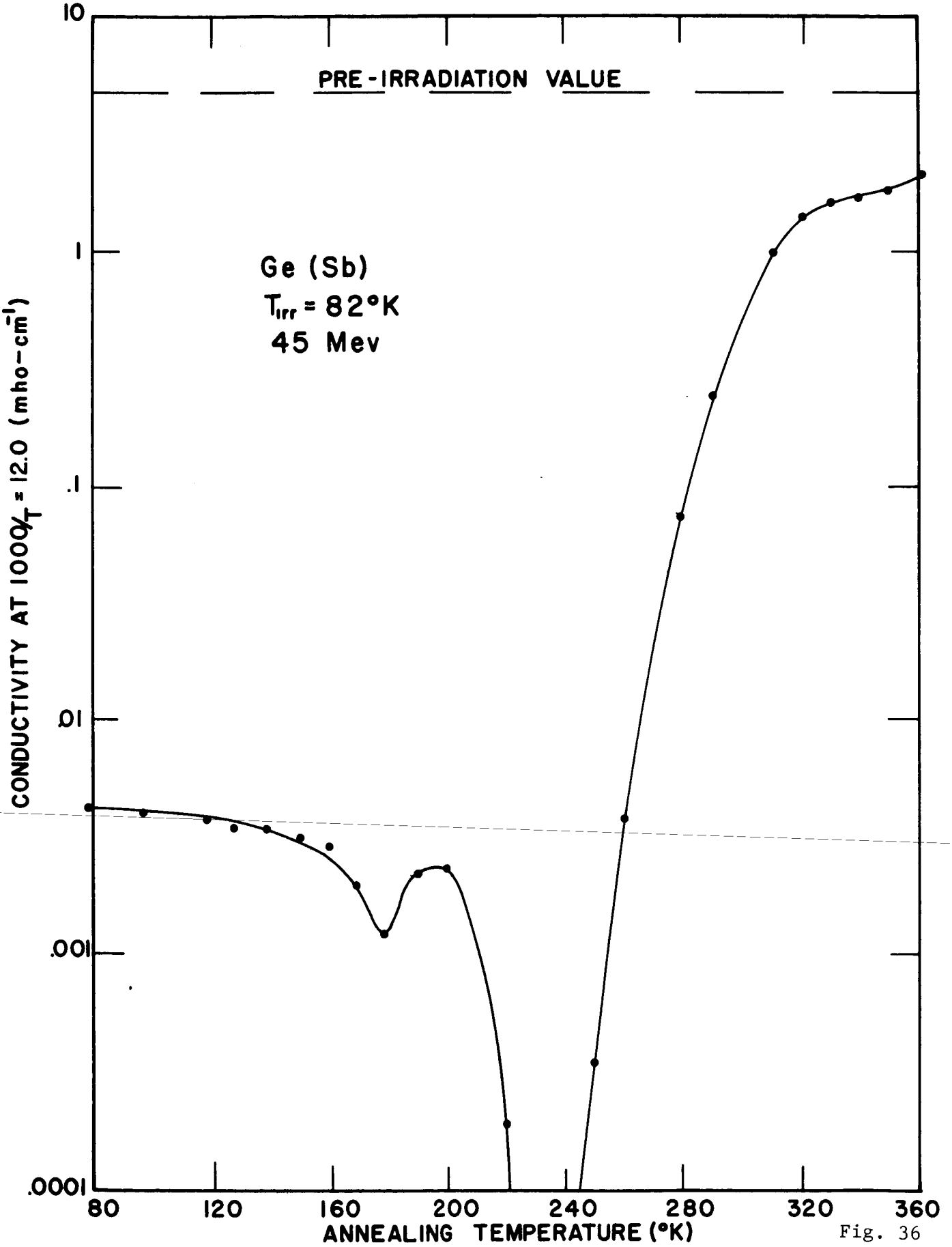
PRE-IRRADIATION VALUE
Ge (Sb)
T_{irr} = 82°K
45 Mev
CONDUCTIVITY AT 1000/T = 12.0 (mho-cm⁻¹)
10
1
.1
.01
.001
.0001
80
120
160
200
240
280
320
360
ANNEALING TEMPERATURE (°K)

Fig. 36